Radar Track Association

by

Michael L. Southcott, B.Sc (Math. Sci.), B.E. (Hons I)

Thesis submitted for the degree of

Doctor of Philosophy

Department of Electrical and Electronic Engineering
The University of Adelaide
March 1998

Table of Contents

List of Figures

List of Tables

Declaration

This thesis has been submitted to the Faculty of Engineering at the University of Adelaide for examination for the Degree of Doctor of Philosophy. This thesis contains no material which has been accepted for the award of any other degree or diploma in any University, and to the best of my knowledge and belief, contains no material previously published or wittern by another person, except where due reference is made in the text of this thesis. However, the reader should note that throughout this thesis, I refer to myself using the formal versions of the first person singular pronoun: we and our.

I hereby consent to this thesis being made available for photocopying and for loans as the University deems fitting, should the thesis be accepted for the award of the Degree.

Signature _____

Date 17/4/1998

Acknowledgments

I am especially indebted to my supervisor, Bob Bogner, for guidance throughout the course of my studies. His most obvious skills lie in his experience, and his depth and breadth of knowledge. This is known by any of his friends, colleagues and students. Along with a multitude of former students, I greatly appreciate this. However, I derived the most benefit from his rare and understated talent, an ability to nurture the process of critical thinking. The student is not explicitly guided, but is trained via a line of subtle and occasional questioning, reminiscent of Socrates. This educational technique is, in my opinion, far superior to explicit guidance, and anyone would do well to master it.

The Centre for Sensor Signal and Information Processing assisted greatly by providing excellent facilities and an environment designed for intellectual interaction between disciplines and across the boundary between industry and academia. My thanks go to fellow students for giving encouragement during difficult times. I am particularly indebted to Tony Zyweck and Brenton Cooper. Thanks also go to the members of my PhD committee, namely Salim Bouzerdoum and Doug Gray without whose encouragement I would never have made it. I am also grateful to my honours supervisor, Andrew Parker, who gave me the inspiration to pursue further study in the first place.

I am also indebted to members of the Wide Area Surveillance Division from the Defence Science and Technology Division. I extend thanks to former Chief Malcolm Golley, acting Chief Bruce Ward, Steve Tucker and Doug Kewley for encouragment but particular thanks go to members of the Data Fusion Group, namely Ian Dall, Andrew Shellshear and Kruger White for meticulous reviews of my work.

Abstract

Ambiguities occur in Over-The-horizon Radar (OTHR) due to multipath propagation from multiple ionospheric layers. Multipath propagation causes multiple instances of each target to be observed and consequently multiple tracks per target are formed. There is a need to determine which tracks correspond to the same target. The process of associating tracks which correspond to the same target is termed track association.

The tracks corresponding to the same target appear in patterns in the radar space which are characteristic of the propagation conditions. These characteristic patterns depend on the ionospheric state and the location of the target with respect to the transmitter and receiver. These patterns have been noticed previously, but have not been used for automated track association.

This dissertation presents a novel system for automated track association, which providess significant improvement on previously proposed methods. The track association system is designed on the premise that the characteristic patterns of multimode propagation are a function of the ionospheric conditions. One component of the track association system models the multimode patterns over the radar coverage. An estimation of the shape and form of a multimode pattern can be made for a required location. The estimated multimode patterns can be compared to the patterns formed by observed tracks, to determine if the observed tracks are multimode tracks from a common target. The comparison of the estimated multimode patterns to the observed track patterns is performed with an association metric. The association metric requires certain parameters of the multimode patterns to be modelled over the radar coverage.

An association metric is proposed for discriminating between 'associated' tracks from a common target and 'non-associated' tracks from different targets. The multimode pattern parameters provided by the model of multimode patterns are used for the computation of the association metric. Propagation modes are hypothesised for the observed tracks and the expected positions of the alternative propagation modes are obtained. The association metric compares the expected position of an observed track's alternative mode to the actual position of another observed track. The discrimination ability of the association metric is compared to that of the alternative association metrics over a range of simulated OTHR scenarios and significant improvement is shown.

Two techniques for modelling parameters of the multimode patterns over the radar coverage are introduced. The first technique employs heuristically chosen functions to model the field of multimode patterns. The second technique models the field via principle component analysis. Deficiencies are noted in both techniques, and a third technique is introduced which combines the advantages of the first two techniques. The third technique employs principle component analysis from the second technique on the coefficients of the basis functions from the first technique. Comparative studies are performed between the three modelling techniques. The technique employing heuristically chosen basis functions performed the worst, while the other two techniques performed similarly.

Glossary

Notation

$\mathbf{a}, \mathbf{b}$	Vectors are denoted by lowercase bold typeface.
$[\mathbf{a}]_k$	The k^{th} component of intermodal vector $\mathbf{a}$.
$\mathbf{A}, \mathbf{B}$	Matrices are denoted by uppercase bold typeface.
$\mathbf{A}^T$	The transpose of matrix $\mathbf{A}$.
$\mathbf{A}^{-1}$	The inverse of matrix $\mathbf{A}$.
$\mathbf{a} \times \mathbf{b}$	The cross product of vectors $\mathbf{a}$ and $\mathbf{b}$.
$\mathbf{a}.\mathbf{b}$	The dot product of vectors $\mathbf{a}$ and $\mathbf{b}$.
$\|\|\mathbf{a}\|\|$	The vector norm of $\mathbf{a}$.
$\forall i$	For all i.
$\hat{\mathbf{a}}$	The estimate of $\mathbf{a}$
$\mathcal{A}, \mathcal{B}$	Sets are denoted by calligraphic typeface.
$E[a]$	The expectation of a.
$\Pr(a)$	The probability of event a.
$\chi^2(r)$	Chi-squared distribution with r degrees of freedom.
$X \sim N(\boldsymbol{\mu}, \boldsymbol{\Sigma})$	Random variable X has normal distribution with mean $\boldsymbol{\mu}$ and covariance $\boldsymbol{\Sigma}$

Symbols

$\mathcal{A}_{mn}$	The set of associated pairs of tracks corresponding to modes m and n.
ΔR	Range disparity component of intermodal vector.
ΔA	Azimuthal disparity component of intermodal vector.
$\mathcal{F}_I$	Abstract representation of ionospheric conditions.
$[H : \{i, j\} \in \mathcal{A}_{mn}]$	The hypothesis that tracks i and j are associated, and correspond to modes m and n, respectively.
$\{i, j\}$	The ordered pair of tracks i and j.
$M_{mn}(\mathbf{y}_i, \mathbf{y}_j)$	Proposed association metric between measurements $\mathbf{y}_i$ and $\mathbf{y}_j$.
$\hat{\mathbf{d}}_{mn}$	The estimate of disparity vector $\mathbf{d}_{mn}$.

Σ_{mn}	Covariance matrix of intermodal vector $\boldsymbol{x}i_{mn}$.
$\mathcal{S}_m$	The set of tracks due to mode m.
T_{mn}	The coordinate transform from mode m to mode n.
$\mathbf{y}$	Vector of radar measurements.
$\mathbf{y}_i$	The vector of radar measurements for track i.
$\mathbf{d}_{mn}(\mathbf{y})$	The intermodal vector function between modes m and n.
$\mathbf{z}_{ij}$	The intertrack vector between tracks i and j.

Bases

Υ_i	Generic basis function for modelling disparity functions.
Φ_i	Cosine basis function for modelling disparities.
Γ_i	Empirical basis function for modelling disparities.
Ψ_i	Combined basis function for modelling disparities.

Acronyms

ARD	Azimuth-Range-Doppler (page 3).
DCT	Discrete Cosine Transform (page 57).
FMCW	Frequency Modulated Continuous Waveform (page 1).
HF	High Frequency (page 1).
IDCT	Inverse Discrete Cosine Transform (page 85).
MP	Multimode Pattern (page 3).
OTHR	Over-The-Horizon Radar (page 1).
SNR	Signal-to-Noise Ratio.

Terms

coning effect	In a linear array, the angle of elevation cannot be distinguished from the azimuthal angle. Only the conical angle can be measured. (page 3).
disparity field	A vector field of difference between mode measurements from a common target (page 4).
intermodal vector	The difference in measurements between modes from a common target (page 7).
M-distance	Mahalanobis distance (page 38).

CHAPTER I

Introduction

1.1 Overview

The ionosphere can be used as a propagation medium for high frequency (HF) radio signals [32]. Over-The-Horizon Radar (OTHR) exploits this propagation medium, and provides a capability for long-range surveillance [19], including the detection and tracking of targets and the remote sensing of the sea state [18], which is important in the detection and monitoring of cyclones or rough weather. Using the information obtained from remote sensing, ships can save fuel by avoiding rough weather. The ionosphere is a complex medium and it is not uncommon for more than one propagation path or *mode* to exist from the transmitter to the receiver via the target. This situation is illustrated in figure 1.1; the E and F layers of the ionosphere, which typically contribute to multimode propagation are shown. Multiple detections received from a common target via different propagation modes are usually tracked as distinct tracks, resulting in multiple tracks per target. This process is termed *track association*. It is important to determine which tracks correspond to the same target, so that an integrated picture of the surveillance region can be obtained [14, 15, 27]. The track association task is a fundamental problem in OTHR and the results of this task can assist other OTHR signal processing tasks. This thesis addresses the problem of track association, and contributes a systematic approach for solving this problem.

1.2 Over-The-Horizon Radar Overview

In this section, we explain the context of OTHR track association by providing a brief overview of OTHR signal processing. We discuss the concepts of OTHR operation and signal processing which are relevant to this thesis. OTHR signal processing is discussed in more detail in chapter 2.

The work in this thesis was inspired by some of the outstanding challenges of the Australian Jindalee radar, near Alice Springs. This HF skywave radar transmits a frequency modulated continuous waveform (FMCW) which consists of multiple sweeps with a linear saw-tooth frequency modulation [24]. The radar transmits and subsequently receives a *dwell*

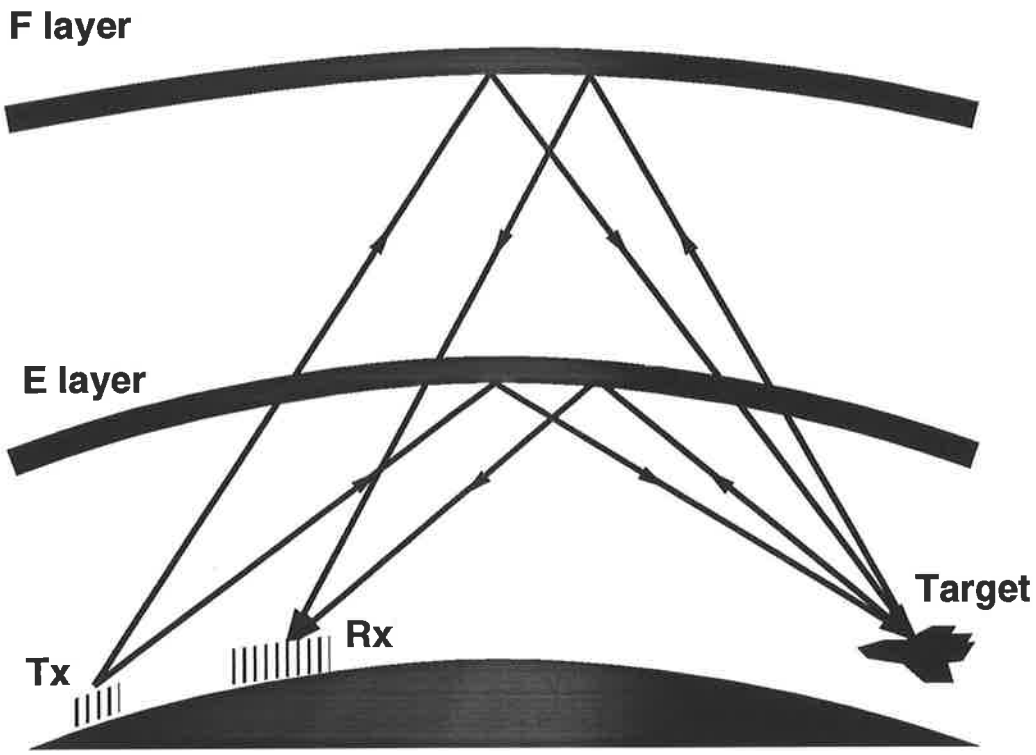

Figure 1.1: OTHR operation in the presence of multipath propagation.

of data, which is a coherent pulse train for measuring delay, apparent azimuth and Doppler shift data. The processes of ranging, beamforming and Doppler processing are applied to received data; thus the data is processed into azimuth-range-Doppler (ARD) *cells*.

Possible detections are identified from the ARD cells, and these detections are associated into tracks by an automatic tracker. This process of determining which detections correspond to a common track is sometimes termed *data association* [2], as distinct from track association [14, 15], which is the process of determining which tracks correspond to a common target. We discuss difficulties of detection and tracking in Section 2.6.2.

1.3 Multimode patterns

In the presence of multimode propagation there are differences in the radar measurements of the multiple detections from a common target. The multipath returns from a common target appear in characteristic patterns in the radar measurement space. These patterns are referred to as *multimode patterns* (MPs) . The shape and size of the MPs depend on the relative differences in the propagation geometry of the different modes. The propagation geometry varies significantly in different circumstances. The propagation geometry depends on the location of the target with respect to the transmitter and receiver and the ionospheric conditions. Consequently the multimode patterns vary geographically (due to changing propagation geometry over the radar coverage), and temporally (due to changes in the ionospheric conditions).

Different modes have different propagation paths, and consequently multiple returns from a common target have different delay, apparent (For economic reasons, OTHR receiver arrays can generally not discriminate between the angle of elevation and the azimuthal angle of return signals. For such receivers, the apparent azimuthal angle is the conical angle of arrival of return signals, which is different from the actual azimuthal angle of the target.) azimuth and Doppler shift measurements. The difference in propagation path length causes a difference in the delay of multipath returns from the same target. The difference in the elevation angle of the different paths causes a difference in apparent azimuthal angle of multipath returns from the same target; we refer to the cause of this difference as the *coning effect* . For economic reasons, OTHR receiver arrays can generally not discriminate between the angle of elevation and the angle of apparent azimuth of return signals. For such receivers, the apparent azimuthal angle is the conical angle of arrival of return signals, which is different from the actual azimuthal angle of the target. The differences between the angles of incidence and reflection at the target with respect to the velocity of the target for different paths cause a difference in the Doppler shift returns from the same target.

A simulation of a single target traversing a large distance within the coverage of an OTHR illustrates the MPs between associated tracks. It is common for two ionospheric layers to

exist at the radar operating frequency; three or more layers occur more infrequently. The simulation assumes two ionospheric layers and therefore two propagation paths between the target and the radar as in figure 1.1. Typical layer heights for the E and F layers of the ionosphere are 100km and 250km respectively, and these values were used in the simulation. Note therefore that there are four paths from the transmitter to the receiver via the target, resulting in the formation of four tracks. The results of the simulation of OTHR propagation are shown in figure 1.2. OTHR track data consists of delay, apparent azimuth and Doppler shift information, but for the sake of simplicity, only the delay and apparent azimuth components of the track data are displayed in figure 1.2. The tracks are displayed as dotted lines and are labelled by mode with two letters (for example "Mode EF") to represent the ionospheric propagation layers which correspond to that mode; the first letter indicates the ionospheric layer reflecting the transmitted signal to the target, while the second indicates the ionospheric layer reflecting the return from the target. The multimode patterns are shown at regular time intervals by solid lines linking the tracks. Note that the shape of the multimode patterns changes as the target moves across the radar coverage.

1.4 Multimode field

The term *disparity field* refers to a field, given in the radar measurement space, which is used to describe the value of MPs throughout the radar space. The disparity field represents the variable shape and size of the MPs throughout the radar space. The disparity field is an indicator of the current ionospheric propagation conditions. The observed MPs are samples of the disparity field.

An illustration of a disparity field is shown in figure 1.3. The figure shows the variation in the MPs over the radar measurement space. The simulation is a snapshot of the multimode patterns at one time instant when there are two ionospheric layers present. Each multimode pattern consists of four detections from the same target which are connected by solid lines to highlight the patterns. Note the variation in multimode patterns throughout the radar coverage due only to variations in the propagation geometry, not variations in the ionosphere. At larger azimuthal angles from boresight (a reference angle, perpendicular to the antenna array and is the direction of maximum resolution), the apparent azimuthal component of the disparity vector between certain modes is larger, due to the coning effect. At shorter ranges, the delay component of the disparity vector between certain modes is larger. The characteristic multimode patterns have been noticed previously [14, 43], but have not been used for automated track association.

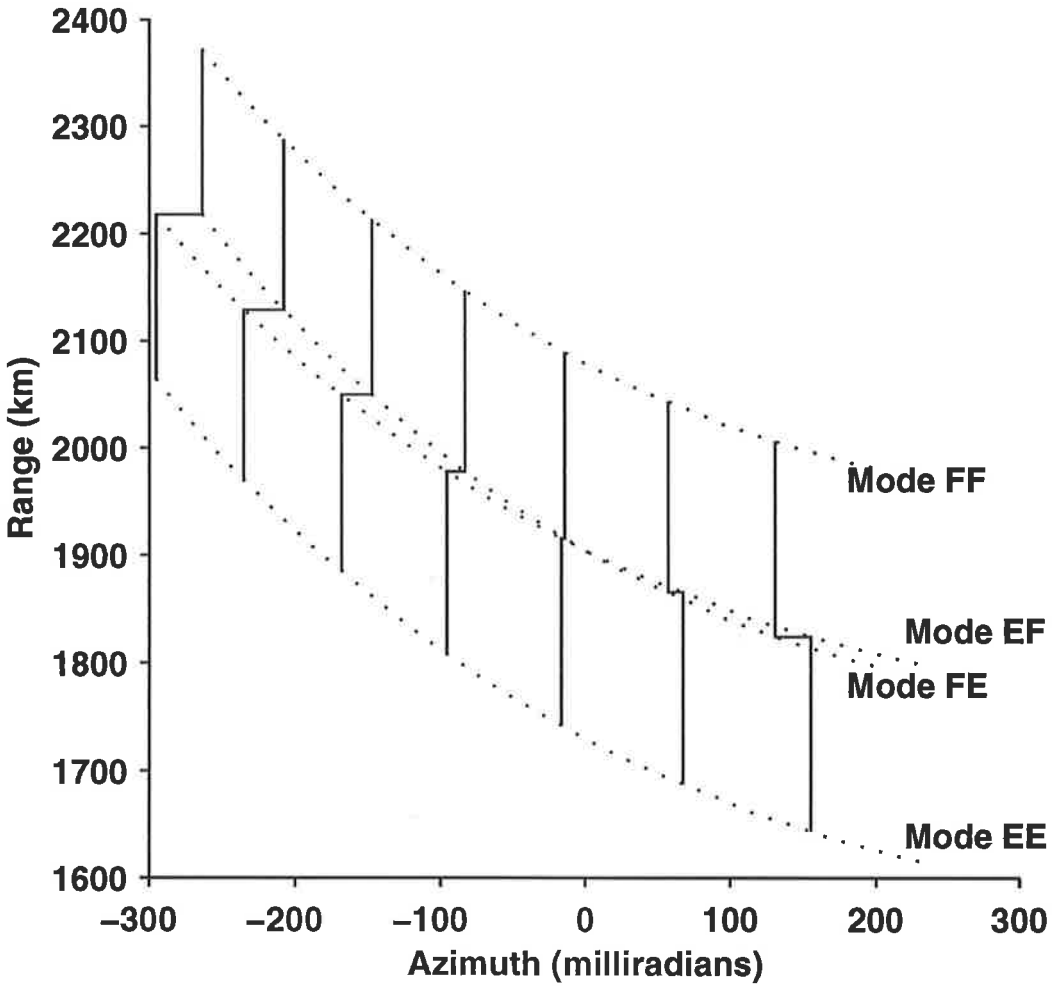

Figure 1.2: Simulation of four tracks from a common target.

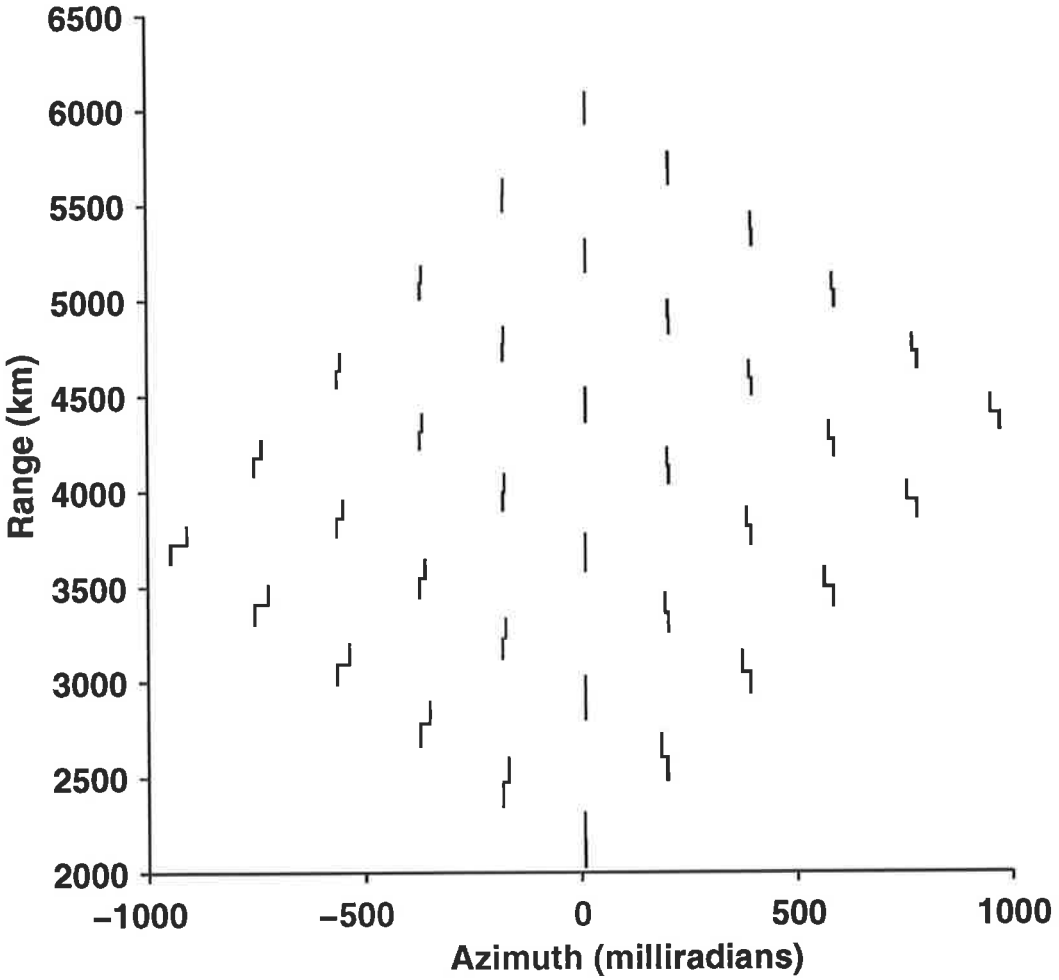

Figure 1.3: Samples of the disparity field throughout the radar coverage.

1.5 disparity vector

The *disparity vector* is defined as the difference in measurements between modes from a common target. Each multimode pattern in figure 1.3 consists of detections due to four modes; thus six (C_2^4) mode pairs and twelve unique disparity vectors exist. Only three disparity vectors are shown in figure 1.3. The disparity vector between a pair of modes varies throughout the radar measurement space.

There are two factors other than the target position which contribute to the variation in an disparity vector. The first is caused by changes in the propagation geometry due to ionospheric perturbations. The second is caused by radar measurement error. These sources of variation cause an disparity vector to vary at a particular location in the radar coverage.

We simulate a typical distribution of an disparity vector at a particular location, which is shown in figure 1.4. The figure shows the variation in the expected measurements of the mode EF track with respect to the mode EE track. This variation is shown as a two dimensional probability density function at a particular location in the radar coverage. The dark regions indicate high probability density and the light regions indicate low probability density. The variation of the expected position of mode EF in this example is caused by changes in the propagation geometry due to perturbations in the heights of the ionospheric layers. Only the variation in the disparity vector due to ionospheric perturbation is considered. The other source of variation, radar measurement error, depends on specific radar characteristics but could be included in an analogous way.

The distribution of the disparity vector in figure 1.4 is generated by a Monte Carlo simulation with a target observed via the E and F layers of the ionosphere. The simulated target is observed via 10,000 different ionospheric conditions at a ground range of 1000km, with an actual azimuth of 400 milliradians from boresight. The height of the E layer is sampled from a normal distribution with mean 100km, and standard deviation 2.5km. The height of the F layer is also sampled from a normal distribution with mean 250km, and standard deviation 12.5km. The heights of the ionospheric layers vary independently according to normal distributions which correspond to physically plausible ionospheric states [32].

1.6 Contributions of this thesis

The major contribution of this thesis is a systematic approach for *associating* OTHR tracks corresponding to the same target. Association is the process of determining which tracks are multimode tracks from a common target. The approach exploits the patterns which are characteristic of multimode propagation. Significant components of the association system are an association metric for track association, and a model of the multimode patterns in the radar measurement space. An overview of the system appears in section 3.3, and it is

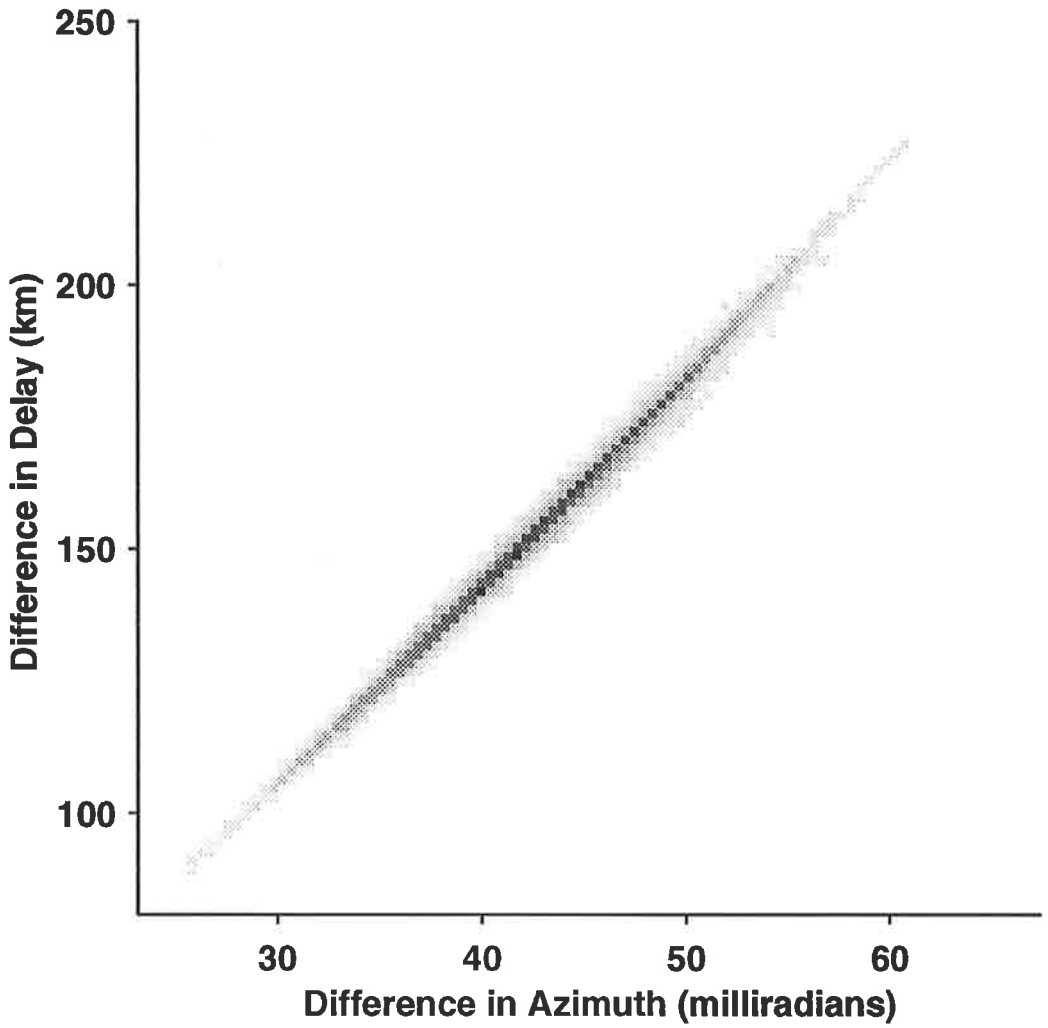

Figure 1.4: Monte Carlo simulation of disparity vector between mode EF and FF.

illustrated in figure 3.1. We summarise specific contributions of the thesis as follows:

- A contribution which lies at the heart of the systematic approach is the formulation of the coordinate transform between propagation modes as a function of the radar measurements and ionospheric propagation conditions. This formulation appears on page 30, in equation (3.1) of section 3.3.2.

- Another contribution at the core of the system is the concept of modelling the statistical parameters of the disparity vector in the radar measurement space. A formulation of this concept appears on page 31 in equation (3.4) of section 3.3.4.

- We propose to model the disparity vector functions as a linear combination of basis functions on page 56 in equation (5.1) of section 5.2. We propose three techniques of finding a suitable set of basis functions:

    1. Firstly, we propose a technique for modelling the disparity vector as a linear combination of heuristically chosen basis functions in section 5.3, beginning on page 57. We illustrate this technique using multidimensional cosine functions.
    2. We propose a second technique for modelling the disparity vector as a linear combination of empirically determined, discretely sampled functions in section 5.4, beginning on page 58. We determine the functions using principle component analysis.
    3. Finally, we propose a third technique for modelling the disparity vector in section 5.5, beginning on page 63. The third technique combines the advantages of the previous two approaches, modelling the disparity vector via principle component analysis (PCA) on the coefficients of multidimensional cosine functions.

- We perform a comparative study of the three techniques for modelling the disparity vector in section 5.7.

- A major component of the system is the association metric, proposed in chapter 4. The association metric operates on a pair of tracks and it is designed to discriminate between pairs of tracks associated with the same target (*associated tracks*) and pairs of tracks associated with different targets (*non-associated tracks*). The association metric is based on the Mahalanobis distance of the disparity vector function, and is formulated on page 38 in equations 4.2 and 4.2 of section 4.2. The disparity vector function is used so that the warping caused by multimode transmission is accounted for, and thus the metric provides a measure of track similarity with uniform accuracy across the radar coverage. We perform a comparative study of the proposed metric to alternative metrics in section 4.3.

- We formulate *cumulative association metrics* in section 4.4, which are a combination of sequential association metrics. We propose equation (4.6) on page 50 for the case of independence between sequential measurements. We propose equation (4.8) on page 50 for the case of dependence between sequential measurements. We propose an additional, more tractable, cumulative association metric for the case of dependence, potentially trading off accuracy for tractability in equation (4.9) on page 51.

1.7 Organisation

The remainder of this thesis is organised as follows:

Chapter 2 provides an introduction to Over-The-Horizon Radar, and some necessary background for the work presented later in the thesis.

Chapter 3 introduces a systematic approach to track association, the significant details of which appear as separate chapters in this thesis.

Chapter 4 introduces a novel association metric, based on a model of the disparity vectors, and compares the association metric to alternative association metrics.

Chapter 5 contains details of novel techniques for modelling the disparity vectors. One method models the disparity vector as a linear combination of cosine functions, while another models the disparity vector via principle component analysis. A third technique, which combines the advantages of each of the first two techniques is proposed, and a comparative study of the three techniques is performed.

Chapter 6 summarises the important results from this thesis, and discusses the direction of future work.

Appendix A contains details of a simplified model of ionospheric propagation used for the comparative study of association metrics in chapter 4.

CHAPTER II

Over-The-Horizon Radar

2.1 Introduction

This chapter introduces some of the background theory required for the work presented later in the thesis. It is intended as an introduction to the relevant concepts and is not a general exposition of OTHR. This chapter is organised as follows.

Some important terms are defined in Section 2.2. The ionosphere and the processes which make it suitable for refraction of HF radio signals are briefly discussed in Section 2.3. In Section 2.4, some important background history of HF radar with respect to the ionosphere is introduced. Relevant issues of OTHR operation are discussed in Section 2.5. There are many problems in OTHR, primarily due to the complex nature of the propagation medium. Some of the problems in OTHR are discussed in Section 2.6. Previous work is discussed in Section 2.7, and a summary of the Chapter appears in Section 2.8.

2.2 Definitions

The definitions in this section, appearing in italics, are necessary for the discussion in this chapter and are used throughout the rest of this thesis.

A *propagation mode* is the the path taken by a radio wave when propagating from the transmitter to the receiver [33]. In OTHR, the radio wave propagates from the transmitter to a remote site and is partially scattered back to the receiver. There are many possible propagation modes. The propagation modes active for a radio wave depend on the frequency of that radio wave, and there are often frequencies for which multiple propagation modes are simultaneously active.

The radio waves make one or more *hops* when propagating in either direction. Single hop propagation has one reflection from the ionosphere, while double hop propagation has two reflections from the ionosphere and one reflection from the surface of the earth in between.

The term *target* is used to refer to reflectors of HF radio waves which are of interest for surveillance. The physical area monitored by the radar in which targets exist is termed the *target space*. The target space is measured in *ground coordinates*, in some global coordinate

system. This global coordinate system can be actual range and actual azimuth from the radar or the geographical coordinate system of latitude and longitude. The radar measurements, which include quantities corresponding to delay, apparent azimuth and Doppler shift, define the *radar space*. There is a need to transform radar measurements into a system of global coordinates. This transformation problem is commonly termed the *coordinate registration* problem. To transform points from the measured radar space (in radar coordinates) to the target space (in ground coordinates) it is necessary to know how ground range and azimuth vary as a function of the propagation path through the ionosphere.

Multimode registration is the process of transforming measurements from multiple propagation modes so that they correspond exactly to a common position in ground coordinates. The common position is the location of the reflector in ground coordinates.

The *association decision* is the process of determining whether a group of tracks is in fact multimode from a common target.

2.3 The Ionosphere

The ionosphere is the medium which makes OTHR possible, but is also the source of many problems. A thesis addressing some of the problems of Over-The-Horizon Radar would be incomplete without giving some background on the ionosphere.

The ionosphere is a roughly spherical region, concentric with the earth's surface in which ionised particles exist. The ionosphere is a complex medium for several reasons. The neutral atmosphere consists of a range of atoms such as oxygen, nitrogen and nitric oxide; the proportion of these atoms varies with altitude but the total density of the atoms decreases as altitude increases. Ionised particles are formed from the atoms by a process termed photoionisation, in which solar radiation strips electrons from atoms [32]. The intensity of solar radiation decreases as altitude decreases, because the radiation has been partially absorbed. The two contributing effects to ionised particles, atomic density and solar radiation both vary in a complex manner and are both functions of height. The combination of these two effects causes the variation of electron densities with height. Consequently, there are several regions of high electron densities at different altitudes. These regions are referred to as layers because they form within height bounds. There are up to four different layers at different altitudes.

The layers of high electron density partially refract electromagnetic radiation of between approximately 0 and 50 MHz, according to Snell's Law of refraction. Consequently, some energy of HF[1] rays transmitted from the earth's surface to be refracted back towards a receiver at another point on the earth's surface. The degree of refraction of the rays depends on the

[1] Between 3 and 30 MHz.

electron density. However, the electron density and hence the path of refracted rays can only be coarsely estimated. The path length of the refracted ray from the transmitter to the receiver is often estimated via a simplification. The ray is considered to be reflected by a virtual reflecting layer in the ionosphere; this layer is known archaically as the Heaviside layer [20], but is referred to in this thesis as the *virtual reflecting layer*. The height of the virtual reflecting layer is determined as the height which causes the path length of a virtual *reflected* ray to equal to the path length of the actual *refracted* ray. For the purposes of this thesis, it is sufficient for the ionospheric regions which refract HF radio waves back to the earth's surface to be considered as distinct reflecting layers.

The suitability of the ionosphere as a reflector depends mainly on solar radiation. The amount of solar radiation incident at a particular point on the ionosphere depends largely on the zenith angle and the degree of solar activity. The zenith angle varies with latitude and with the diurnal and seasonal cycles. Solar activity is also cyclic and has a period of approximately 11 years. There are other factors which contribute to ionospheric variability such as thermospheric winds, and chemical reactions [32].

The ionospheric layers can be considered to be roughly spherical, but there are many large scale perturbations from the spherical. For instance, the heights of ionospheric layers vary immensely at the sunrise and sunset transition. Other effects which contribute to a gradient in the ionospheric include ionospheric storms, the equatorial anomaly, and travelling ionospheric disturbances [17].

2.3.1 Previous work on modelling the ionosphere

Theoretical models of the ionosphere are very complicated due to the nature of the medium being modelled. The primary ionospheric variable estimated by a model is usually electron density as a function of height. Due to the complex chemical and physical processes at work in the ionosphere, the estimation is invariably difficult. The literature has an abundance of ionospheric models and ionospheric prediction techniques, and they continue to be developed [40, 53, 11, 30]. A review of ionospheric radio propagation models is out of the scope of this thesis, but one is provided in [40].

2.4 History of Over-The-Horizon Radar

It has long been known that the ionosphere can be used for the propagation of HF radio signals. The ionosphere's ability to act as a propagation medium for radio signals was first suggested following Marconi's successful transatlantic radio transmissions in December 1901 [46]. Heaviside and Kennelly independently suggested the existence of an ionised layer in the upper atmosphere which acts as a reflecting surface for radio signals [20, 46].

Further important precursors to OTHR occurred in the mid 1920's, when the first experiments relating to the propagation of HF radio signals for ionospheric sounding were being conducted in Germany, Britain and the USA [47].

During World War II, Britain's Chain Home radar series was intended as a ground-wave radar, but often received backscattered returns at extreme ranges [29, 44]. It was known that these returns were from the earth's surface via ionospheric propagation. Due to the magnitude of clutter from the earth's surface it was not possible to interpret the returns. The pulse repetition frequency (PRF) had to be reduced to ensure that these unwanted returns were not confused with the desired ground-wave returns via range ambiguity.

Following World War II it was recognised that distinguishing between targets and the backscattered surface clutter (see Section 2.5) required that the Doppler of moving targets be used. Perhaps the first attempts at exploiting the ionosphere for over-the-horizon surveillance was in World War II when HF radars attempted to detect sea convoys. Without the ability to use Doppler to distinguish between targets and clutter, the attempts were in vain. OTHR has only become a possibility with the advent of high quality signal sources, which enable the Doppler of targets to be resolved from that of clutter via signal processing. Furthermore, OTHR requires the processing of a vast amount of data, which has been made possible through advances in digital signal processing.

2.5 OTHR principles of operation

In Section 2.3 the effect of the ionosphere on high frequency radio signals was discussed. The essential principles of OTHR operation are discussed in this section.

OTHR provides a capability for long range surveillance [43] by exploiting the ionosphere as a propagation medium for HF radio signals. HF radio waves are transmitted with some directivity and propagate through the ionosphere, where they are effectively reflected back to the earth. The transmitted radio waves illuminate a large area on the surface of the earth *over the horizon* from the transmitter. Some of the radio energy is backscattered from the target and return to the receiver array via the ionosphere.

The radio signals travel through a large propagation distance (thousands of kilometres) and a highly variable propagation medium. The received electromagnetic energy diminishes as the fourth power of distance from the transmitter, so a large amount of energy must be transmitted to obtain significant backscatter returns [43]. To prevent the transmitted energy from saturating the receiver, the OTHR must operate as a bi-static radar (with the transmitter and receiver not colocated) with the receiver usually being over the horizon from the transmitter. At the Jindalee OTHR facility near Alice springs in Australia, the transmitter and receiver are geographically separated by more than 100km and a mountain range [43].

OTHR provides a look-down view from the ionosphere, so backscatter returns from

the earth's surface, also known as *clutter returns*, are significant [24]. The sea contributes particularly strong clutter returns to the received signal, and meteorological parameters relating to the sea state can be obtained from the sea clutter via signal processing [18]. Consequently, the long range surveillance provided by OTHR contributes remote sensing of the sea state in addition to the detection and tracking of targets. Analysis of the Bragg lines of sea clutter returns enables maps of the wind speed, wind direction and sea state to be produced. Such maps provide valuable information to many bodies with an interest in meteorology. For instance, the information provides a capability for the tracking of tropical cyclones, and the information also enables ships to save fuel by avoiding rough seas [19].

The area illuminated on the earth's surface is of the order of tens of thousands of square kilometres, and the resolution of a delay-beam cell is of the order of hundreds of square kilometres, which is much larger than the size of an aircraft or even a ship. Hence the energy backscattered from the earth's surface is of far greater magnitude than the energy backscattered by a target. A target, typically an aircraft or a ship, has an effective radar cross section in the range 5 to 500 square metres [5]. Most of the radar energy returned is clutter from the sea or land; the clutter power typically dwarfs target returns by more than a million-fold [43, 24]. Consequently, Doppler is an important feature for discriminating between the returns from moving targets and the returns from the earth's surface. To use the Doppler effect as a discriminator between moving targets and clutter, the propagation path length must be stable during the coherent integration time (CIT).

2.6 Present challenges of OTHR

2.6.1 Introduction

There are many areas in OTHR signal processing where the interpretation of signals is often challenging. These areas include detection and tracking, multimode track association, coordinate registration and mode identification. Each of these areas is discussed in turn in this section.

The ionosphere is the medium which makes OTHR possible, but is also the source of many challenges in the interpretation of received OTHR signals. The geometry of OTHR propagation paths are dependent on the ionosphere, whose unpredictable nature is the main cause of the challenges in interpretation. The ionosphere is a highly complex medium, affected by changes in the earth's upper atmosphere and incident solar radiation [32, 39] and its state can only be predicted in gross features. The geometry of the propagation path thus varies over the radar coverage and with the ionosphere over the diurnal, seasonal and sunspot activity cycles. Other factors contribute to the challenges of interpreting OTHR signals; these include uncertainty in the propagation mode, impulsive noise (from noise sources such

as thunderstorms and meteors), and multimode propagation.

The detection of OTHR targets is not as reliable as in other radar applications due to the highly variable propagation environment. There are several aspects of the variable environment which deteriorate the signal-to-noise ratio (SNR). The deterioration of SNR can lead to missed detections and false detections. Difficulties in the detection and tracking of OTHR targets are discussed in Section 2.6.2.

Multiple detections received from a common target via different propagation modes are usually tracked as distinct tracks, resulting in ambiguous situations with multiple tracks per target. It is necessary to resolve these ambiguous situations by determining which tracks correspond to the same target [14, 15]. This process is termed *track association*. The track association task is a fundamental problem in OTHR and the results of this task can assist other OTHR signal processing tasks (see Section 2.6.6). The problem of multimode track association is discussed in Section 2.6.3.

An important part of OTHR signal processing is the determination of the physical location of the targets which correspond to observed tracks. Coordinate registration (see Section 2.2) is used to convert tracks from radar coordinates to ground coordinates. The key to coordinate registration is knowledge of the ionospheric propagation conditions along the entire propagation path [22]. However, the ionosphere and thus the propagation path can only be estimated in gross features. Hence coordinate registration is still considered a difficult problem. Furthermore even the propagation mode of tracks is not always known. The coordinate registration problem is discussed in Section 2.6.4.

Identification of propagation modes is a necessary step for the coordinate registration process to be successful. However, the propagation mode is often ambiguous. The problem of mode identification is discussed in Section 2.6.5.

Detection and tracking, multimode track association, coordinate registration and mode identification are closely linked problems in OTHR signal processing. The similarities of these problems and their solutions are discussed in Section 2.6.6.

2.6.2 *Detection and tracking*

The first stage of OTHR signal processing involves processing the received waveforms into delay-Doppler shift-beam cells [24]. The next stage of signal processing involves the detection of potential targets in the delay-Doppler shift-beam cells. The detection of targets is difficult for the following reasons:

Clutter

The clutter power is of the order of a million times greater than the signal power. Slowly moving targets are particularly difficult to detect because they often occupy the same Doppler cells as the clutter.

Noise

Noise sources can often severely deteriorate the background noise level in frequency modulated continuous waveform (FMCW) radar [48]. The two significant contributors to noise are impulsive noise and radio frequency interference (RFI). Impulsive noise is usually caused by environmental phenomena such as meteors and lightning strikes. Impulsive noise causes a higher than average background noise level in several delay-Doppler shift-beam cells [28], but is localised in one or more domains [24]. RFI consists of transmissions by other users of the HF spectrum. RFI is spread across many delay and beam cells but is localised in Doppler. The degree of localisation in Doppler depends on the bandwidth of the transmitted interference. Some successful methods have been proposed for suppressing noise [35, 36], but the suppression of target signals is an unavoidable consequence.

Smearing

The Doppler of moving targets is not always a reliable discriminator; fluctuations in the electron density of the ionosphere effectively change the height of the equivalent reflecting layer and thus also change the length of the propagation path. When the length of the propagation paths change during the coherent integration time, the Doppler of signal returns are effectively smeared across several Doppler bins. The Doppler smearing property of the ionosphere reduces the quality of the returned signal and therefore reduces the probability of a successful detection.

Polarisation

The polarisation of the radio wave can affect the detectability of a target. The transmitted wave is vertically polarised. The polarisation of the wave changes as it propagates through the ionosphere. For significant backscatter from the target, the polarisation of the wave must be suited to the orientation of the major reflector(s) in the target. Furthermore, polarisation of the returning wave changes as it propagates through the ionosphere from the target to the receiver. An array of vertical receivers only detects the vertical component of the returning wave's polarisation.

Tracking of OTHR detections is difficult due to the poor quality and reliability of the detections. Multiple detections received from a common target via different propagation modes are usually tracked as distinct tracks, resulting in multiple tracks per target [12, 13]. The idea of tracking several multimode detections as a single target was introduced in [37] and extended in [38]. Multimode tracking will theoretically provide improved tracking performance, and is discussed further in section 2.7.3.

The detection and tracking of ships is a particularly difficult problem. Sea going ships travel at a speed similar to the speed of the waves. Hence the Doppler shifts from sea waves

are similar to the Doppler shifts from sea going ships. Consequently, a long CIT is needed to obtain the Doppler resolution necessary to distinguish between ship detections and clutter. It is necessary for the ionosphere to be stable during the CIT if the signals received are to be interpretable. This is important over longer coherent integration times, such as those used to detect ships (approximately 30 seconds). The ionosphere is often not sufficiently stable over the coherent integration time because movements in the ionosphere cause Doppler variations as a function of delay, apparent azimuth and time. Over shorter coherent integration times, such as those used to detect aircraft (approximately 2 seconds), the effect of ionospheric fluctuations on Doppler returns is not as great.

2.6.3 *Multimode track association*

The ionosphere is a complex medium and it is not uncommon for more than one propagation path or *mode* to be active from the transmitter to the receiver via the target [33]. OTHR operation in the presence of multiple propagation modes is illustrated in Figure 1.1. Simultaneously active propagation modes contribute what is termed *multimode interference* to the received signals. Multimode interference is effectively a superposition of the returns from several distinct propagation modes.

Multimode interference causes difficulties for the interpretation of OTHR signals. Hence in OTHR operation it is preferable for signals to propagate from the transmitter to the target and back to the receiver via one propagation mode [32]. A simple way to avoid multimode propagation is to choose a radar frequency sufficiently high so that the signal can only propagate by the lowest order mode. However for optimal detection probability, it is important to maximise the SNR, regardless of multimoding [14]. Hence multimode propagation cannot always be avoided, and multiple detections of each target are observed. The multiple detections from the same target are usually tracked as distinct tracks, resulting in multiple tracks per target. *Track association* is the process of determining which tracks correspond to the same target [14]. In some parts of the literature, track association is also known as *dual designation resolution.*

Multipath interference occurs in many other areas, such as communications and sonar applications, where signals propagate via multiple paths. Multipath interference is usually modelled as the sum of amplitude scaled and time shifted copies of a known signal plus white noise. There are many established methods in the signal processing literature for determining the relative amplitudes and time shifts of multiple propagation paths [3]. These established methods are not applicable to the problem of resolving multipath interference in OTHR, where the signals propagating via different modes have different Doppler shifts [14].

There are two essential components of track association. The first involves the computation of *association metrics* (also known as similarity measures in some parts of the literature)

which are tools for estimating the probability that a pair of tracks is associated. The second component of track association is the combination and interpretation of these metrics in a meaningful way. The association metrics considered in this thesis all operate on a pair of tracks. Previous approaches for track association are discussed in Section 2.7.

2.6.4 Coordinate registration

OTHR data is of interest to many bodies including meteorological bureaus, customs authorities, drug enforcement agencies and the military. However, the processed data is not useful to these bodies. The radar coordinates in which measurements are made do not have a direct correspondence with the real world, and therefore it is necessary to transform the data to a global coordinate system.

Coordinate registration is the process of registering measurements in the radar space to the locations of the corresponding reflectors in the target space. The locations of measurements in radar space are given in terms of delay (also known as slant range) and apparent azimuth. However the locations of the corresponding reflectors in the target space are the actual range and azimuth with respect to the radar, which can be readily converted to geographical coordinates (when the geographical coordinates of the radar are known). Note that the apparent azimuth of the target is not the same as the actual azimuth of the target due to the coning effect.

A coordinate transformation is used to convert measurements in the radar space to the corresponding locations in the target space. It is important to estimate the transformation between the radar coordinates of measurements and the ground coordinates of the corresponding reflectors in the target space as accurately as possible. Knowledge of the propagation conditions, and hence the propagation mode, is necessary for the coordinate transformation.

Coordinate registration is a difficult problem due to uncertainty in the propagation conditions [22]. The ionosphere must be modelled as precisely as possible for accurate coordinate registration. Various techniques for observing the ionosphere are used to reduce the uncertainty in the coordinate registration model. In addition to the analysis of backscatter ionograms, the ionosphere is observed by networks of vertical incidence ionosondes, oblique incidence ionosondes, fixed frequency HF beacons and HF transponders [34]. Despite these techniques for observing the ionosphere, the ionospheric state can only be reliably estimated in gross features. The heights of the equivalent reflecting layers cannot always be accurately estimated throughout the entire radar coverage.

Measurements due to different propagation modes but from the same target should be registered to the same ground coordinates, via multimode registration. The existence of multiple echoes can actually enhance the reliability of the ground range estimation. However, to use the multiple echoes for ground range estimation, the track association process needs

to determine the correct associations.

2.6.5 Mode identification

The coordinate registration process transforms tracks from radar coordinates to ground coordinates. To perform the registration, a coordinate transform is estimated for each possible mode of propagation. The mode of propagation of a track must be known for the correct transform to be applied. This is where the challenge lies: a track's mode of propagation is not always known with certainty.

The set of active propagation modes can usually be established from other sources, such as ionospheric sounders. The situation is unambiguous when only one propagation mode is known to exist. However, when multiple propagation modes are known to exist, it is necessary to establish the propagation mode of a track so that the appropriate coordinate transform can be applied. Mode ambiguity can arise when there are fewer echoes observed than there are active modes, which can happen when one layer is only reflecting weakly. The mode identification problem is easier if the elevation angles are measured [34], but the cost of building a two dimensional array to measure the elevation angles is often prohibitive.

2.6.6 Closely linked problems

Many of the problems in OTHR are closely related [27]. Figure 2.1 is a block diagram showing the relationships between some of the OTHR processing tasks. The coordinate registration task relies upon the results from the mode identification task. The track association results can assist the mode identification task, and vice versa. The accuracy of the coordinate registration task can be validated by the track association results.

The key to successful coordinate registration is knowledge of the propagation conditions but particularly the propagation mode. Hence coordinate registration is reliant upon the resolution of mode ambiguities (see Section 2.6.4). Many mode ambiguities can be resolved as a by-product of the multiple hypotheses techniques employed in multimode track association [14, 45]. Thus successful mode identification can enhance the accuracy of coordinate registration. Furthermore, the accuracy of the coordinate registration task can be validated by the track association results. Thus track association and coordinate registration are closely related tasks. The track association process provides a valuable enhancement to the task of estimating the position of the target in global coordinates. For instance, if you know that two tracks should be associated, then they should be registered to the same location in ground coordinates.

The track association task and the detection and tracking task are closely linked. Knowledge of the difference between multimode measurements from the same target can help the detection process. For instance, if the correct associations and correct mode assignments of

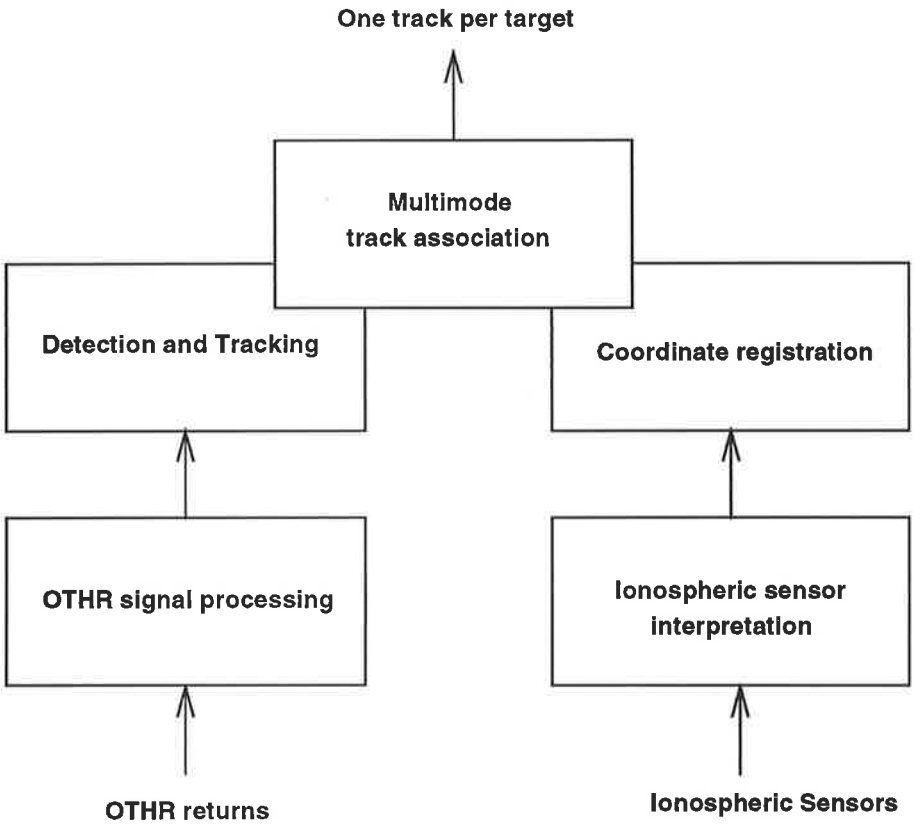

Figure 2.1: The related processes in the multimode track association problem.

a group of tracks are known, then the location of any undetected mode can be estimated, thus assisting the detection process. If a set of detections are known to be multimode detections from a common target, then the multimode detections can theoretically be tracked as a single target [37].

The usefulness of a successful technique for associating multimode tracks is not limited to this area; the results of multimode association can provide valuable information for the coordinate registration task and other OTHR signal processing tasks, because the problems are so closely related.

2.7 Previous Methods for Multimode Track Association

The literature is rich in some areas of data association, specifically in areas relating to target tracking: track initiation and track maintenance. However, the open literature[2] is sparse in the area of track association. Multimode track association for OTHR is a far more difficult problem, due to the inherent difficulties of ionospheric propagation, which has been largely overlooked in the open literature. The previously proposed methods and concepts are outlined in this section. Some work has been done in the area of multiradar track association for OTHR, but this is an entirely different challenge, so a review of this work is out of the scope of this thesis.

2.7.1 Dall-Kewley

One method for multimode track association is proposed in [14], evaluated in [15], and refined in [16]. We refer to this technique as Dall's method. The proposed method is reliant on an explicit model of ionospheric propagation to provide coordinate transformations from radar coordinates to ground coordinates and back into radar coordinates. A pair of tracks is compared by calculating a "correlation score". Tracks are deemed to be associated if they have a high correlation score. The correlation score proposed in [14] between two tracks is,

$$S = -\sum_{n=1}^{N} \boldsymbol{\delta}_n^T \boldsymbol{\Gamma} \boldsymbol{\delta}_n \tag{2.1}$$

where $\boldsymbol{\delta}_n$ is the difference in the radar measurements of the two tracks in consideration at sample n, and $\boldsymbol{\Gamma}$ is a matrix to normalise the weight given to each component of the difference. The matrix contains the statistical variances of each of the components of $\boldsymbol{\delta}_n$. There is no mention of covariances between components of $\boldsymbol{\delta}_n$.

A major shortfall with the method is that the $\boldsymbol{\Gamma}$ matrix does not vary over the radar coverage, whereas the dependence between measurements does. A further shortfall is that

[2]The literature which is publicly available.

$\boldsymbol{\Gamma}$ is a diagonal matrix, and thus the method does not take the dependence in the components of $\boldsymbol{\delta}$ into account.

Another problem is in the calculation of the correlation score; the score is formed by summing the contributions of the Mahalanobis distance $\boldsymbol{\delta}_n^T \boldsymbol{\Gamma} \boldsymbol{\delta}_n \forall n$. This summation is a valid way to combine Mahalanobis distances of independent normal random variables [21]. The correlation score would then have a χ^2 distribution with $n \times r$ degrees of freedom, where r is the length of vector $\boldsymbol{\delta}_n$. However, in this case the $\boldsymbol{\delta}_n$ are not independent for different values of n, because each δ_n represents the difference in measurements between the same pair of tracks. Therefore the threshold for the correlation score cannot be chosen in accordance with a χ^2 test. Furthermore, the proposed correlation score will vary, depending on both the location and length of the tracks. There is no mention in either paper of how the decision threshold for the correlation score is chosen.

Dall's method is reliant on an explicit ionospheric model (in the form of coordinate registration tables), and thus any errors in the propagation model will result in errors in the coordinate transformations, and thus errors in the correlation score. Without taking the dependence in measurements into account, the errors in the correlation score will be larger than necessary. A generalisation of the algorithm has been proposed which allows for the possibility of refining the ionospheric model [50].

The performance of Dall's method was reported in [15]. The associations made by human operators were compared with the associations made by the data fusion algorithm. The data used for the comparison was collected at the Jindalee Facility at Alice Springs, over 240 hours (ten days). The performance of the data fusion algorithm was found to be comparable to the performance of the human operators.

2.7.2 Feature based methods

Methods for track association based on track features alone have been proposed in [9, 10, 52]. These methods are inspired by the ability of a human operator to associate tracks on a radar display. The association decision is based on the comparison of heuristically chosen track features. The features are selected on their ability to discriminate between associated and non-associated tracks. Typical track features are mean position, track shape (curvature), angular velocity and speed.

The performance of the above-mentioned feature based methods was reported in [7, 51]. The association decision is based on the combination of features. Two approaches for combining the features were proposed in [6, 8]: a linear, statistically determined combination, and a non-linear combination found by training a multi-layer perceptron. Both approaches were evaluated in [7, 51]. A data set was simulated for evaluating several permutations of the proposed methods. All permutations of the proposed methods performed extremely

well on this data set: the error rate of the association decisions was around 0.1% for every permutation.

2.7.3 Pulford-Evans

The idea of tracking a multimode pattern as a single target was introduced in [37] and discussed in detail in [38]. Multimode tracking is conceptually appealing, because it will theoretically improve tracking performance. However, a comparison of the relative advantages of track-level fusion and measurement level fusion suggests that "although measurement level fusion is technically superior, in many scenarios track fusion is more appropriate" [49]. Multimode tracking is difficult due to variations in the relative positioning of associated tracks (see section 1.5). The tracking process can be enhanced by improving the *a priori* knowledge of the intermodal field. Hence we anticipate that this work could benefit from contributions in this thesis, such as modelling the intermodal vector field chapter 5. Details of the performance of this approach are not publicly available.

2.7.4 Other work

The association of tracks between multiple OTHRs is receiving attention [50, 27, 4]. The technique proposed in [27] has similarities with Dall's approach [14]. The track data is transformed from the radar space to the target space. The linkage between the problems of mode propagation and multiradar track association is recognised in [27], but the problem of multimode track association is overlooked. The association of tracks between multiple OTHRs does not fall within the scope of this thesis; instead, we focus on the challenge of associating multimode tracks due to a single OTHR.

2.7.5 Limitations of previous work

There is an inherent distortion between multimode measurements over the radar coverage due to variations in the propagation geometry. A significant limitation of previous track association work is that the association metrics do not take this inherent distortion into account. This oversight causes the previously proposed association decisions to vary in quality over the radar coverage.

Multimode data is potentially a very useful source of information for addressing the challenges faced in OTHR, and yet it has not been exploited by previous work to address these challenges.

2.8 Summary

The ionosphere is the medium by which long range surveillance can be achieved. However, there are many challenges in the interpretation of OTHR returns due to the complex nature of the ionosphere as a medium for propagation. Many of the processing tasks in OTHR are interrelated, and the success of one affects the success of the others. Multimode track association is a key operation, which is related to several OTHR signal processing tasks.

Multimode data can be used to assist the track association task, and also to assist other related OTHR processing tasks. However, previous methods for multimode track association have significant limitations in that they do not exploit the multimode patterns to their full potential.

CHAPTER III

Systematic Approach To Track Association

3.1 Introduction

In Section 2.6 some challenges in OTHR were outlined. In this chapter, the problem of multimode track association is discussed in more detail, and a systematic approach to this problem is presented. This system is outlined in this chapter, and certain aspects thereof are discussed in detail in subsequent chapters.

The methodology for the approach taken is described in Section 3.2. An overview of the system for track association is presented in Section 3.3. Several features of the system are introduced in this chapter, including the association metric, the model of multimode patterns and the association decision. Finally, we summarise the important aspects of this chapter in section 3.5.

3.2 Methodology of proposed system

The methodology for the systematic approach to track association is discussed in this section. The system contains several distinct components which act together to exploit the information contained in the multimode patterns for track association.

3.2.1 Motivation

Differences in the radar measurements of multimode detections from a common target appear in patterns which have been noticed previously, but have not been used for automated track association. Knowledge of the multimode patterns is potentially of great assistance for the association decision.

A system proposed in this chapter exploits prior knowledge of the characteristic patterns of multimode propagation. The motivation for using the multimode patterns is firstly to provide a systematic approach for track association based chiefly upon the valuable, but as yet

unexploited, multimode patterns; and secondly to enable mutual verification of the association decisions. The verification of the association decisions enables conflicting decisions to be identified, and provides a framework for resolving the conflicting decisions.

3.2.2 Exploiting the multimode patterns

Multimode patterns are a previously unexploited source of information in OTHR. The multimode patterns are characteristic of the propagation paths, which are dependent on the ionospheric propagation conditions and the location of the target with respect to the transmitter and receiver. Estimating the multimode patterns from their cause is difficult because the ionospheric propagation conditions and the location of the target can only be crudely estimated. However note that accurate estimates of the radar measurements (delay, apparent azimuth and Doppler shift) of tracks are available from the tracking process. The proposed system for track association models the multimode patterns in terms of their radar measurements, thus exploiting the multimode patterns. The approach of modelling the multimode patterns in terms of the radar measurements is a key aspect of the systematic approach to track association presented in this thesis.

Let the radar measurement space be denoted by $\mathcal{M}$. The vector field given in $\mathcal{M}$ of the difference between radar measurements of multimode tracks is referred to as the *disparity field* (first introduced in section 1.4 of this thesis). Simultaneously observed multimode patterns are *samples* of the disparity field for a particular moding. Hence the disparity field is modelled from the observed multimode patterns and the resulting model reflects the current ionospheric state.

The approach of modelling the multimode patterns in $\mathcal{M}$ from observed multimode patterns avoids reliance on an explicit ionospheric model. The cause of the multimode propagation, the ionosphere, is not modelled; instead the effects of multimode propagation are modelled. Hence the model of the disparity field constitutes a *partial ionospheric model.* The model of the disparity field can not only assist the task of track association, but also other OTHR signal processing tasks. Such tasks include coordinate registration and the tracking of multimode detections.

3.2.3 Verification of association decisions

The systematic approach is inspired by the exploitation of simultaneously observed multimode patterns to assist association decisions, and enhance the confidence with which they are made. In contrast to previous track association methods (see section 2.7), in which each association decision is based solely on the measurements of the pair of tracks in consideration, the systematic approach incorporates information from other (potentially multimode) pairs of tracks. The systematic approach's association decisions will thus be consistent with

each other, and also more reliable overall.

Example: We give an example of conflicting decisions. There are three tracks, labelled A, B and C. Consider a scenario in which the following association decisions have been made:

1. tracks A and B are associated with a common target;

2. tracks B and C are associated with a common target;

3. tracks A and C are not associated with a common target.

The association decisions are clearly conflicting, because *if* A and B are from a common target, and *if* B and C are from a common target, then A and C *must* also be from a common target. In this case, at least one of the decisions is incorrect. We hypothesise that some conflicts can be resolved by verifying association decisions against each other.

3.3 System Overview

The proposed system for associating multimode OTHR tracks is shown as a block diagram in Figure 3.1. The measurements of observed track i are denoted $\mathbf{y}_i$. The measurements of observed track j are denoted $\mathbf{y}_j$. The estimated value of the disparity vector and its covariance are denoted by $\hat{\mathbf{d}}_{mn}$ and $\boldsymbol{\Sigma}_{mn}$. There are several aspects of the systematic approach shown in the figure. Details of each of the main blocks are outlined in this section, but discussed in detail in subsequent chapters.

3.3.1 Mode hypotheses

The model introduced in chapter 5 provides an estimate of the difference in multimode measurements between propagation modes at a specified location in radar coordinates. The mode of propagation of each track is not known, but can be deduced by the relative positioning with respect to other tracks, so classical hypothesis testing is performed to determine the correct associations. Each possible mode of propagation is hypothesised for each observed track and the association metric is computed under these hypotheses. Note that mode classification is a by-product of the multiple hypothesis approach.

The set of track measurements is denoted as $\{\mathbf{y}_i | i = 1, \ldots, N\}$, where i refers to the track. The subset of tracks due to propagation mode m is denoted $\mathcal{S}_m$. The hypothesis that track i is due to mode m is denoted $[H : \{i\} \in \mathcal{S}_m]$.

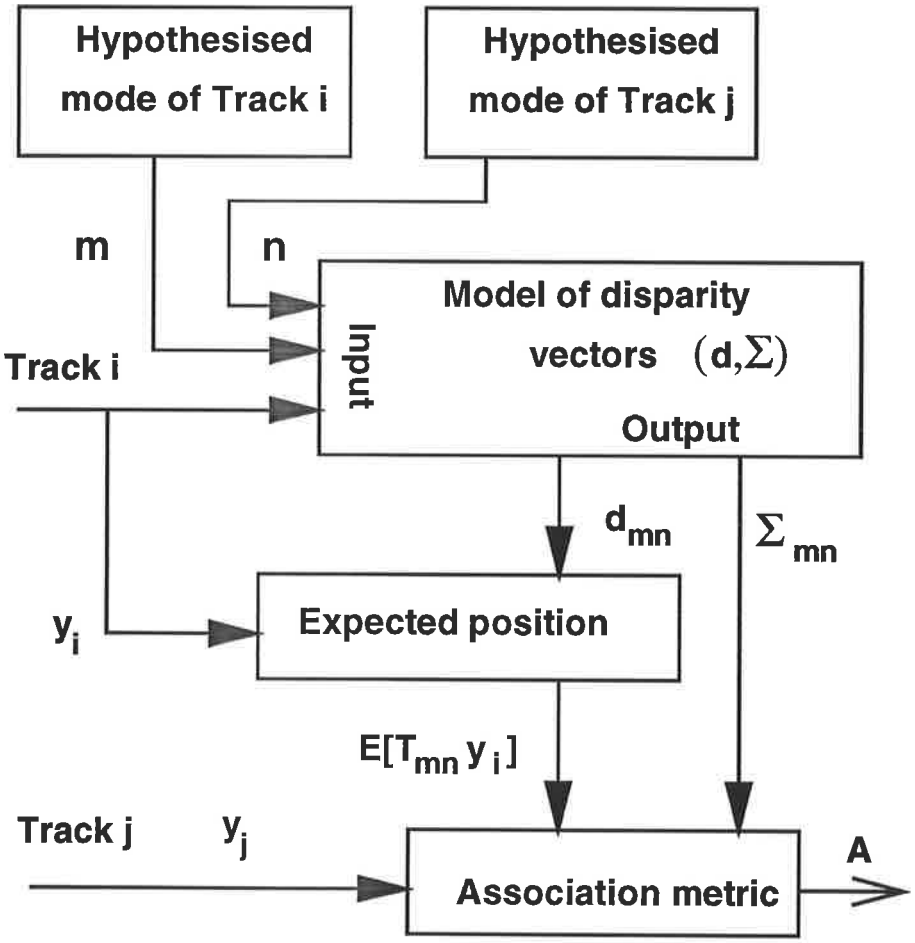

Figure 3.1: Overview of proposed system for track association.

3.3.2 Intermodal coordinate transformation

The expected measurements of a track are calculated with respect to an observed track under the specific mode hypotheses outlined in section 3.3.1. We represent the difference in radar measurements from alternate modes as a coordinate transformation. The transform T_{mn} is a coordinate transformation of radar measurements due to mode m to radar measurements, from a common source, due to mode n. We make the hypothesis that an observed track i is due to mode m. The measurements of a track corresponding to the same target as track i, but due to propagation mode n, are represented by the transformation of the measurements $\mathbf{y}_i$ under transform T_{mn}, expressed

$$T_{mn}\mathbf{y}_i.$$

The radar measurement space has a variable relationship with the geographical space, due to variations in the propagation geometry. The intermodal transform depends on two things; firstly, it depends on the the ionospheric conditions, which are abstractly represented by $\mathcal{F}_I$ and secondly it depends on the location of the vector in the radar measurement space $\mathbf{y}_i$. We express the intermodal coordinate transform in terms of the *disparity function* $\mathbf{d}_{mn}(\mathbf{y}_i, \mathcal{F}_I)$; thus

$$T_{mn}\mathbf{y}_i = \mathbf{y}_i + \mathbf{d}_{mn}(\mathbf{y}_i, \mathcal{F}_I). \tag{3.1}$$

The disparity function $\mathbf{d}_{mn}(\mathbf{y}_i, \mathcal{F}_I)$ is a vector function defined in the radar measurement space $\mathcal{M}$ and represents the the difference in measurements between tracks from a common target due to modes m and n.

3.3.3 The disparity function

The disparity function is a vector function in $\mathcal{M}$; there is an disparity function in $\mathcal{M}$ for every pair of propagation modes. The components of the disparity functions corresponding to delay, apparent azimuth and Doppler shift are discussed here, but other radar measurements, such as range rate and azimuth rate can be treated in an analogous way.

There is a component of the disparity function which corresponds to the difference in delay between two modes from a common target, denoted by ΔR. This component is due to the differences in length of the propagation paths. Another component of the disparity function corresponds to the difference in apparent azimuth between two modes from a common target, and this component is denoted by ΔA. The return radar signals propagate via different ionospheric layers, and therefore arrive at the receiver from different elevation angles. The difference in elevation angle of the different paths causes a difference in the apparent azimuthal angle of multipath returns from the same target.

The Doppler refers to the Doppler shift in frequency in returns from a moving target. The shift is proportional to the component of velocity in the direction of the radar beam, which

is related to but not the same as the ground velocity. The Doppler is proportional to the radial component of the target's velocity multiplied by the cosines of the elevation angles of the incoming beam to the target θ_i and the outgoing beam from the target θ_o. The incoming angle and outgoing angle are determined by the mode of propagation. Hence the measured Doppler depends on the mode of propagation as well as the radial component of the target's velocity. The measured Doppler is related to the radial component of the target's velocity v_T and the cosine of the angle of the incident signal and the cosine of the angle of the out-bound signal.

$$D_R = v_T \cos\theta_i \cos\theta_o$$

Multimode tracks originating from the same target will have differences in their values of Doppler. Another component of the disparity function is the difference in Doppler of the multimode returns from a common target. This component is denoted by ΔD.

3.3.4 Model of disparity function

An estimate of the intermodal coordinate transform T_{mn} of equation (3.1) is needed to compute the association metric in Section 3.3.5. Yet T_{mn} is dependent on the ionospheric propagation conditions and should be estimated from ionospheric models. Ionospheric modelling is a large field in its own right, and is out of the scope of this thesis. Suffice it to say that ionospheric models are not sufficiently reliable for the purpose of accurately estimating the transform T_{mn}. We consider the ionospheric state $\mathcal{F}_I$ as a random variable. The expectation of the transform T_{mn} can be reduced, via equation (3.1), to the expectation of $\mathbf{d}_{mn}(\mathbf{y}_i, \mathcal{F}_I)$; thus

$$\begin{aligned} E\left[T_{mn}\mathbf{y}_i | \mathbf{y}_i, [H : \{i\} \in \mathcal{S}_m]\right] &= E\left[\mathbf{y}_i + \mathbf{d}_{mn}(\mathbf{y}_i, \mathcal{F}_I) | \mathbf{y}_i, [H : \{i\} \in \mathcal{S}_m]\right] \\ &= \mathbf{y}_i + E\left[\mathbf{d}_{mn}(\mathbf{y}_i, \mathcal{F}_I) | \mathbf{y}_i, [H : \{i\} \in \mathcal{S}_m]\right]. \end{aligned} \quad (3.2)$$

The distribution of the disparity function $\mathbf{d}_{mn}(\mathbf{y}_i, \mathcal{F}_I)$ for a particular $\mathbf{y}_i$ is dependent on the ionospheric conditions, and hence the distribution can only be grossly estimated. For simplicity it is assumed that the disparity vector has Gaussian distribution,

$$\mathbf{d}_{mn}(\mathbf{y}_i, \mathcal{F}_I) \sim N\left[\hat{\mathbf{d}}_{mn}(\mathbf{y}_i), \mathbf{\Sigma}_{mn}(\mathbf{y}_i)\right]. \quad (3.3)$$

We denote the expectation of the disparity vector in equation (3.2) in terms of $\hat{\mathbf{d}}_{mn}(\mathbf{y}_i)$. Hence Equation (3.2) becomes

$$E\left[T_{mn}\mathbf{y}_i | \mathbf{y}_i, [H : \{i\} \in \mathcal{S}_m]\right] = \mathbf{y}_i + \hat{\mathbf{d}}_{mn}(\mathbf{y}_i). \quad (3.4)$$

We use the model of disparity functions, which is one of the components in Figure 3.1, to estimate the disparity function $\mathbf{d}_{mn}$ and its covariance $\mathbf{\Sigma}_{mn}$. The inputs to the model are

the track measurements $\mathbf{y}_i$ and hypothesised modes m and n and the outputs from the model are the estimated disparity vector $\hat{\mathbf{d}}_{mn}(\mathbf{y}_i)$ and an estimate of its covariance $\hat{\boldsymbol{\Sigma}}_{mn}(\mathbf{y}_i)$/

The ionosphere is a highly complex medium, and hence it is very difficult to model (see Section 2.3). Instead of modelling the ionosphere explicitly, only the effects of multimode propagation are modelled. The model of the multimode effects is essentially a *partial ionospheric model.* We model the field given by $\mathbf{d}_{mn}(\mathbf{y}_i, \mathcal{F}_I)$ by exploiting prior knowledge of the form of likely disparity fields. The accuracy of the modelled disparity field is improved by adding current observations of the multimode patterns to the prior knowledge. The observed multimode patterns reflect the current ionospheric state $\mathcal{F}_I$. The forms (i.e. shapes) of likely disparity fields are estimated from prior knowledge, and the most likely disparity field to fit the data is used. The disparity field is calibrated to fit the observed multimode patterns so that it is representative of the current ionospheric conditions. Note that the selection of the most likely disparity field may change as more multimode patterns are available.

The model of the disparity field is a major component of the system for track association, and is discussed further in chapter 5. Two alternative techniques for modelling the disparity field are proposed. Limitations of these techniques are identified, and another technique for modelling the disparity field is introduced which combines the advantages of both models.

3.3.5 Association metric

The proposed association metric is a key component of the track association system; it is used to discriminate between pairs of associated tracks and pairs of non-associated tracks. The proposed association metric is the Mahalanobis distance between the radar measurements of an observed track, and the expected transformed measurements of another track. The transformed measurements are calculated relative to another observed track, hypothesised to belong to the same target but due to another propagation mode. The association metric is described in detail and compared to other previously proposed *similarity measures* (measuring the similarity of a pair of tracks) in chapter 4.

We use the association metric to test a hypothesis consisting of three statements for the pair of tracks labelled i and j:

1. that tracks i and j are associated,
2. that track i belongs to mode m, and
3. that track j belongs to mode n.

We denote this hypothesis by

$$[H : \{i, j\} \in \mathcal{A}_{mn}], \tag{3.5}$$

where $\mathcal{A}_{mn}$ is a set, containing ordered pairs of tracks which are associated, and correspond to the modes m and n, respectively.

3.4 Association probability

We use the association metric, denoted by $M_{mn}(\mathbf{y}_i, \mathbf{y}_j)$, to estimate the *association probability* for a pair of tracks. We define the association probability as the probability that a pair of tracks are due to a common target. The association metric operates on a vector referred to as the error vector, denoted $\boldsymbol{\delta}_{mn}$; we mention this vector now, but it is properly introduced later (see equation (4.1)). Note that the association metric only provides *an estimate* of the probability that a pair of tracks are associated. We do not obtain a measure of the actual probability, since the distribution of $\boldsymbol{\delta}_{mn}$, and hence the association metric, are not accurately known.

To estimate the probability, it is necessary to make assumptions regarding the distribution of $\boldsymbol{\delta}_{mn}$ for associated pairs of tracks and non-associated pairs of tracks. We assume the difference vector $\boldsymbol{\delta}_{mn}$ is normally distributed about the estimated disparity vector $\hat{\mathbf{d}}_{mn}$, with covariance matrix $\boldsymbol{\Sigma}_{mn}$. From these assumptions, the distribution of the association metric for associated and non-associated pairs of tracks is implied. Despite the inherent warping of the radar measurement space (see section 2.6.4), the distribution of the association metric is assumed to be invariant over the radar measurement space, because this warping is accommodated by a model of the disparity vectors (see chapter 5). The distribution of the Mahalanobis distance is then $\chi^2(r)$, where r denotes the number of degrees of freedom; r is also the dimension of $\boldsymbol{\delta}_{mn}$. The estimated association probability can then be found from χ^2 tables [26].

We use our estimate of the association probability to test the hypothesis $[H : \{i,j\} \in \mathcal{A}_{mn}]$. We calculate the confidence interval that the association metric corresponds to a pair of associated tracks; the confidence interval is defined by

$$\Pr(M_{mn}(\mathbf{y}_i, \mathbf{y}_j) \leq \alpha) = \gamma, \tag{3.6}$$

where γ is the degree of confidence of the interval. γ is usually chosen to be close to unity (99% or 99.9%). The association metric is the Mahalanobis distance and therefore has a χ^2 distribution. Hence the bound of the confidence interval α can be found from chi-square tables (as in [26]) for the chosen value of γ.

The combination of successful hypotheses is complex, since the successful hypotheses can be mutually conflicting (see the example in section 3.2.3, page 28). The combination of hypotheses is dealt with in the following subsection.

3.4.1 Association decision

A pair of observed tracks which are potentially multimode tracks from a common target is referred to as a *multimode candidate*. Multimode candidates which actually correspond to a common target provide samples of the actual disparity field and thence must be compatible

with the disparity field. We divide this requirement into two criteria, which are both necessary conditions for multimode candidates to be deemed associated. The first criterion determines which association candidates are possibly associated. The second criterion is applied to successful association candidates from the first criterion. The second criterion determines which subset of the association candidates are associated.

First Criterion

The first criterion is a simple test performed locally on each multimode candidate to eliminate candidate pairs which are incompatible with every possible disparity field of a certain mode combination. One way of expressing this test as a question in English is, **"Is this pair of tracks possibly associated?"**.

The assumption is made that the range of all possible ionospheric states $\mathcal{I}$ can be known a priori. This is not an unreasonable assumption, as solar activity is cyclic and the range of all ionospheric states have been observed for a longer period of time than the longest cycle, the 11-year solar cycle. The disparity field given in $\mathcal{M}$ depends directly on the ionospheric state $\mathcal{F}_I$, and thus the range of all possible disparity fields can be known a priori. The range of possible disparity fields may be analytically derived from the range of possible ionospheric states $\mathcal{I}$.

In other words, the difference in measurements (between a certain mode pair) must lie within a bound corresponding to possible ionospheric states. This bound, denoted $\mathcal{R}_{mn}$ for mode pair mn is variable over the radar coverage and is a function of the radar measurement $\mathbf{y}_i$; thus

$$\mathcal{R}_{mn}(\mathbf{y}_i) = \{\mathbf{d}_{mn}(\mathbf{y}_i, \mathcal{F}_I) \forall \mathcal{F}_I \in \mathcal{I}\}.$$

The first criterion for track pair $\{i, j\}$ where track i is hypothesised to belong to mode m, i.e. $[H : \{i\} \in \mathcal{S}_m]$, and track j is hypothesised to belong to mode n, i.e. $j \in \mathcal{S}_n$ is formulated as

$$\mathbf{y}_i - \mathbf{y}_j \in \mathcal{R}_{mn}(\mathbf{y}_i).$$

The projection of $\mathcal{R}_{mn}$ onto any one dimension of the radar measurement space would not be a good discriminator, and thus the first criterion would not be very successful. However, there is a high degree of correlation between the components of the difference in measurements, so the bound is a good discriminator in the radar measurement space. Independent targets are unlikely to maintain the appearance of multimode tracks for long, even if this is their objective.

Second Criterion

The second criterion verifies the global compatibility of the multimode candidates which have satisfied the first criterion. The multimode candidates which actually correspond to a

common target must all be compatible with the same (plausible) disparity field.

We make the hypotheses that every successful candidate from the local criterion is an associated pair. We denote the corresponding set of hypotheses by the unordered set $\mathcal{H}$; thus

$$\mathcal{H} = \langle [H : \{i,j\} \in \mathcal{A}_{mn}], [H : \{k,l\} \in \mathcal{A}_{mn}], \ldots \rangle, \tag{3.7}$$

where $\{i,j\}$ and $\{k,l\}$ denote the track pairs of association candidates. As explained in section 3.3.5, each hypothesis is tested using the association metric M_{mn}. The association metric requires an estimate of $\mathbf{d}_{mn}$, obtained via the model of disparity vectors (see section 3.3.4). The model is calibrated to observed disparity vectors, which are not known. However, we do have observed *inter-track vectors*, denoted by

$$\mathbf{z}_{ij} = \mathbf{y}_i - \mathbf{y}_j$$

for track pair $\{i,j\}$. The hypothesis $[H : \{i,j\} \in \mathcal{A}_{mn}]$, if true, implies that the corresponding inter-track vector $\mathbf{z}_{ij}$ is a disparity vector. Hence, under the hypotheses of $\mathcal{H}$, the corresponding inter-track vectors are samples of the disparity field. Thus, we calibrate the model of disparity vectors using the inter-track vectors $\mathbf{z}_{ij}$ corresponding to every hypothesis of $\mathcal{H}$.

The second criterion is satisfied if, for every multimode candidate $\{i,j\}$ the association metric M_{mn} lies inside the confidence interval; thus

$$M_{mn}(\mathbf{y}_i, \mathbf{y}_j) \leq \alpha, \ \forall \, [H : \{i,j\} \in \mathcal{A}_{mn}] \in \mathcal{H} \tag{3.8}$$

However, it is important for the reader to note that if we calibrate the model based on all the hypotheses of $\mathcal{H}$, we run the risk of false hypotheses biasing our estimate $\hat{\mathbf{d}}_{mn}$ away from the actual value $\mathbf{d}_{mn}$. If the second criterion is not satisfied for the desired confidence interval γ, we apply the criterion to all subsets of $\mathcal{H}$; satisfied for a subset of the hypotheses $\mathcal{H}$; thus

$$M_{mn}(\mathbf{y}_i, \mathbf{y}_j) \leq \alpha, \ \forall [H : \{i,j\} \in \mathcal{A}_{mn}] \in \mathcal{G}$$

where $\mathcal{G}$ denotes a subset of $\mathcal{H}$. For each subset, the model is recalibrated to the inter-track vectors corresponding to the hypotheses in the subset. We choose the subset $\mathcal{G}$ for which α corresponds to the greatest confidence level γ of equation (3.6). We decide that this subset (perhaps the full set $\mathcal{H}$ and perhaps the empty subset) contains all the hypotheses for associated tracks, and only the hypotheses for associated tracks.

3.5 Chapter summary

This chapter proposes a systematic approach for solving the challenge of multimode track association in OTHR. The system exploits the characteristic patterns of multimode propagation. The methodology of the systematic approach, including motivation for exploiting the multimode patterns, is discussed in section 3.2.

We present an overview of the proposed system in section 3.3, and discuss each of the major subcomponents in turn. The difference between radar measurements from a common target, but due to different propagation modes, are expressed as a disparity function; the disparity function is a function of location in the radar measurement space. A major component of the system is a model of the disparity function, discussed briefly in section 3.3.4; the model is discussed at length in chapter 5. Another major component of the system is an association metric for discriminating between pairs of associated tracks and pairs of non-associated tracks. The association metric is mentioned in section 3.3.5, but discussed in detail in chapter 4. The final component of the system is the association decision, discussed in section 3.4.1. We separate the association decision into two criteria, applied consecutively. The first criterion selects candidates which are possibly associated. The second criterion determines which set of candidates are associated, while ensuring that conflicting association decisions are avoided.

CHAPTER IV

Association metric

4.1 Introduction

A key component of the track association system of chapter 3 is the association metric, introduced in section 3.3.5. The purpose of the association metric is to discriminate between pairs of tracks from a common target and pairs of tracks from different targets. The association metric is essentially a tool for estimating the probability that a pair of tracks are due to a common target, and it forms the basis for the association decision. This chapter is organised as follows. The proposed association metric is discussed in detail in section 4.2. It is compared to alternative association metrics, similar to those previously proposed [9, 10, 52], in section 4.3. The combination of several values of an association metric over several dwells is discussed in section 4.4. Finally, we summarise the important aspects of this chapter in section 4.5.

4.2 Association metric

The association metric operates on the difference between the measurements of an observed track and the expected transformed measurements of another track. An illustration of the spatial relationship between an observed track position, in the radar measurement space, and the expected track position is shown in figure 4.1. In this figure, the observed track i, shown as a solid line, is hypothesised to correspond to mode m and the expected measurements (in the radar measurement space) of the transformed track corresponding to mode n is shown as a dotted line. The observed track j, shown as another solid line, is hypothesised to belong to mode n. The estimated disparity vector $\hat{\mathbf{d}}_{mn}$ is shown at both of ends of track i; note that $\hat{\mathbf{d}}_{mn}$ has changed over the radar coverage. The measurements of track i are denoted $\mathbf{y}_i$, and the expected transformed measurements due to mode n are expressed $E[T_{mn}\mathbf{y}_i]$. The measurements of observed track j, which is hypothesised to be due to propagation mode n are denoted by $\mathbf{y}_j$. The difference between the estimated measurements of mode n and the observed measurements of track j is also shown in figure 4.1. This difference is referred to

as the *error vector*; it is denoted by δ_{mn}, and formulated thus

$$\delta_{mn}(\mathbf{y}_i, \mathbf{y}_j) = E\left[T_{mn}\mathbf{y}_i | \mathbf{y}_i, i \in \mathcal{S}_m\right] - \mathbf{y}_j.$$

Through application of equation (3.4) the error vector is expressed as

$$\delta_{mn}(\mathbf{y}_i, \mathbf{y}_j) = \mathbf{y}_i + \hat{\mathbf{d}}_{mn}(\mathbf{y}_i) - \mathbf{y}_j. \tag{4.1}$$

For the association decision, we require an estimate of the the probability that a pair of tracks are associated. The N-dimensional Mahalanobis distance is the distance from the centre of a N-dimensional, multivariate, normally distributed population, normalised with respect to the covariance of the population. We choose the Mahalanobis distance [21] (hereafter referred to as *M-distance*) as a tool to estimate this probability, since there is a high degree of correlation between the components of the disparity vector. The correlation between the delay and apparent azimuth components is clearly evident in figure 1.4. The association metric is the Mahalanobis distance of $\delta_{mn}(\mathbf{y}_i, \mathbf{y}_j)$, formulated thus:

$$M_{mn}(\mathbf{y}_i, \mathbf{y}_j) = \delta_{mn}(\mathbf{y}_i, \mathbf{y}_j)^T \boldsymbol{\Sigma}_{mn}^{-1}(\mathbf{y}_i)\delta_{mn}(\mathbf{y}_i, \mathbf{y}_j), \tag{4.2}$$

where $\boldsymbol{\Sigma}_{mn}$ denotes the covariance matrix of δ_{mn}. The covariance matrix varies over the radar coverage and hence is a matrix function of the radar measurements $\mathbf{y}_i$. We estimate the disparity function, $\mathbf{d}_{mn}(\mathbf{y}_i)$ and its covariance $\boldsymbol{\Sigma}_{mn}(\mathbf{y}_i)$.

The primary benefit of using the M-distance as the association metric is the fact that it accounts for the covariance between radar measurements. We do not ignore the possibility that there may be a choice of association metric which provides better discrimination between associated and non-associated pairs of tracks. We expect an association metric with greater discriminatory performance to improve the performance of the track association system. However, to maintain the focus of this thesis, we omit a rigorous investigation into the merits of different metrics. We perform a limited comparison of the proposed association metric to other association metrics in section 4.3.

4.3 Comparative study

A demonstration of the proposed association metric is presented in this section. The demonstration compares the proposed metric to alternative metrics using the track measurements of a pair of tracks. For simplicity, we only consider two components of the track measurements, the components corresponding to delay and apparent azimuth. The alternative metrics are similar to those which have been previously proposed in [9, 10, 52].

For the purpose the demonstration, we designed an OTHR simulator, and used it to generate the demonstration's data set. The simulated ionospheric layers are spherical and the heights of these layers drift by a small amount between each radar dwell. Details of the

propagation geometry used for the simulation appear in appendix A. Two ionospheric layers are considered and the initial heights of these layers, and the distribution of their rates of drift are chosen according to known ionospheric priors (see appendix A.5).

The data set consists of two types of scenarios. Each scenario consists of two targets, travelling with constant speed and constant heading. Only two of the multimode tracks are considered from each target. The first type of track association scenario comprises two targets travelling in significantly different directions and travelling with significantly different speeds. It should be easy for any method, including a human operator, to determine the correct track association. This type of scenario is referred to as the *easy association scenario*. An easy scenario is shown in figure 4.2. Both targets have two corresponding multimode tracks: tracks #1 and #2 correspond to the one target and tracks #3 and #4 correspond to another target. The second type of track association scenario is chosen to be difficult for track association. The targets have similar locations, speeds and headings. This scenario is referred to as the *difficult association scenario*. The difficult association scenarios comprise two targets travelling on parallel flight paths with a separation of approximately 50km. A difficult scenario is shown in figure 4.3, two multimode tracks per target. As in the easy scenario, tracks #1 and #2 correspond to the one target, whereas tracks #3 and #4 correspond to another target.

The simulated data set for the comparison comprises 500 easy association scenarios (such as Figure 4.2) and 500 difficult association scenarios (such as Figure 4.3). The heights of the ionospheric layers are the same throughout every scenario. The height of the E layer is 110km, while the height of the F layer is 250km; we refer the interested reader to appendix A.5 for justification of these values. Each scenario contains data for 4 tracks from 100 dwells and is divided into 10 windows of 10 dwells each, making 5,000 windows of track history for each type scenario. There are 4 tracks in every scenario and therefore 6 pairs of tracks in every scenario which are candidates for track association. Therefore there are 30,000 cases for track association for both types of association scenario. The alternative metrics and the proposed metric are applied to every case.

4.3.1 Alternative Association Metrics

We heuristically choose alternative association metrics for their potential ability to discriminate between pairs of associated tracks and pairs of non-associated tracks. The alternative metrics are based on features which are derived from the difference in track measurements over time, which we refer to as track velocity. Note that the track velocity of a target is not the same as the actual velocity of the target due to the geometry of OTHR propagation paths. Track velocity is computed in the *radar space* in Cartesian coordinates, as in [52], and is measured as the change in target position between radar dwells.

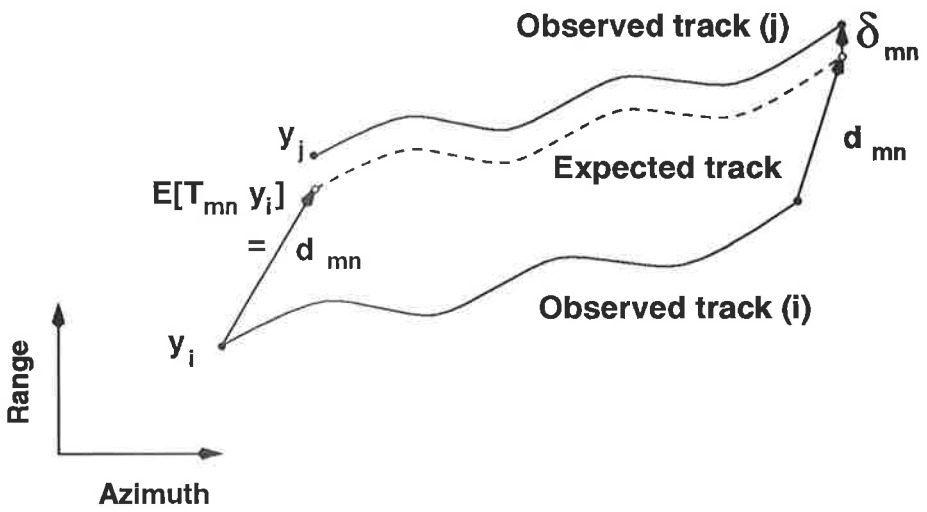

Figure 4.1: Expected measurements of transformed track.

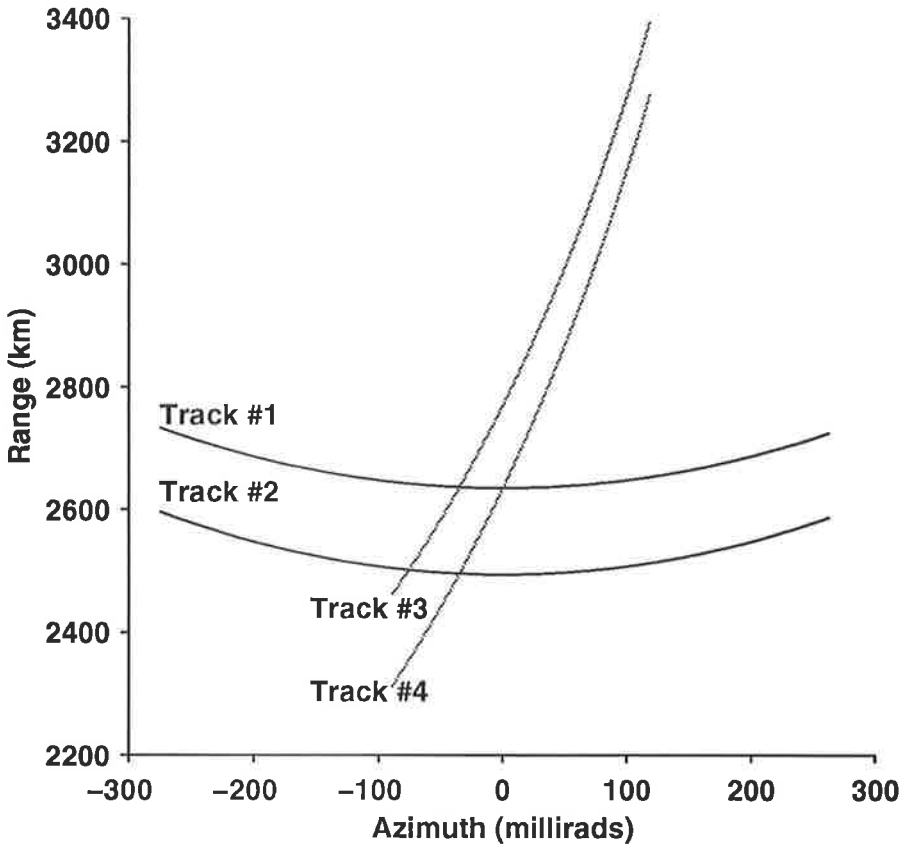

Figure 4.2: Easy association scenario.

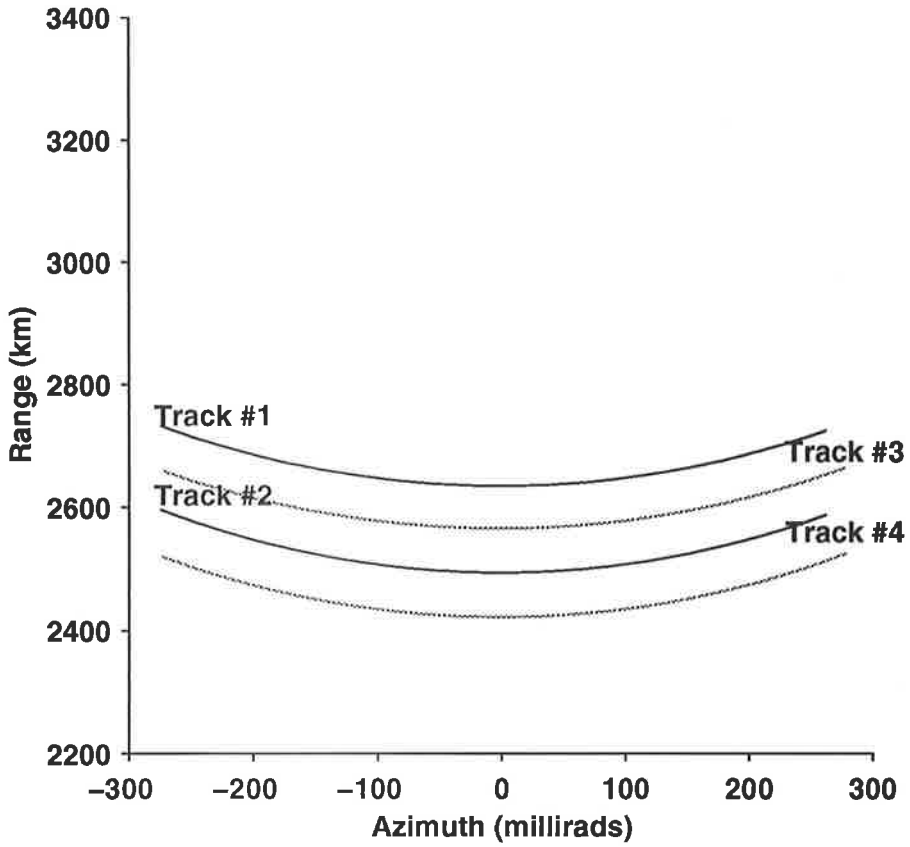

Figure 4.3: Difficult association scenario.

The track features for the alternative metrics are all computed as vectors over a window of n points of track data. The length of the resulting feature vectors will not necessarily be n, because more than one point is needed to compute track velocity. Each alternative metric measures an aspect of track similarity. The metrics used for the comparison of a pair of tracks are:

(1) Projection of velocity vectors

(2) Rate of change in heading

(3) Track speed

Projection of velocity vectors

The first alternative metric is a measure of the similarity of the velocity vectors of a pair of tracks. The metric discriminates between:

- tracks with similar velocity (both magnitude and direction), and
- tracks with dissimilar velocity (both magnitude and direction).

The similarity of the velocity vectors, denoted p, is computed over two dwells using the projection of the one velocity vector in the direction of the other velocity vector. For the metric to preserve symmetry, the choice of the velocity vector projected and the velocity vector projected upon must be unambiguous. We arbitrarily choose to project the shorter of the two vectors onto the longer of the two vectors, so that the metric approaches unity for velocity vectors with similar magnitudes and directions,. We denote the velocity vector at dwell k for track i by $\mathbf{v}_i(k)$. The velocity vector is the difference in the radar measurements of two sequential dwells; thus

$$\mathbf{v}_i(k) = \mathbf{y}_i(k+1) - \mathbf{y}_i(k).$$

The projection of the shorter vector $\mathbf{v}_i$ onto the longer vector $\mathbf{v}_j$ is formulated

$$p = \frac{\mathbf{v}_i.\mathbf{v}_j}{\|\mathbf{v}_j\|}, \text{ where } \|\mathbf{v}_j\| > \|\mathbf{v}_i\|.$$

The ratio of the length of projection p and the magnitude of the vector projected upon, $\mathbf{v}_j$, is the association metric for one dwell; thus

$$M_p\left(\begin{bmatrix} y_i(1) \\ y_i(2) \end{bmatrix}, \begin{bmatrix} y_j(1) \\ y_j(2) \end{bmatrix}\right) = \frac{\mathbf{v}_i.\mathbf{v}_j}{\|\mathbf{v}_j\|^2}, \text{ where } \|\mathbf{v}_j\| > \|\mathbf{v}_i\|.$$

The metric is computed for a window of track data by averaging over a number of dwells. The projections are averaged over a window of N sequential dwells, and therefore $N-1$

values of $\mathbf{v}_i$. The association metric between tracks i and j is

$$M_p\left(\begin{bmatrix} y_i(1) \\ \vdots \\ y_i(N) \end{bmatrix}, \begin{bmatrix} y_j(1) \\ \vdots \\ y_j(N) \end{bmatrix}\right) = \sum_{k=1}^{N-1} \frac{\mathbf{v}_i(k).\mathbf{v}_j(k)}{(N-1)\ \max\left(\|\mathbf{v}_i(k)\|^2, \|\mathbf{v}_j(k)\|^2\right)}.$$

Alternately, M_p can be expressed as

$$M_p\left(\begin{bmatrix} y_i(1) \\ \vdots \\ y_i(N) \end{bmatrix}, \begin{bmatrix} y_j(1) \\ \vdots \\ y_j(N) \end{bmatrix}\right) = \sum_{k=1}^{N} \min\left(\frac{\|\mathbf{v}_i(k)\|}{\|\mathbf{v}_j(k)\|}, \frac{\|\mathbf{v}_j(k)\|}{\|\mathbf{v}_i(k)\|}\right) \cos\theta_{ij}(k), \tag{4.3}$$

where $\theta_{ij}(k)$ is the angle between vectors $\mathbf{v}_i(k)$ and $\mathbf{v}_j(k)$. It is apparent from equation (4.3), that the metric is related to two aspects of the velocity vectors:

- the similarity in magnitude, as either ratio $\frac{\|\mathbf{v}_i(k)\|}{\|\mathbf{v}_j(k)\|}$, or ratio $\frac{\|\mathbf{v}_j(k)\|}{\|\mathbf{v}_i(k)\|}$, and
- the similarity in direction, as $\cos\theta_{ij}(k)$.

Contrastingly, the correlation coefficient between vectors $\mathbf{v}_i$ and $\mathbf{v}_j$, formulated as

$$C(\mathbf{v}_i, \mathbf{v}_j) = \sqrt{\frac{\mathbf{v}_i.\mathbf{v}_j}{\|\mathbf{v}_i\|\ \|\mathbf{v}_j\|}},$$

is merely equivalent to the cosine of the angle between vectors $\mathbf{v}_i$ and $\mathbf{v}_j$, which is not sufficient to discriminate between vectors similar or dissimilar in magnitude.

Similarity in rate of change in heading

One would expect that tracks from the same target would have similar headings, and similar rates of change in heading. The second alternative metric, due to [52], represents the similarity of the rate of change in heading of a pair of tracks. The measure of rate of change in heading is calculated over three consecutive track points. The rate of change in heading of track i at dwell k is denoted $\omega_i(k)$, and formulated as

$$\omega_i(k) = \arcsin \frac{\|\mathbf{v}_i(k-1) \times \mathbf{v}_i(k)\|}{\|\mathbf{v}_i(k-1)\|\ \|\mathbf{v}_i(k)\|} \quad \text{radians/dwell}$$

where $\times$ represents the vector cross product operation. The computation of rate of change in heading over a window of n consecutive dwells results in a feature vector for every track in consideration. The rate of change in heading feature vector of track i is

$$\omega_i = \begin{bmatrix} \omega_i(2) \\ \vdots \\ \omega_i(n-1) \end{bmatrix}.$$

Note that the feature vector is of length $n-2$ (two elements shorter than the track window), because the computation of every element of the feature vector requires two consecutive velocity measurements, and therefore positional data from three consecutive dwells.

The association metric is a tool to estimate the probability that a pair of tracks are associated; in this case the metric uses the similarity in the rate of change in heading of the tracks in question. The association metric is the sample correlation coefficient between feature vector $\boldsymbol{\omega}_i$ from track i and feature vector $\boldsymbol{\omega}_j$ from track j; thus

$$M_\omega\left(\begin{bmatrix} y_i(1) \\ \vdots \\ y_i(N) \end{bmatrix}, \begin{bmatrix} y_j(1) \\ \vdots \\ y_j(N) \end{bmatrix}\right) = \sqrt{\frac{[\boldsymbol{\omega}_i - \overline{\boldsymbol{\omega}}_i]^T\,[\boldsymbol{\omega}_j - \overline{\boldsymbol{\omega}}_j]}{\|[\boldsymbol{\omega}_i - \overline{\boldsymbol{\omega}}_i]\|\ \|[\boldsymbol{\omega}_j - \overline{\boldsymbol{\omega}}_j]\|}} \tag{4.4}$$

where $[\boldsymbol{\omega}_i - \overline{\boldsymbol{\omega}}_i]$ is the demeaned version of feature vector $\boldsymbol{\omega}_i$.

Similarity in track speed

The third alternative metric is a measure of the similarity in track speed for a pair of tracks. Track speed is calculated as the magnitude of the change in track position between dwells. The track speed of track i at dwell k is denoted $\|\mathbf{v}_i(k)\|$. The computation of this metric over a time window of length n results in a feature vector of track speed for every track in consideration. Note that the computation of track speed uses two points, so the resulting feature vector is one element shorter than the track window, N. The feature vector for the speed of track i is

$$\mathbf{s}_i = \begin{bmatrix} \|\mathbf{v}_i(1)\| \\ \vdots \\ \|\mathbf{v}_i(N-1)\| \end{bmatrix}$$

The association metric for the similarity in track speed is calculated as the correlation coefficient between the two speed vectors from the respective tracks. The correlation coefficient between feature vectors $\mathbf{s}_i$ and $\mathbf{s}_j$ is formulated by analogy with equation (4.4); thus

$$M_s\left(\begin{bmatrix} y_i(1) \\ \vdots \\ y_i(N) \end{bmatrix}, \begin{bmatrix} y_j(1) \\ \vdots \\ y_j(N) \end{bmatrix}\right) = \sqrt{\frac{[\mathbf{s}_i - \overline{\mathbf{s}}_i]^T\,[\mathbf{s}_j - \overline{\mathbf{s}}_j]}{\|[\mathbf{s}_i - \overline{\mathbf{s}}_i]\|\ \|[\mathbf{s}_j - \overline{\mathbf{s}}_j]\|}}. \tag{4.5}$$

where $[\mathbf{s}_i - \overline{\mathbf{s}}_i]$ is the demeaned version of feature vector $\mathbf{s}_i$.

4.3.2 Proposed Metric

The proposed association metric is described in Section 4.2. The proposed metric uses only one point, chosen at random from the same track window as the alternative association metrics. The computation of this association metric requires a model to compute the distribution

of the disparity vector for associated tracks. Details of the propagation geometry and priors of this model can be found in appendix A.

The model does not have perfect knowledge of the ionospheric conditions. The ionospheric state lies within the total range of possible ionospheric states, which are known *a priori*. The modelled parameters are the estimated disparity vector $\hat{\mathbf{d}}_{mn}$ and the eigenvectors and eigenvalues of its covariance matrix $\boldsymbol{\Sigma}_{mn}$.

4.3.3 Results

The values for every metric are accumulated and are plotted as histograms for associated and non-associated tracks. The results of the association metrics applied to the easy scenario are plotted in figure 4.4, while the results from the difficult scenarios are plotted in figure 4.5. Both figures contain four sub-figures, showing one histogram for each method. The distribution for non-associated tracks is shown as a gray line, while the distribution for associated tracks is shown as a black line. The methods are based on the following association metrics (by sub-figure):

(a) projection of velocity vectors;

(b) correlation of rate of change in heading;

(c) correlation of track speed and

(d) proposed metric.

The values of the proposed metric span such a large range that the histograms need to be plotted on a log scale; the histograms of the alternative association metrics are only plotted on a linear scale. To aid the visual comparison of the metrics, we plot the values of the proposed metric on a reversed log scale; thus in all sub-figures, the distributions of associated tracks and non-associated tracks appear to the right and left of the scale, respectively.

An association decision based on any association metric is prone to errors when the distribution of the association metric for associated tracks overlaps the distribution of the association metric for non-associated tracks. The histograms in figure 4.4 show that, in the case of the easy association scenario, all of the association metrics provide some degree of discrimination between associated and non-associated tracks. However, in figure 4.5 distributions of associated tracks and non-associated tracks are significantly overlapped for the alternative metrics. Note that in figures 4.5(a) and 4.5(b), there is significant overlap in the distributions. The histograms in figures 4.5(a), 4.5(b) and 4.5(c) indicate that, in the case of the difficult association scenario, the alternative metrics provide little or no discrimination between associated and non-associated tracks. For these metrics, there is significant overlap

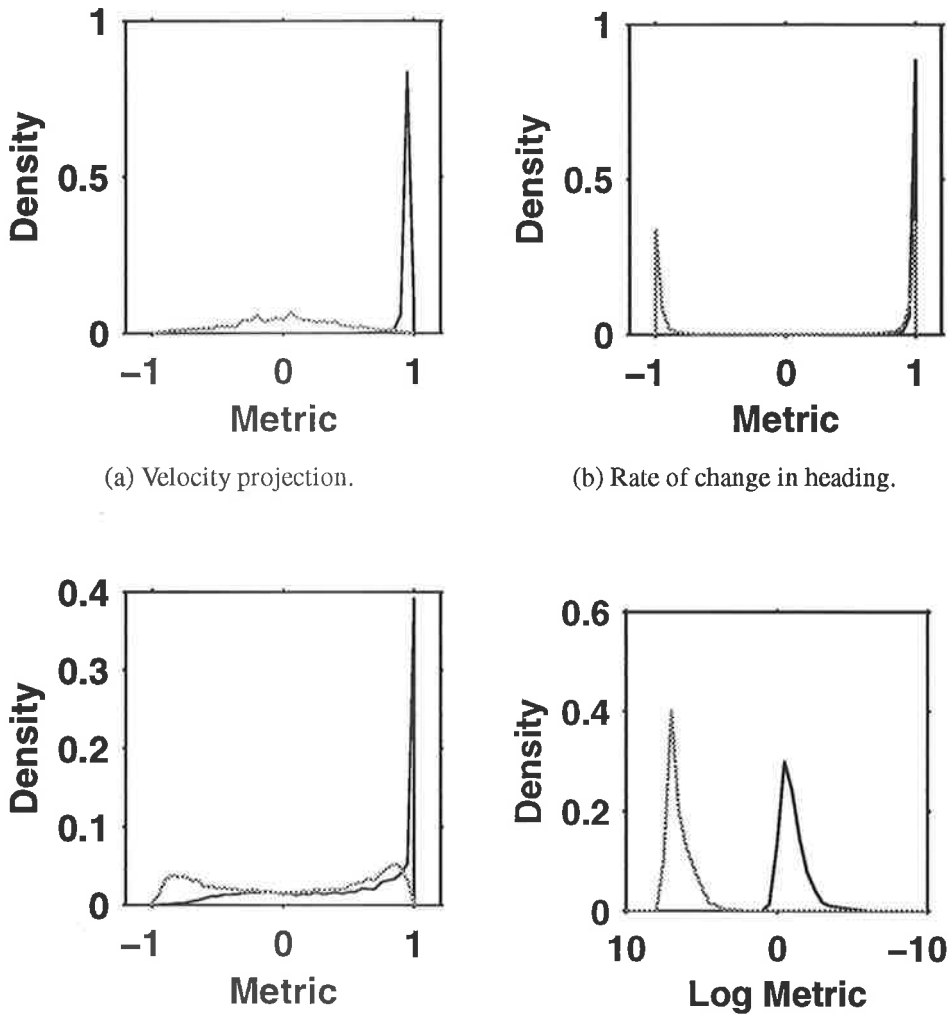

(a) Velocity projection.

(b) Rate of change in heading.

(c) Track speed.

(d) Proposed metric.

Figure 4.4: Easy association scenario results.

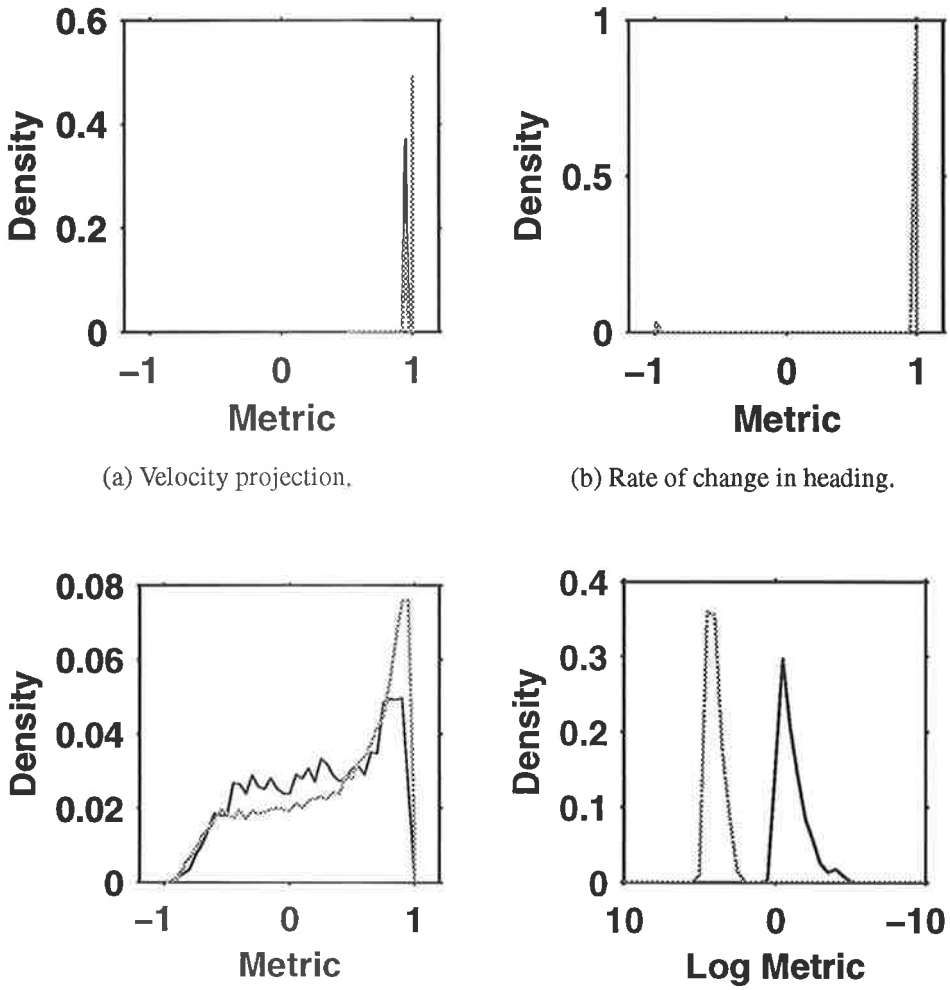

(a) Velocity projection.

(b) Rate of change in heading.

(c) Track speed.

(d) Proposed metric.

Figure 4.5: Difficult association scenario results.

between the histograms of the association metrics for associated tracks and for non-associated tracks, particularly in the case of the difficult association scenarios.

We decide that a pair of tracks are associated if $M < t$ where t is the threshold. The error rate is calculated as the sum of Type I (missed association) and Type II (false association) errors, and is calculated for each metric as an indication of its discrimination ability. We make the simplification that Type I errors and Type II errors have equal prior probabilities and equal cost. The threshold which minimises the sum of Type I and Type II errors has been calculated for each metric and is shown in Table 4.1 as t. In other words, the error rate e is calculated as if the best possible threshold t were known and used. The error rate e is the ratio of the erroneous cases (including both Type I and Type II errors) to the total number of cases (30,000). It is tabulated in Table 4.1.

Scenario	Metric	M_p	M_ω	M_s	M
	Subfigure	(a)	(b)	(c)	(d)
Easy	t	0.92	0.96	0.92	~ 10
	e	2%	31%	39%	0.0%
Difficult	t	0.93	0.91	0.01	~ 10
	e	53%	67%	71%	0.0%

Table 4.1: Comparative performance of association metrics.

4.3.4 Discussion

In the case of the easy association scenario, shown in figure 4.4, every association metric provides some degree of discrimination between associated tracks and non-associated tracks. Each of the alternative metrics produced some errors, with the projection of velocity vectors in figure 4.4(a) having the lowest error rate of the alternative metrics. Note, in table 4.1, the outstanding difference in the error rate of the proposed association metric and the alternative association metrics. The proposed association metric in figure 4.4(d) produces no errors for the easy association scenarios.

In the case of the difficult association scenario, only the proposed association metric in Figure 4.5(d) performs better than a random guess. The alternative metrics in Figures 4.5(a), 4.5(b) and 4.5(c) have an error rate, shown in table 4.1, which is greater than 50%. As in the easy scenario, the proposed association metric has an error rate of 0%, which is achievable over a range of values for the decision threshold.

The outcome of the association decision for the proposed metric is not sensitive to the exact choice of threshold, and the minimum sum of errors is zero. For the easy scenarios, a threshold in the range of 3 to 300 resulted in no errors. For the difficult scenarios, a threshold

in the range of 3 to 200 resulted in no errors. In contrast, the outcome of the association decision for the alternative association metrics is sensitive to the choice of threshold and the minimum sum of errors is not zero. The choice of threshold is therefore a critical issue for the alternative metrics. Due to the overlap in the distributions of associated and non-associated tracks for the alternative metrics, errors are unavoidable. Contrastingly, the histograms of the proposed association metric for associated and non-associated tracks are substantially separated, as shown in figures 4.4(d) and 4.5(d).

The proposed method has no errors in either the easy scenario or the difficult scenario, and is not as sensitive to the choice of threshold as the alternative metrics. The decision threshold for the proposed association metric can be chosen over a wide range with no resulting errors. It is both desirable and possible to have a measure of association calculated instantly instead of having to wait for a window of data to process as in [14] and [52]. The alternative metrics discussed in this paper are all derived from the change in radar measurements over a period of time, and therefore require a window of track data for their computation. The alternative metrics become less reliable over shorter windows.

The proposed association metric presents a significant reduction in errors over the alternative metrics. However this metric is based on the comparison of the observed disparity vector to the expected disparity vector, and thus the metric can be calculated from just one point. Naturally, one could expect the proposed association metric to have greater reliability if it were calculated over more points. In section 4.4, we propose extensions to the association metric so that it can accommodate more than one data point.

With respect to the variation in disparities, only the contribution due to ionospheric perturbation has been considered. Radar specific effects due to measurement errors have been deliberately ignored for simplicity. Radar errors can be included in the simulation. The inclusion of radar errors would change the distribution of the disparity vector, and therefore the parameterisation. The performance of all of the association metrics would be slightly impaired by the inclusion of radar measurement errors.

4.4 Cumulative association metrics

The association metric proposed in this chapter puts a lot of dependence on one detection, which may be in error in real data. In this section, we discuss a way of improving the discrimination between associated tracks and non associated tracks, by combining several sequential association metrics for an association candidate. This improvement reduces the possibility of erroneous association in cases when a pair of non-associated tracks are separated by the correct disparity distance for associated tracks for a small number of dwells; for instance, when two non-associated tracks cross. We refer to a combination of sequential association metric as a *cumulative association metric*.

The association metric in [14] is accumulated (see equation (2.1)) over a length of track, and an arbitrary threshold is applied to the sum. However, the application of a threshold to a sum of M-distances, as in [14], is only correct if the M-distances are independent. In the case of independence, we test the sum of M-distances using the $\chi^2(r)$ test [21], where r represents the degrees of freedom of the random variable to be tested, since M-distances have a χ^2 distribution. The number of degrees of freedom r is $M \times N$, where M is the dimensionality of the disparity vector, and N is the number of M-distances which have been added.

We propose a cumulative association metric of the M-distances of equation (4.2) for the case of independence, denoted M_{mn}^{ind}. The radar measurements of track i at dwell t are contained in vector $\mathbf{y}_t$. The cumulative association metric M_{mn}^{ind} is formulated as

$$M_{mn}^{ind} = \sum_{t=1}^{N} \boldsymbol{\delta}_{mn}^T(t) \boldsymbol{\Sigma}_{mn}^{-1}(\mathbf{y}_i(t)) \boldsymbol{\delta}_{mn}(t). \tag{4.6}$$

where the error vector $\boldsymbol{\delta}_{mn}$ at time t is

$$\delta_{mn}(t) = \mathrm{y}_i(t) + \hat{\mathrm{d}}_{mn}(\mathbf{y}_i(t)) - \mathbf{y}_j(t). \tag{4.7}$$

Unfortunately, the temporally sequential M-distances are not independent. If we properly account for the dependence between sequential M-distances the cumulative association metric is formulated as

$$M_{mn}^{dep} = \begin{bmatrix} \boldsymbol{\delta}_{mn}(t_1) \\ \boldsymbol{\delta}_{mn}(t_2) \\ \vdots \\ \boldsymbol{\delta}_{mn}(t_N) \end{bmatrix}^T \begin{bmatrix} \boldsymbol{\Sigma}_{t_1} & \boldsymbol{\Sigma}_{t_1,t_2} & \cdots & \boldsymbol{\Sigma}_{t_1,t_N} \\ \boldsymbol{\Sigma}_{t_2,t_1} & \boldsymbol{\Sigma}_{t_2} & \cdots & \boldsymbol{\Sigma}_{t_2,t_N} \\ \vdots & \vdots & \vdots & \vdots \\ \boldsymbol{\Sigma}_{t_N,t_1} & \boldsymbol{\Sigma}_{t_N,t_2} & \cdots & \boldsymbol{\Sigma}_{t_N} \end{bmatrix}^{-1} \begin{bmatrix} \boldsymbol{\delta}_{mn}(t_1) \\ \boldsymbol{\delta}_{mn}(t_2) \\ \vdots \\ \boldsymbol{\delta}_{mn}(t_N) \end{bmatrix} \tag{4.8}$$

where $\boldsymbol{\Sigma}_{t_j}$ denotes $\Sigma_{mn}(\mathrm{y}_i(t_j))$. $\boldsymbol{\Sigma}_{t_i,t_j}$ represents the covariance between the elements of $\boldsymbol{\delta}_{mn}(t_i)$ and $\boldsymbol{\delta}_{mn}(t_j)$. The difference between the independent metric of equation (4.6) and the dependent metric of equation (4.6) is the off-diagonal matrices $\boldsymbol{\Sigma}_{t_i,t_j}$, $t_i \neq t_j$.

The covariance matrix Σ_{mn} of equation (4.2) accounts for the covariance in the error vector $\boldsymbol{\delta}_{mn}$ about the estimated disparity vector $\hat{\mathrm{d}}_{mn}$. There are two major contributors to the covariance of the error vector:

1. errors in the estimate $\hat{\mathrm{d}}_{mn}$ due to mismodelling, and

2. errors in the measurement of y_i and y_j.

The off-diagonal matrices are difficult to determine. We propose a method of calculating the cumulative association metric M_{mn}^{dep} of equation (4.8) which avoids the need to calculate the off-diagonal matrices. This method discriminates between tracks based on the variation

in the disparity vector $\boldsymbol{\delta}_{mn}$ over the track window. This discriminator exploits the fact that the variation in $\boldsymbol{\delta}_{mn}$ over the track window is smaller for associated tracks than for non-associated tracks. We demean the disparity vector $\boldsymbol{\delta}_{mn}$ over the track window in consideration. The covariance matrix $\boldsymbol{\Sigma}$ then only needs to account for the errors in the measurement of $\mathbf{y}_i$ and $\mathbf{y}_j$. Thus,

$$M_{mn}^{dep} \simeq \begin{bmatrix} \boldsymbol{\delta}_{mn}(t_1) - \overline{\boldsymbol{\delta}}_{mn} \\ \boldsymbol{\delta}_{mn}(t_2) - \overline{\boldsymbol{\delta}}_{mn} \\ \vdots \\ \boldsymbol{\delta}_{mn}(t_N) - \overline{\boldsymbol{\delta}}_{mn} \end{bmatrix}^T \begin{bmatrix} \boldsymbol{\Sigma}_{t_1}^{meas} & 0 & \cdots & 0 \\ 0 & \boldsymbol{\Sigma}_{t_2}^{meas} & \cdots & 0 \\ \vdots & \vdots & \vdots & \vdots \\ 0 & 0 & \cdots & \boldsymbol{\Sigma}_{t_N}^{meas} \end{bmatrix}^{-1} \begin{bmatrix} \boldsymbol{\delta}_{mn}(t_1) - \overline{\boldsymbol{\delta}}_{mn} \\ \boldsymbol{\delta}_{mn}(t_2) - \overline{\boldsymbol{\delta}}_{mn} \\ \vdots \\ \boldsymbol{\delta}_{mn}(t_N) - \overline{\boldsymbol{\delta}}_{mn} \end{bmatrix}$$

where $\boldsymbol{\Sigma}_{t_j}^{meas}$ denotes the component of covariance in $\boldsymbol{\delta}_{mn}(t_1)$ due to measurement errors. Then the resultant M-distance is given by

$$M_{mn}^{dep} = \sum_{t=1}^{N} (\boldsymbol{\delta}_{mn}(t) - \overline{\boldsymbol{\delta}}_{mn})^T \boldsymbol{\Sigma}^{meas}(\mathbf{y}_i(t))^{-1} (\boldsymbol{\delta}_{mn}(t) - \overline{\boldsymbol{\delta}}_{mn}). \tag{4.9}$$

4.5 Summary

In this chapter, a novel association metric for track association based on a model of the intermodal vectors is presented. The association metric is a tool for estimating the probability that a pair of tracks are due to a common target. Since the components of the difference in multimode radar measurements are correlated significantly, we propose an association metric which can exploit the correlation in the difference components: the Mahalanobis distance (M-distance). The parameters of the M-distance, the estimated disparity vector $\hat{\mathbf{d}}_{mn}$ and its covariance matrix $\boldsymbol{\Sigma}_{mn}$ are modelled as functions in the radar measurement space.

The proposed metric is compared to alternative, heuristically chosen methods similar to those previously proposed. The success of the proposed metric is demonstrated for both easy association scenarios and difficult association scenarios. The proposed metric provides better discrimination between pairs of associated tracks and pairs of non-associated tracks than the alternative, heuristically chosen metrics. For the data set in the demonstration, no errors result from this proposed metric. The proposed association metric is not as sensitive to choices in decision threshold as the alternative metrics.

The fundamental difference between the proposed metric and the alternative metrics is that the proposed metric uses prior knowledge to estimate the distributions of intermodal vectors. The success of the proposed metric is due to the incorporation of a model of the multimode propagation. The alternative association metrics, by comparison, do not incorporate a propagation model, and we demonstrated that these metrics perform significantly worse.

Finally, in section 4.4, we proposed three ways of computing cumulative association metrics. The proposed association metric performs well on one dwell (see section 4.3.3).

However, we anticipate that a cumulative association metric, based on several dwells, will enhance the discrimination ability of the association metric, and hence the performance of the entire track association system. To maintain focus on the track association system, a demonstration of cumulative association metrics is out of the scope of this thesis.

CHAPTER V

Modelling the disparity vector

5.1 Introduction

The argument for modelling the intermodal disparity function (which we refer to as the disparity function), which defines the intermodal disparity field (which we refer to as the disparity field), appears in section 3.3.4. In this chapter, we introduce three techniques for modelling the disparity function throughout the radar measurement space. Samples of a simulated disparity field typical of those to be modelled are shown in figure 5.1. There are two ionospheric layers present in the simulation; the E layer with a virtual height of 100km, and the F layer with a virtual height of 250km. Figure 5.1 shows the multimode detections at a set of grid-points throughout the radar coverage. The set of four detections for a common target are connected for clarity, and the connecting lines form a zig-zag pattern for each target. The vertices of each zig-zag pattern correspond to the four detections, and the edges correspond to three disparity vectors. In figure 5.2, we show the azimuthal disparity between modes EF and FE as a function of the radar measurements range and azimuth for one mode. The radar measurements correspond to one mode of the pair detection, which we arbitrarily choose to be the FE mode.

One important aspect of all three techniques presented in this chapter is that the modelling of the disparity function occurs in the radar measurement space. We choose to model in the radar measurement space because the multimode data is observed in the radar measurement space, and the correspondence to the geographical space can only be crudely estimated. It is important for the reader to note that any point fixed in the radar measurement space is not fixed in geographical space due to the variability of the measurement transform.

Note that the disparity field between modes m and n is defined by the disparity function $\mathbf{d}_{mn}$. We denote our estimate of the disparity function by $\hat{\mathbf{d}}_{mn}$. The three techniques demonstrated in this chapter are illustrated for a generic component of the disparity field; the specific components of the disparity field can be treated analogously. We denote the k^{th} component of the estimated disparity function by $\hat{\mathbf{d}}_{mn,k}(\mathbf{y})$, which is a function of the radar measurements, such as range, azimuth and Doppler, denoted by the vector $\mathbf{y}$.

We explain how each technique models the disparity function as a linear combination of

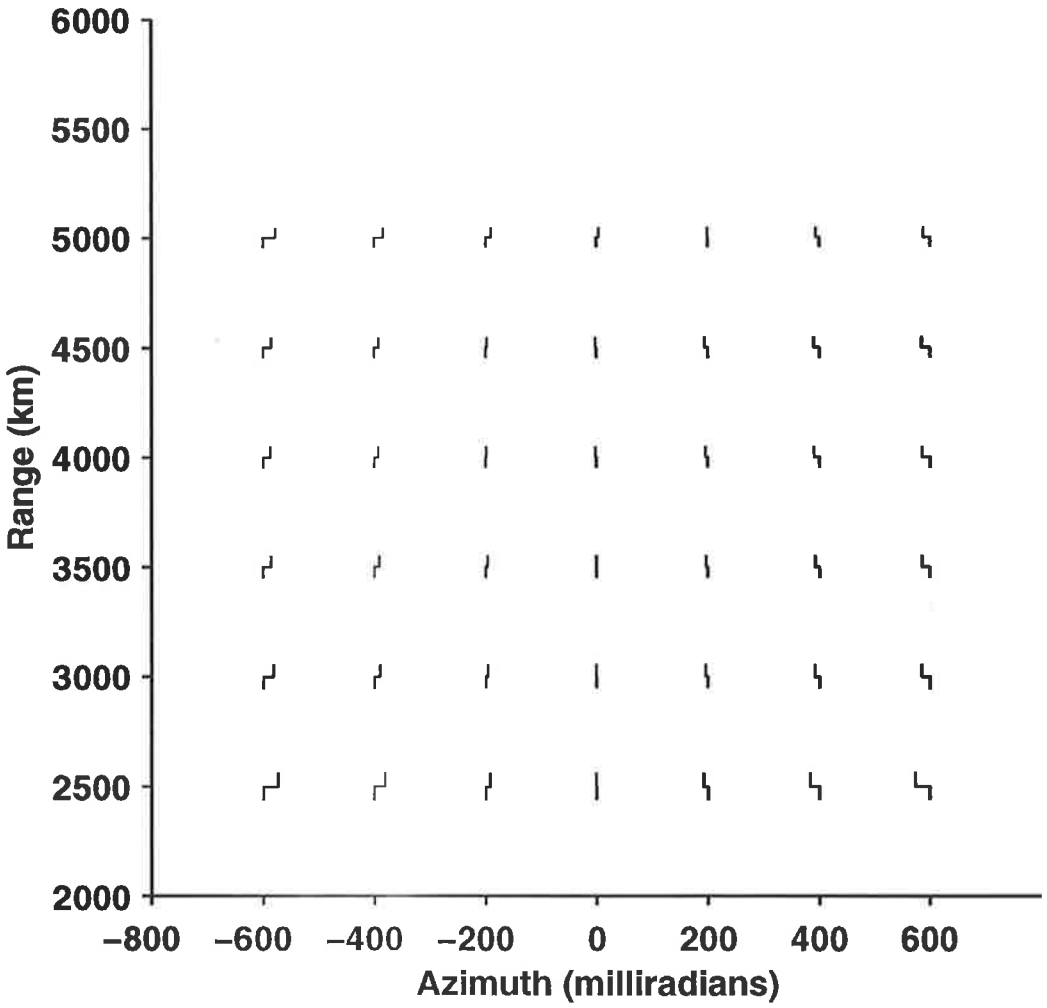

Figure 5.1: Multimode patterns over the radar coverage.

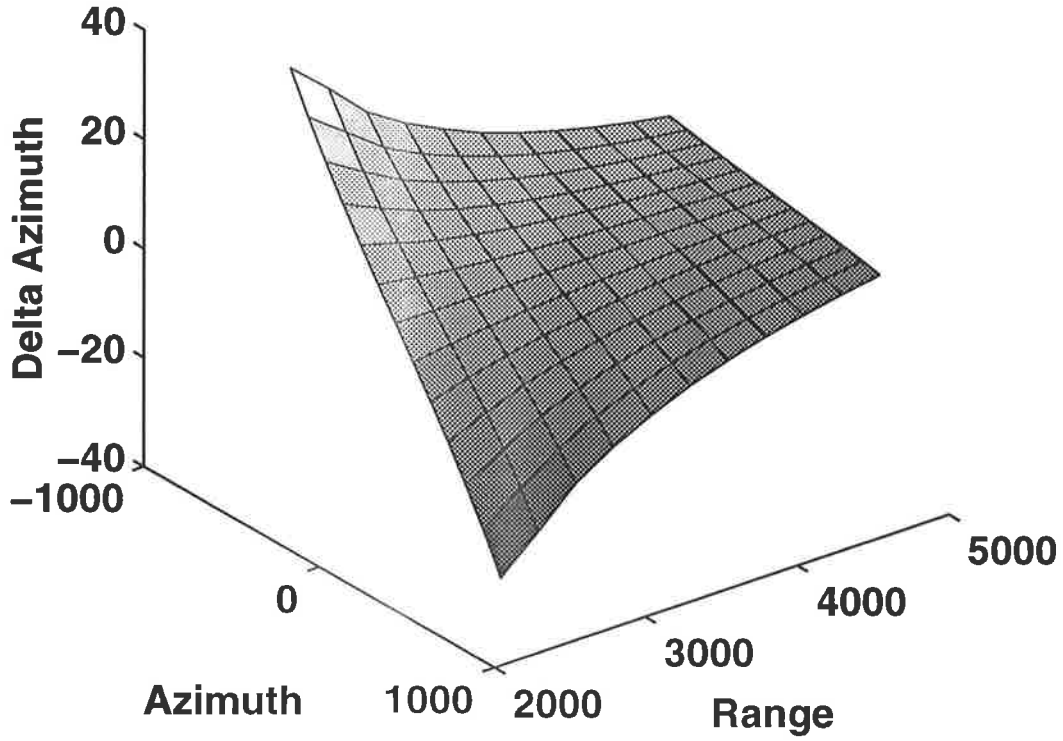

Figure 5.2: ΔA component of the intermodal disparity field.

basis functions in section 5.2. The first technique represents $\hat{\mathbf{d}}_{mn}$ as a linear combination of discrete cosine functions, and is described in section 5.3. The second technique represents $\hat{\mathbf{d}}_{mn}$ by basis functions determined via principle component analysis (PCA), and is described in section 5.4. By contrast, the first technique represents $\hat{\mathbf{d}}_{mn}$ with analytical functions, whereas the second technique represents $\hat{\mathbf{d}}_{mn}$ at discrete locations with empirical vectors. The third technique combines the strengths of each of the first two techniques by analysing basis function coefficients via PCA; this technique is presented in section 5.5. A limited demonstration of each of the three techniques is presented in section 5.6. For each of the three techniques presented in sections 5.3, 5.4 and 5.5, the estimated values of $\mathbf{d}_{mn}(\mathbf{y})$ are denoted by $\hat{\mathbf{d}}^{cos}_{mn}(\mathbf{y})$, $\hat{\mathbf{d}}^{emp}_{mn}(\mathbf{y})$ and $\hat{\mathbf{d}}^{com}_{mn}(\mathbf{y})$, respectively. A comparative study of the three techniques, in which $\hat{\mathbf{d}}^{cos}_{mn}(\mathbf{y})$, $\hat{\mathbf{d}}^{emp}_{mn}(\mathbf{y})$ and $\hat{\mathbf{d}}^{com}_{mn}(\mathbf{y})$ are compared to the actual values of $\mathbf{d}_{mn}(\mathbf{y})$ appears in section 5.7. Finally, we summarise and discuss the important aspects of this chapter in section 5.8.

5.2 Modelling with basis functions

Each of the three techniques introduced in this chapter is illustrated modelling the disparity function $\mathbf{d}_{mn,k}(\mathbf{y})$ as a linear combination of basis functions. We denote a set of N basis functions in the radar measurement space by

$$\{\Upsilon_0, \Upsilon_1, \ldots, \Upsilon_N\}.$$

The linear combination of basis functions for modelling $\hat{\mathbf{d}}_{mn,k}(\mathbf{y})$, adopted by all of the three techniques proposed in this chapter is formulated as

$$\hat{\mathbf{d}}_{mn,k}(\mathbf{y}) = \sum_{j=0}^{N} a_{kj} \Upsilon_j(\mathbf{y}), \tag{5.1}$$

where each a_{kj} is the coefficient of the j^{th} basis function $\Upsilon_j(\mathbf{y})$.

If the disparity function component $\mathbf{d}_{mn,k}$ is to be estimated from only p multimode samples, then only p basis function coefficients can be determined. Hence it is important to represent the estimated disparity $\hat{\mathbf{d}}_{mn,k}$ in terms of a few basis functions. The criterion for finding $\hat{\mathbf{d}}_{mn,k}(\mathbf{y})$ is to minimise the expression

$$E\left[\left(\hat{\mathbf{d}}_{mn,k}(\mathbf{y}) - \mathbf{d}_{mn,k}(\mathbf{y})\right)^2\right]$$

with a limited number of basis functions. Consequently, we determine the proportion of the disparity field's total spatial variation represented by each basis function. We refer to the basis function which accounts for the most spatial variation as the dominant basis function. We choose the set of basis functions so that the mean squared error between a combination of p basis functions and the disparity function is minimised. The basis functions are the first p functions, in terms of dominance.

5.3 Modelling via Cosine Functions

In this section, we introduce a technique for modelling the disparity using a heuristically chosen set of basis functions. The choice of basis functions will depend on the data used, and any modelling must be performed with simulated data since there is no suitable data publicly available. We avoid a rigorous study into the choice of basis functions, since it would have only limited value on the simulated data. Instead, we choose a set of basis functions from a visual inspection of a typical disparity field, such as the one in figure 5.1. The most noticeable feature of figure 5.1 is the component of the disparity field corresponding to the azimuthal disparity ΔA, since it exhibits the maximum amount of variance throughout the field. Furthermore, ΔA exhibits a symmetry about bore-sight, which is apparent from figure 5.1, but glaringly obvious in figure 5.2.

From our observations, we choose the cosine functions [1] of the discrete cosine transform (DCT) as the basis functions. Hence we refer to this technique as the cosine technique. From a visual inspection of the field it is apparent that most of the spatial variation of the disparity field might be represented by a few of the low frequency cosine functions; thus the cosine functions seem to be a good choice, heuristically speaking. However, there may be other sets of basis functions which are more suitable because they can express the disparity field in terms of fewer basis functions. The cosine functions are commonly used as functions of a single variable, in which case the j^{th} cosine function, with j a non-negative integer, is denoted $\phi_j(y)$ and formulated thus:

$$\phi_j(y) = \cos(jy),$$

where the variable y is normalised to a range between 0 and π. The first basis function covers half the period of the cosine function, and subsequent functions cover multiples thereof. Bases are also defined for cosine functions of more than one variable. For instance, the widely used JPEG image compression standard represents an image in terms of the two dimensional (2D) cosine functions [41].

For simplicity, we represent only two dimensions of the disparity vector function using 2D cosine functions, but an extension to higher dimensionality is trivial. We denote the 2D basis functions of equation (5.2) by $\Phi_{ij}(x, y)$. The 2D cosine functions are defined as the multiplicative combination of two 1D cosine functions; thus

$$\begin{aligned} \Phi_{ij}(y_1, y_2) &= \phi_i(y_1)\phi_j(y_2) \\ &= \cos(iy_1)\cos(jy_2). \end{aligned}$$

The k^{th} component of the estimated disparity function $\hat{\mathrm{d}}_{mn,k}(y_1, y_2)$ is then modelled as

$$\hat{\mathrm{d}}^{cos}_{mn,k}(y_1, y_2) = \sum_{i=0}^{N_1-1} \sum_{j=0}^{N_2-1} \alpha_{kij}\Phi_{ij}(y_1, y_2) \tag{5.2}$$

$$= \sum_{i=0}^{N_1-1} \sum_{j=0}^{N_2-1} \alpha_{kij} \phi_i(y_1) \phi_j(y_2),$$

where α_{kij} denotes the coefficient of the 2D basis function Φ_{ij}, used to represent function $\hat{\mathbf{d}}^{cos}_{mn,k}$, and N_1 and N_2 denote the dimensions of the set of 2D basis functions.

Normalisation

The chosen basis functions, the cosine functions, operate on angles (in radians) between 0 and π radians. Hence the choice of basis functions requires that the radar measurements be normalised to this range.

In all simulations of this chapter, the slant range R_s lies between 2500 and 5000 kilometres, and the apparent azimuth A_s lies between -600 and +600 milliradians. We therefore normalise R_s and A_s to normalised values (in radians):

$$\begin{aligned} R_{Ns} &= \frac{\pi(R_s - 2500)}{2500} \\ A_{Ns} &= \frac{\pi(A_s + 600)}{1200} \end{aligned} \quad . \tag{5.3}$$

5.3.1 Summary

A technique is proposed for modelling the disparity function as a linear combination of heuristically chosen basis functions. We choose the set of basis functions to be the cosine functions.

5.4 Modelling via Principle Component Analysis

In this section, we introduce a technique for modelling the disparity field via principle component analysis (PCA). By contrast to the technique introduced in section 5.3, this technique determines the model from empirical data, and hence is referred to as the *empirical technique*. The empirical technique is inspired by the use of PCA in meteorology for modelling the field of a meteorological parameter; such use of PCA is described in section 5.4.1. The application of PCA for modelling the disparity function is proposed in section 5.4.2. Finally, we discuss the merits of this proposed technique in section 5.4.3. A limited demonstration of the proposed technique appears later in the chapter, in section 5.6.2.

5.4.1 PCA for meteorological modelling

Principle Component Analysis (PCA) is an established tool in meteorology for describing the spatial variance of a meteorological parameter in a condensed form [25]. A meteorological parameter, such as pressure or temperature, is observed (i.e. measured) at several weather stations. These stations simultaneously measure the meteorological parameter at regular time

intervals. A set of simultaneous measurements from the stations constitute an observation of the spatial field of the meteorological parameter, at discrete locations. The field varies from observation to observation, since the parameter varies over time. PCA decomposes the sequence of spatial fields into a set of eigenvectors, ordered by the amount of spatial variation they represent. Each observation of the spatial field can be represented by a combination of eigenvectors, which are found via PCA. The merit of PCA in meteorological modelling is that the bulk of the spatial variance in the field of a meteorological parameter can be represented by a linear combination of just a few eigenvectors.

We form a matrix, termed the *sample* matrix. A row of the sample matrix contains a set of measurements of the meteorological parameter, made simultaneously; there is one measurement for each weather station. Each column of the sample matrix contains all the measurements at one weather station. In the simplest case of the PCA, each set of measurements receives equal attention, which corresponds to the case where the evenly spaced measurement intervals.

Consider the case in which the meteorological parameter has been measured simultaneously at the p weather stations on n occasions; n is much greater than p. The sample matrix $\mathbf{X}$ is $(n \times p)$, with n observations on the p variables; thus

$$\mathrm{X} = \begin{bmatrix} w_1(1) & w_2(1) & \cdots & w_p(1) \\ w_1(2) & w_2(2) & \cdots & w_p(2) \\ \vdots & \vdots & \cdots & \vdots \\ w_1(n) & w_2(n) & \cdots & w_p(n) \end{bmatrix},$$

where $w_j(i)$ is the i^{th} measurement at the j^{th} weather station. We perform PCA by determining the eigenvectors, or principle components (PCs), of $\mathbf{X}^T\mathbf{X}$. The eigenvectors of $\mathbf{X}^T\mathbf{X}$ are sometimes referred to as the *empirical orthogonal functions* (EOFs) in the meteorological literature [31].

The singular value decomposition (SVD) is a computationally efficient way to compute the eigenvectors of $\mathbf{X}^T\mathbf{X}$. Another virtue of the SVD is that it provides a useful means of representing the results of the PCA, in the form of the eigenvectors. The data matrix $\mathbf{X}$ is decomposed via the SVD as follows

$$\mathbf{X} = \mathbf{U}\mathbf{L}\mathbf{V}^T, \tag{5.4}$$

where $\mathbf{V}$ is a $(p \times p)$ matrix with orthonormal columns so that $\mathbf{V}^T\mathbf{V} = \mathbf{I}_n$ ($\mathbf{I}_n$ being the identity matrix of dimension n); V contains the eigenvectors of $\mathbf{X}^T\mathbf{X}$. $\mathbf{L}$ is a $(n \times p)$ matrix, containing the square roots of the eigenvalues of $\mathbf{X}^T\mathbf{X}$. $\mathbf{U}$ is a $(n \times n)$ matrix, also having orthonormal columns. Each row corresponds to an observation of the spatial field, and contains the coefficients for the linear combination of eigenvectors which represents that field.

The eigenvectors of $\mathbf{X}^T\mathbf{X}$, contained in the columns of $\mathbf{V}$ each represent an aspect of the spatial variation of the meteorological parameter. The simultaneous measurements of the meteorological parameter at the weather stations, denoted by the $(1 \times p)$ row vector $\mathbf{w}$, are representable as a unique linear combination of the columns of $\mathbf{V}$; thus

$$\mathrm{w} = \sum_{j=1}^{n} a_j \mathrm{v}_j^T, \tag{5.5}$$

where the $(p \times 1)$ vector v_j denotes the j^{th} column of $\mathbf{V}$, and a_j is the corresponding coefficient in the linear combination.

5.4.2 Modelling the disparity function via PCA

We derive inspiration from the above-mentioned use of PCA in meteorology to develop a technique for modelling the principle components of spatial variation in the disparity field. The disparity field is analogous to the meteorological field of section 5.4.1; the spatial variation of the disparity field is modelled in the radar measurement space using PCA. In our analogy, the weather stations correspond to fixed locations in the radar measurement space, which we term grid-points, and which are, in general, not uniformly spaced. We require measurements of the disparity function at fixed points, also termed grid-points, as an intermediate result for estimating the disparity at other locations; however, these measurements are not available. Therefore, we estimate disparity measurements at these locations.

The technique proposed in this section represents $\hat{\mathrm{d}}_{mn}$ by exploiting empirical data of the disparity field; hence we refer to this technique as the empirical technique. An outline of the technique follows: Firstly, we obtain observations of several disparity fields. Then we interpolate the observations of each field to fixed grid-points. We then apply PCA to the disparity fields at the grid-points. The disparity function is modelled at the grid-points as a linear combination of eigenvectors. These eigenvectors are basis functions, albeit discretely sampled in the radar measurement space. Each basis function represents some of the disparity function's spatial variation. The eigenvector corresponding to the largest eigenvalue of $\mathbf{X}^T\mathbf{X}$ accounts for the maximum spatial variance in the disparity field.

Simultaneously observed multimode patterns are samples of the disparity field. These samples are rarely available at the required grid-points, and hence the disparity function must be estimated at these grid-points. We estimate the disparity function at the required grid-points by extrapolating from, and interpolating between, the available samples of the disparity field. We make an assumption about the form of the disparity field, since we lack accurate ionospheric information for estimating it. Any such assumption is arbitrary, so for the sake of simplicity, we assume that the form of the disparity field is maximally smooth between the available samples. The criterion for maximal smoothness in the estimated disparity field

is the minimisation of the second derivative with respect to the spatial coordinates. The interpolation method estimates the required disparity function component $\mathrm{d}_{mn,k}$ at the p grid-points using a maximally smooth interpolation function. Details of the interpolation method, which employs biharmonic splines to achieve the criterion for maximal smoothness, are not relevant to the immediate discussion, and therefore do not appear here; instead we refer the interested reader to [42].

We form a data matrix $\mathbf{X}$, analogous to the meteorological data matrix $\mathbf{X}$ of section 5.4.1, for each component of the disparity field. We denote data matrix for the k^{th} component of the disparity field by $\mathbf{X}_k$. The data matrix $\mathbf{X}_k$ is $(n \times p)$, with n estimates on the p variables. The variables are the estimated values of the disparity function at fixed grid-points in the radar measurement space. Stated explicitly, the p variables have been simultaneously estimated at all grid-points, on n occasions. Each column of the data matrix $\mathbf{X}_k$ contains all the estimates of one variable, and each row of $\mathbf{X}_k$ contains one estimate of all the variables; thus

$$\mathbf{X}_k = \begin{bmatrix} m_{k1}(1) & m_{k2}(1) & \cdots & m_{kp}(1) \\ m_{k1}(2) & m_{k2}(2) & \cdots & m_{kp}(2) \\ \vdots & \vdots & \cdots & \vdots \\ m_{k1}(n) & m_{k2}(n) & \cdots & m_{kp}(n) \end{bmatrix},$$

where $m_{kj}(i)$ is the estimate of the k^{th} disparity function component $\mathrm{d}_{mn,k}$, on the i^{th} occasion, at the j^{th} grid-point, measured about its mean $\overline{m}_{kj}$. Thus the temporal variation in the disparity field is represented in the columns of the data matrix, while the spatial variation is represented in the rows of the data matrix.

By analogy with equation (5.4), we perform PCA via the SVD on each data matrix $\mathbf{X}_k$. The decomposition is formulated as

$$\mathbf{X}_k = \mathbf{U}_k \mathbf{L}_k \mathbf{V}_k^T, \tag{5.6}$$

where $\mathbf{V}_k$ is a $(p \times n)$ matrix, having orthonormal columns; these columns contain the eigenvectors of $\mathbf{X}_k^T \mathbf{X}_k$. $\mathbf{L}_k$ is a $(n \times n)$ diagonal matrix, containing the square roots of the eigenvalues of $\mathbf{X}_k^T \mathbf{X}_k$. $\mathbf{U}_k$ is a $(n \times n)$ matrix, also having orthonormal columns, whose rows contain coefficients for the eigenvectors for each observation.

The eigenvectors are contained in the columns of $\mathbf{V}_k$. These eigenvectors form a basis which can represent different disparity fields with a different set of coefficients. We denote the j^{th} column of $\mathbf{V}_k$ by the $(p \times 1)$ vector $\mathbf{v}_{kj}$. The i^{th} element of $\mathbf{v}_{kj}$, denoted v_{kij} is the value of the j^{th} eigenvector at the i^{th} grid-point. We denote the radar measurements of the i^{th} grid-point by $\mathbf{y}_i$. We estimate the disparity function $\mathrm{d}_{mn,k}(\mathbf{y}_i)$ at the i^{th} grid-point by a linear combination of the n eigenvectors; thus

$$\hat{\mathrm{d}}_{mn,k}^{emp}(\mathbf{y}_i) = \sum_{j=1}^{n} a_j v_{kij}, \tag{5.7}$$

where a_j is the coefficient of the j^{th} eigenvector.

The coefficient of the dominant eigenvector (that is, the eigenvector which accounts for the most spatial variation) can be determined from just one sample of the corresponding disparity function. However, if we have q samples, we can obtain the coefficients of the q dominant eigenvectors. Note that the coefficients change if more samples are available.

We estimate the disparity function component $\mathbf{d}_{mn,k}$ at the grid-points as a linear combination of the eigenvectors. The estimated disparity function $\hat{\mathbf{d}}^{emp}_{mn,k}(\mathbf{y})$ at a location $\mathbf{y}$ in the radar measurement space, is obtained by interpolating the values at the grid-points $\mathbf{y}_i \forall i \in 1 \ldots p$. We denote the function which is the biharmonic spline interpolation [42] of the j^{th} eigenvector by $\boldsymbol{\Gamma}_{kj}(\mathbf{y})$, and express it thus

$$\boldsymbol{\Gamma}_{kj}(\mathbf{y}) = \mathcal{F}(\mathbf{v}_{kj}, \mathbf{y}). \tag{5.8}$$

$\mathcal{F}$ is the interpolation function which uses the elements of vector $\mathbf{v}_{kj}$ as the pivotal points [26]. The interpolated eigenvectors are continuous functions in the radar measurement space. We insert equation (5.8) into equation (5.7) to obtain a general expression for the estimated disparity function $\hat{\mathbf{d}}_{mn,k}(\mathbf{y})$ at location $\mathbf{y}$ in the radar measurement space; thus

$$\hat{\mathbf{d}}^{emp}_{mn,k}(\mathbf{y}) = \sum_{j=1}^{n} a_j \boldsymbol{\Gamma}_{kj}(\mathbf{y}), \tag{5.9}$$

with the coefficient a_j the same as in equation (5.7).

5.4.3 Summary and Discussion

In this section, we introduced a technique for modelling the disparity function as a linear combination of empirically determined basis functions. Hence we refer to this technique as the empirical technique. Our inspiration for this technique comes from the field of meteorological modelling, which is discussed in section 5.4.1. In section 5.6.2, we demonstrate that a significant proportion of the spatial variation in the disparity function can be represented by a few empirically determined functions.

The empirical technique has an apparent advantage over the cosine technique, in that it is able to represent the majority of the spatial variance in the disparity function by a smaller number of functions. This advantage is demonstrated in section 5.7. The empirical technique estimates the disparity function by determining a smaller number of coefficients; thus requiring a smaller number of samples.

The assumption about the form of the interpolated disparity field is arbitrary and thus is the most obvious weakness of this technique. While maximal smoothness is an adequate choice for demonstrating the empirical technique of modelling the spatial variation in the disparity field, the choice of a maximally smooth disparity field may not be appropriate in some circumstances. For instance, at dawn and dusk there is a significant change in the

incident solar radiation (these conditions are referred to in the literature as the dawn and dusk *terminators*), and therefore there is a change in ionospheric propagation conditions. There may be better choices for the form of the disparity field, but an assumption is necessary to demonstrate the technique and the emphasis of this work is on the modelling technique and not the assumption of the form of the disparity field.

5.5 Combined model of disparity vectors

In this section, we discuss limitations of the techniques proposed in sections 5.3 and 5.4. A third technique is proposed for modelling the disparity function which incorporates the strengths of both previous techniques, without the weaknesses of either. We refer to the technique introduced in this section as the *combined technique*, since the technique combines aspects of both of the previous techniques. We illustrate the combined technique in section 5.6.3. Finally, in section 5.5.4, we summarise and discuss the important points of this section.

5.5.1 Limitations of previous techniques

The techniques introduced in sections 5.3 and 5.4 both have obvious weaknesses. The most obvious weakness of the cosine technique is that the basis functions are arbitrarily chosen. The most obvious weakness of the empirical technique is the interpolation method, which is reliant on an arbitrary assumption: that the disparity field is maximally smooth.

Since the set of analytical basis functions is chosen arbitrarily, and the empirical functions are determined from the data, we hypothesise that the functions of the empirical technique represent a greater proportion of the spatial variance in the disparity field than the functions of the cosine technique. In the section 5.7, we test this hypothesis by measuring the proportion of the spatial variation in the disparity field accounted for by various subsets of basis functions.

Cosine technique

The cosine technique of section 5.3 requires a greater number of functions than the empirical technique of section 5.4 to represent the disparity function with the same accuracy (see section 5.7), and therefore a greater number of samples to determine the functions' coefficients. The cosine technique's requirement for a greater number of coefficients restricts the scenarios in which the disparity field can be adequately modelled by this technique, since only q coefficients can be determined from q multimode samples.

Empirical technique

The empirical technique represents the disparity function at a set of fixed grid-points by a linear combination of eigenvectors. As discussed in section 5.4.3, the most significant limitation of the empirical technique is its reliance upon an interpolation method. The interpolation method uses the assumption of a maximally smooth field, which is not necessarily justified. Furthermore, the interpolated field based on the arbitrary assumption of a maximally smooth disparity field may be very different from the actual disparity field.

5.5.2 The Combined Technique

We distinguish between the basis functions of section 5.3 and the basis functions of this section: we refer to the basis functions of section 5.3 as the *cosine* basis functions, denoted

$$\boldsymbol{\Phi} = \{\Phi_0, \Phi_1, \ldots, \Phi_N\};$$

we refer to the basis functions of the combined technique as the *combined* basis functions, denoted

$$\boldsymbol{\Psi}_k = \{\Psi_{k0}, \Psi_{k1}, \ldots, \Psi_{kN}\}.$$

Note the subscript k in the combined basis; the combined basis functions are different for the representation of each component of the disparity function. Basis function Ψ_{ki} is the i^{th} basis function in the representation of the k^{th} disparity function component. The idea is that we choose a linear transformation such that each combined basis function is itself a linear combination of the cosine basis functions. The change of basis, from the cosine basis $\boldsymbol{\Phi}$ to the combined basis $\boldsymbol{\Psi}_k$, is a linear transformation; formulated as

$$\boldsymbol{\Psi}_k = \mathbf{V}_k \boldsymbol{\Phi}$$

where $\mathbf{V}_k$ is termed the *transformation matrix*. Note that the combined functions may no longer be orthogonal.

One strength of the cosine technique of section 5.3 is that it represents the disparity function as a linear combination of analytical basis functions. Hence we embody this representation of the disparity function in the combined technique. However, we aim to represent the disparity function in terms of fewer basis functions than are required by the cosine technique. Consequently, the combined technique should have basis functions which are more representative of the disparity field than the basis functions of the cosine technique.

There is a high degree of correlation between the cosine basis function coefficients in representations of different disparity fields. The proportion of the total spatial variation which can be represented by one basis function of the combined technique is greater than 95%. We refer the interested reader to section 5.6.3 for verification of this statement. One strength of

the empirical technique of section 5.4 is that it models the spatial variation in the disparity field from empirical data. We derive inspiration from the empirical technique in developing a method of determining the transformation matrix $\mathbf{V}_k$; we use PCA.

5.5.3 Modelling via PCA on basis function coefficients

Consider the coefficients corresponding to the first p cosine basis functions selected (by dominance), denoted α_{kj}, $\forall j = 1 \ldots p$. We refer to a row vector of cosine coefficients, used to represent the disparity function by the linear combination of equation (5.2), as an *observation*. We denote the i^{th} observation of the variable α_{kj} by α_{kij}. Note that here we refer to the cosine basis function coefficients as variables, since they are the quantities which vary from observation to observation.

We determine p cosine coefficients of n previously observed disparity fields. We form a $n \times p$ matrix, denoted $\mathbf{A}_k$, containing the n observations of the p variables;

$$\mathbf{A}_k = \begin{bmatrix} \alpha_{k11} & \alpha_{k12} & \cdots & \alpha_{k1p} \\ \alpha_{k21} & \alpha_{k22} & \cdots & \alpha_{k2p} \\ \vdots & \vdots & \cdots & \vdots \\ \alpha_{kn1} & \alpha_{kn2} & \cdots & \alpha_{knp} \end{bmatrix}$$

where each row of the data matrix contains one observation of the variables from historical data.

The transformation matrix $\mathbf{V}_k$ contains row vectors of cosine coefficients. The i^{th} row contains the cosine coefficients for the i^{th} combined basis function Ψ_{ki}. We determine matrix $\mathbf{V}_k$ by performing PCA on the observation matrix $\mathbf{A}_k$, which contains row vectors of cosine coefficients. Each row vector of $\mathbf{A}_k$ contains the cosine coefficients corresponding to one *observation* of the k^{th} disparity function.

The coefficients which account for the maximum variation in the cosine basis function coefficients are the elements of the principle eigenvector (i.e. the eigenvector which corresponds to the largest eigenvalue) of the sample covariance matrix.

We decompose $\mathbf{A}_k$ via the SVD to find the eigenvectors of $\mathbf{A}_k^T\mathbf{A}_k$; thus

$$\mathbf{A}_k = \mathbf{U}_k\mathbf{L}_k\mathbf{V}_k^T \tag{5.10}$$

where $\mathbf{U}_k$, $\mathbf{L}_k$ and $\mathbf{V}_k$ are analogous to equation (5.4).

The *principle* linear combinations of cosine basis functions are contained in the columns of $\mathbf{V}_k$. Hence $\mathbf{V}_k$ is the transformation matrix referred to in section 5.5. We denote the column of $\mathbf{V}_k$ corresponding to the j^{th} largest singular value, i.e. the j^{th} largest element of $\mathbf{L}_k$, by the $(p \times 1)$ vector $\mathbf{v}_{kj}$. The column of $\mathbf{V}_k$ corresponding to the largest element of $\mathbf{L}_k$ represents the maximum variance in the cosine basis coefficients.

The functions of the combined basis Ψ_k are thus represented as

$$\Psi_{kj}(\mathbf{y}) = \sum_{i=1}^{p} v_{kij}\Phi_i(\mathbf{y}), \tag{5.11}$$

where v_{kij} is the element of the j^{th} principle linear combination corresponding to the i^{th} cosine basis function.

We represent the modelled value of the function $\hat{\mathrm{d}}_{mn,k}(\mathbf{y})$ as a linear combination of the n combined basis functions:

$$\hat{\mathrm{d}}^{com}_{mn,k}(\mathbf{y}) = \sum_{j=1}^{n} \omega_{kj}\Psi_{kj}(\mathbf{y}) \tag{5.12}$$

where ω_{kj} is the coefficient corresponding to the j^{th} combined basis function. We express $\hat{\mathrm{d}}^{emp}_{mn,k}$ in terms of the basis Φ by inserting equation (5.11) into equation (5.12);

$$\hat{\mathrm{d}}^{com}_{mn,k}(\mathbf{y}) = \sum_{j=1}^{n} \omega_{kj} \sum_{i=0}^{p} v_{kij}\Phi_i(\mathbf{y}). \tag{5.13}$$

5.5.4 *Summary and Discussion*

The technique of section 5.3 represents the disparity function analytically as a linear combination of basis functions, but has a disadvantage: it lacks a mechanism for incorporating historical data. On the other hand, the technique of section 5.4 incorporates historical data via PCA, but it also has a disadvantage: the form of the disparity field between the grid-points must be arbitrarily chosen.

The technique of section 5.5 combines the advantages of the methods presented in section 5.3 and section 5.4, while avoiding the major disadvantages of both: a function which is defined analytically over the radar coverage but which exploits a lot of historical data.

5.6 Demonstration

We demonstrate each of the proposed techniques of sections 5.3, 5.4 and 5.5 in sections 5.6.1, 5.6.2 and 5.6.3, respectively. In these demonstrations, we measure the error in the estimated disparity function $\hat{\mathrm{d}}_{mn,k}$ when a limited number of basis functions are available. The demonstrations in this section are not intended to be comparative; a comparative study of the three techniques appears in section 5.7.

To reduce the complexity of the demonstration and the comparison in section 5.7, we only consider the range component of $\hat{\mathrm{d}}_{mn,k}$, denoted ΔR, and the azimuthal component, denoted ΔA. These components are the differences in radar measurements of a pair of multimode detections from the same target. We simulate the corresponding radar measurements: the

delay, or *slant range*, denoted R_s, and the apparent azimuth, denoted A_s, for the multimode detections of each target, using the propagation rules in Appendix A. The Doppler data is the most accurate in real data, and also the best discriminator between associated and non-associated pairs of tracks. Therefore we anticipate that all methods will perform better with the inclusion of Doppler data.

5.6.1 Cosine technique

As a demonstration of the technique of section 5.3, we model components of the disparity function as a linear combination of the functions with the greatest coefficients. These functions are also referred to as the dominant functions. The first stage of the cosine technique is the determination of the dominant cosine functions. The discrete cosine transform (DCT) [1], is a standard technique for determining the coefficients of discrete cosine functions, and we employ this transform for such purpose here. To determine the dominant discrete cosine functions, we apply the DCT to a typical disparity field. Note that the DCT operates upon an evenly spaced grid of data. Therefore we generate a grid of data of a typical disparity field. The typical disparity field is obtained either from historical data, or via simulation. We demonstrate the latter case (of a simulated disparity field) here.

The azimuthal component of the simulated disparity field, shown in figure 5.2, varies with respect to both the range and azimuth radar measurements, whereas the range component varies only with respect to range. For demonstration, we apply the DCT on the more 'interesting' of the two components considered, which is the grid of data representing the azimuthal component of the disparity field. We obtain the coefficients of the basis functions by applying the DCT to the grid of simulated data in figure 5.2. The corresponding DCT coefficients are shown in figure 5.3(a). Note that the DCT coefficients corresponding to the even azimuthal functions are zero, because the azimuthal disparity is odd symmetric about bore-sight. The coefficients which are even in azimuth are all zero. For clarity, we display only the odd coefficients of the DCT in figure 5.3(b). Note that the greatest coefficients are those corresponding to the low frequency cosine functions, and size of the coefficients diminishes with an increase in frequency. This property is invariant as the virtual heights of the ionospheric layers vary in the simulation.

The dominant functions apparent from figure 5.3(a), and figure 5.3(b) are (in order of significance):

$$\begin{aligned}
\Phi_{10}(y_1, y_2) &= \cos(y_1) \\
\Phi_{11}(y_1, y_2) &= \cos(y_1)\cos(y_2) \\
\Phi_{30}(y_1, y_2) &= \cos(3y_1) \\
\Phi_{12}(y_1, y_2) &= \cos(y_1)\cos(2y_2)
\end{aligned}$$

$$\begin{aligned}\Phi_{13}(y_1, y_2) &= \cos(y_1)\cos(3y_2)\\ \Phi_{31}(y_1, y_2) &= \cos(3y_1)\cos(y_2)\\ &\vdots\end{aligned}$$

The two dominant cosine functions are the two lowest frequency functions: $\Phi_{10}(y_1, y_2)$, which is simply $\cos(y_1)$ and $\Phi_{11}(y_1, y_2)$, which is $\cos(y_1)\cos(y_2)$. The magnitudes of these two functions are plotted with respect to range and azimuth in figures 5.4 and 5.5, respectively.

In order to demonstrate the proportion of the field representable by the dominant basis functions, we demonstrate a linear combination of the first two dominant functions. The linear combination of the two functions is formulated thus:

$$\hat{\mathrm{d}}^{cos}_{mn,k}(y_1, y_2) = A_{k10}\Phi_{10}(y_1, y_2) + A_{k11}\Phi_{11}(y_1, y_2).$$

We combine these functions in the ratio determined by the DCT of the simulation in figure 5.2, in which case $A_{k10} = 3607$, and $A_{k11} = 1624$. The ΔA component of the disparity function resulting from the linear combination of the 2 dominant basis functions is shown in figure 5.6. The error between the original field of figure 5.2 and the modelled field of figure 5.6 is displayed in figure 5.7.

In addition to the combination of two basis functions, we also demonstrate the proportion of the field represented by a linear combination of the four dominant functions. The coefficients for the linear combination are as determined by the DCT of the simulation in figure 5.2; namely, $A_{k10} = 3607$, $A_{k11} = 1624$, $A_{k30} = 520$ and $A_{k12} = 439$. The ΔA component of the disparity function resulting from the linear combination is shown in figure 5.8. The error between the original field of figure 5.2 and the modelled field is shown in figure 5.9.

It is apparent that a linear combination of the two dominant basis functions represents a significant portion of the azimuthal component of the disparity field. The inclusion of the next two functions, by dominance, in the linear combination improves the approximation slightly.

5.6.2 Empirical technique

In section 5.4 we introduced the empirical technique, and, in this subsection, we perform a demonstration of this technique. We demonstrate the ability of the empirical technique to model the estimated disparity function $\hat{\mathrm{d}}_{mn,k}$, which defines the k^{th} component of the disparity field. Furthermore, we demonstrate that it can describe the majority of the spatial variance of the disparity field in terms of just a few eigenvectors.

We determine the eigenvectors for the azimuthal disparity ΔA and the range disparity ΔR from a set of simulated data. To generate the data set, our simulation contains two ionospheric layers; the E layer and the F layer. We denote the heights of the corresponding

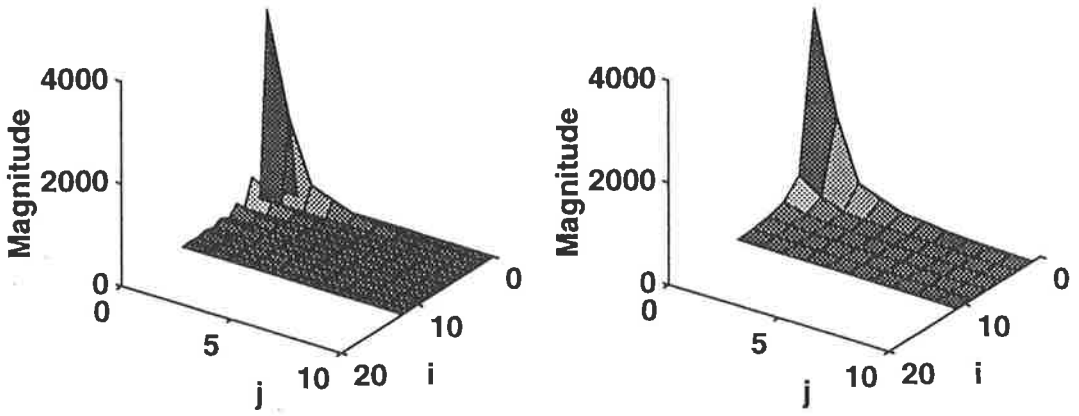

(a) All cosine coefficients.

(b) Odd cosine coefficients.

Figure 5.3: Coefficients of 2D DCT, applied to ΔA grid.

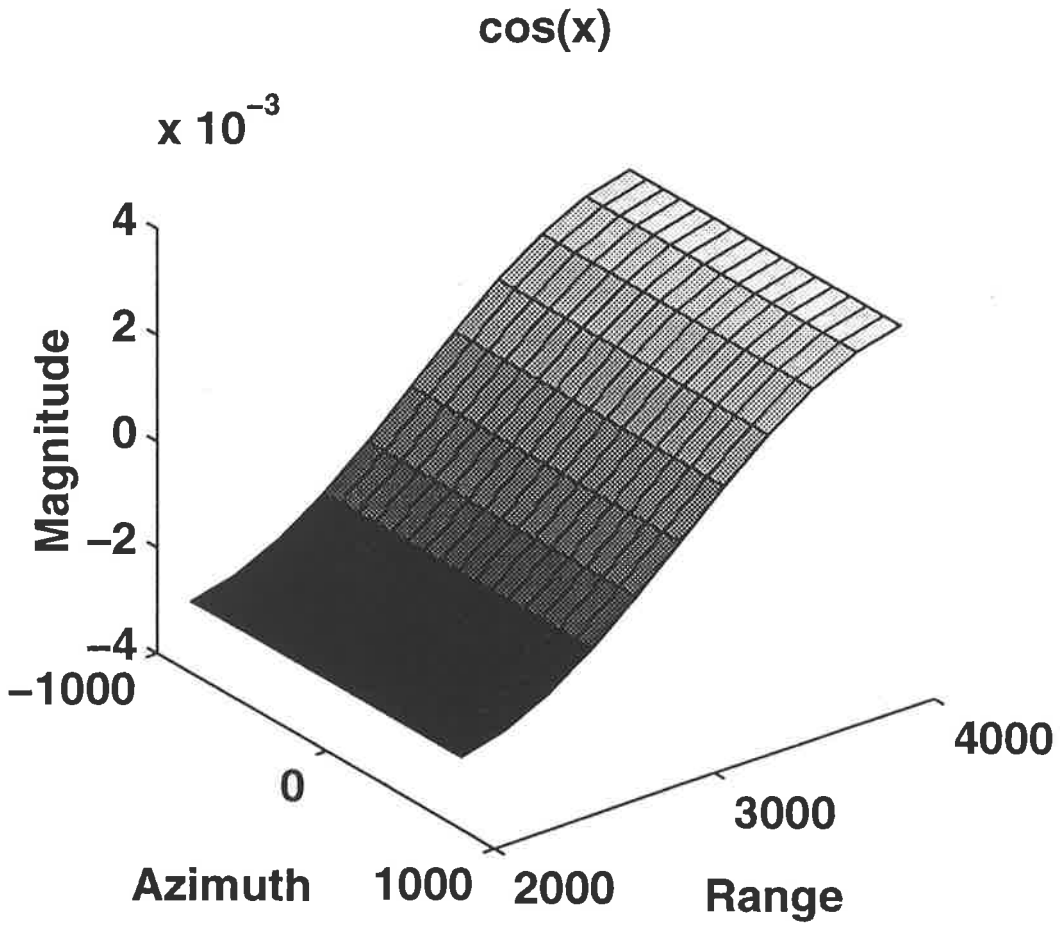

Figure 5.4: The dominant basis function

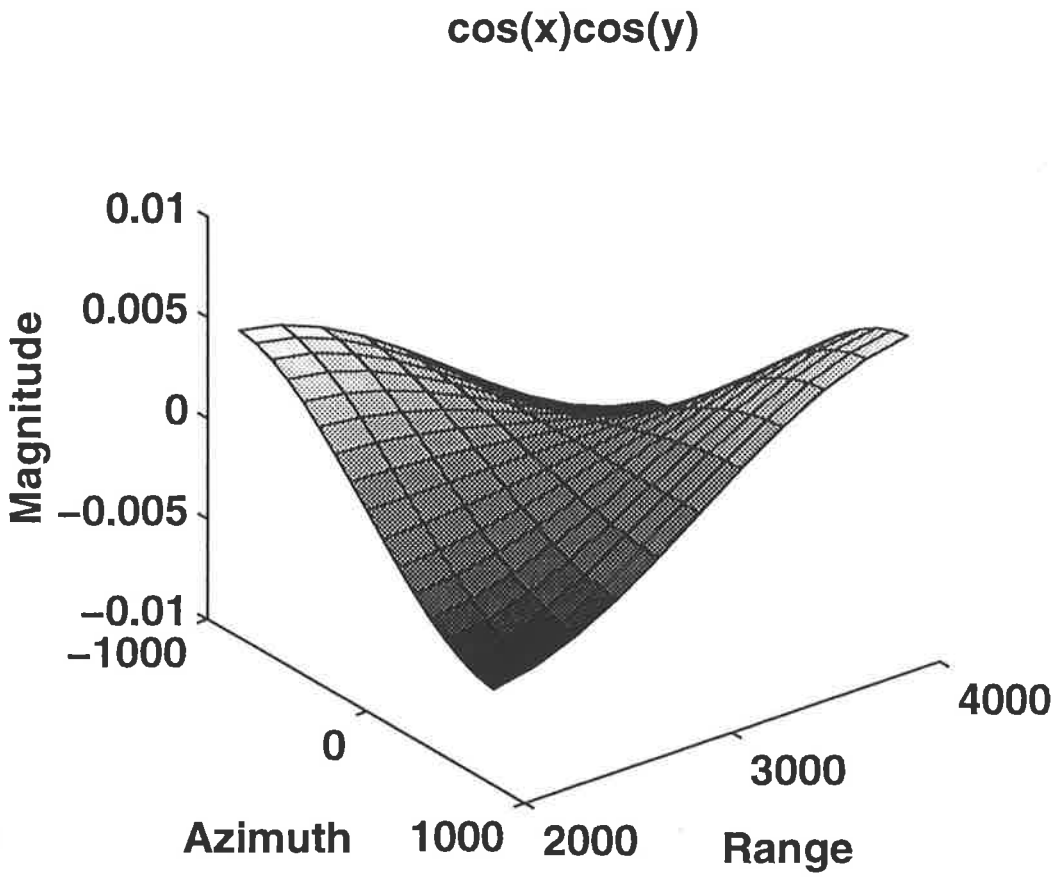

Figure 5.5: The 2^{nd} basis function, by dominance.

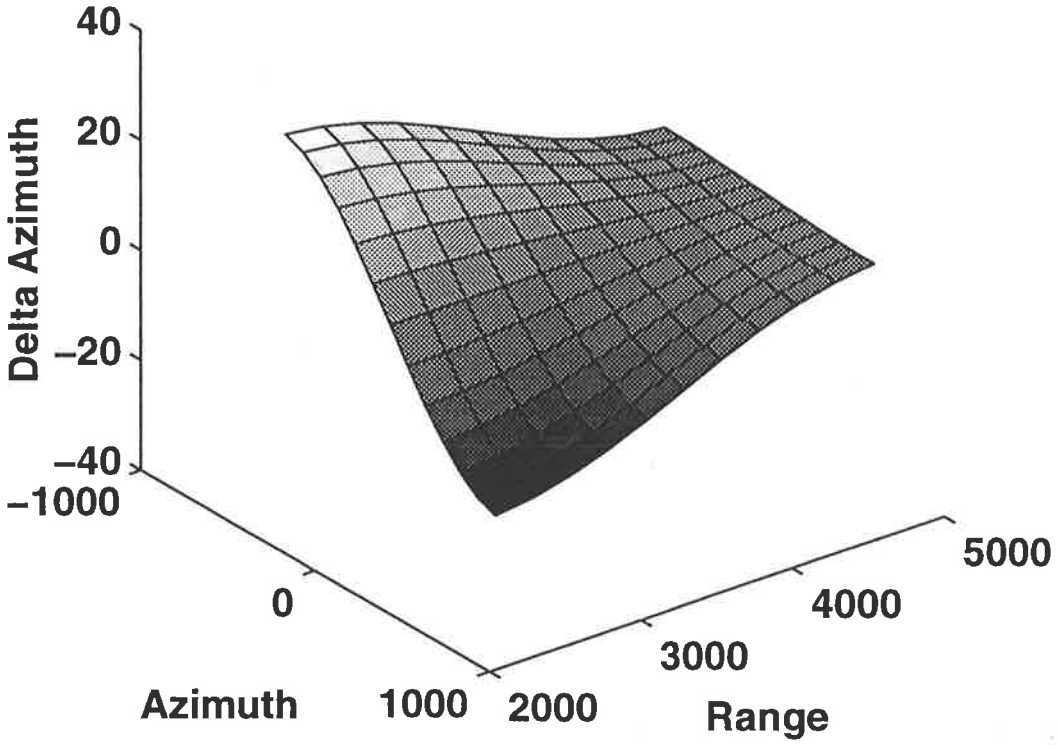

Figure 5.6: ΔA modelled by 2 basis functions.

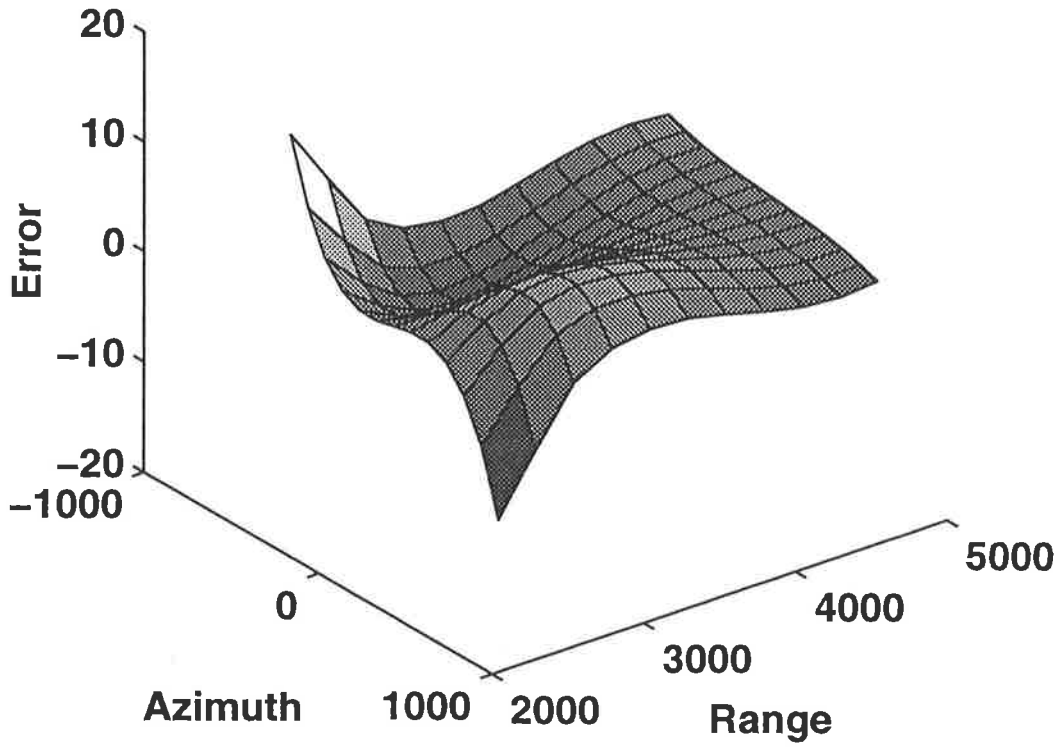

Figure 5.7: Difference between actual field and field modelled by 2 basis functions.

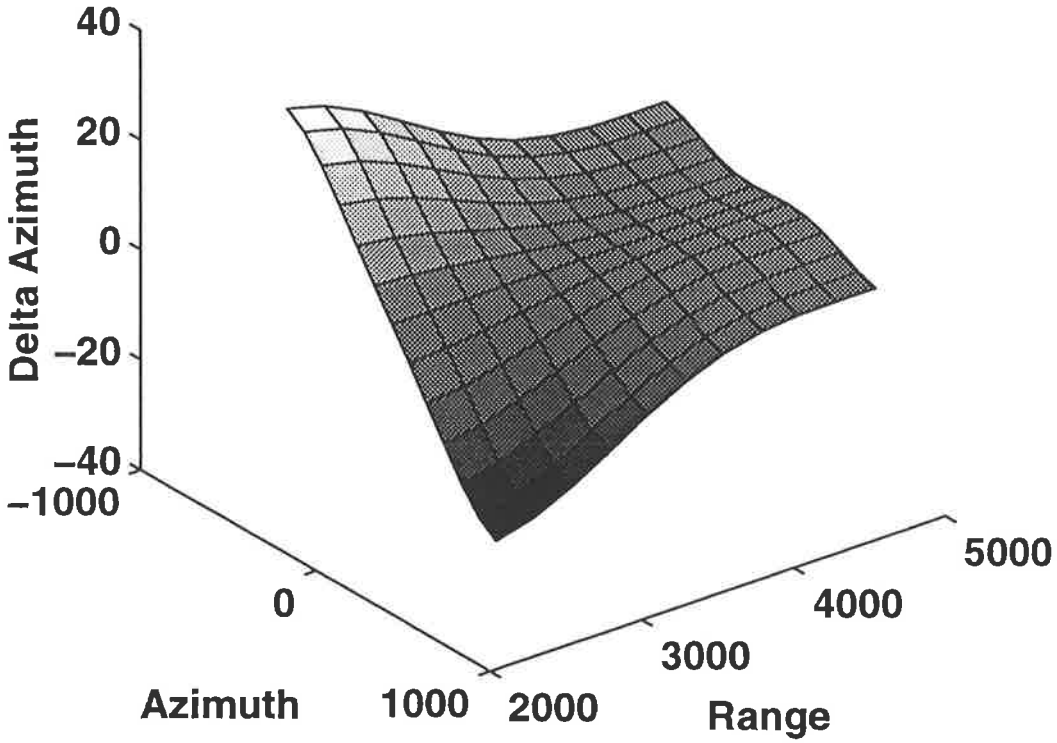

Figure 5.8: ΔA modelled by 4 basis functions.

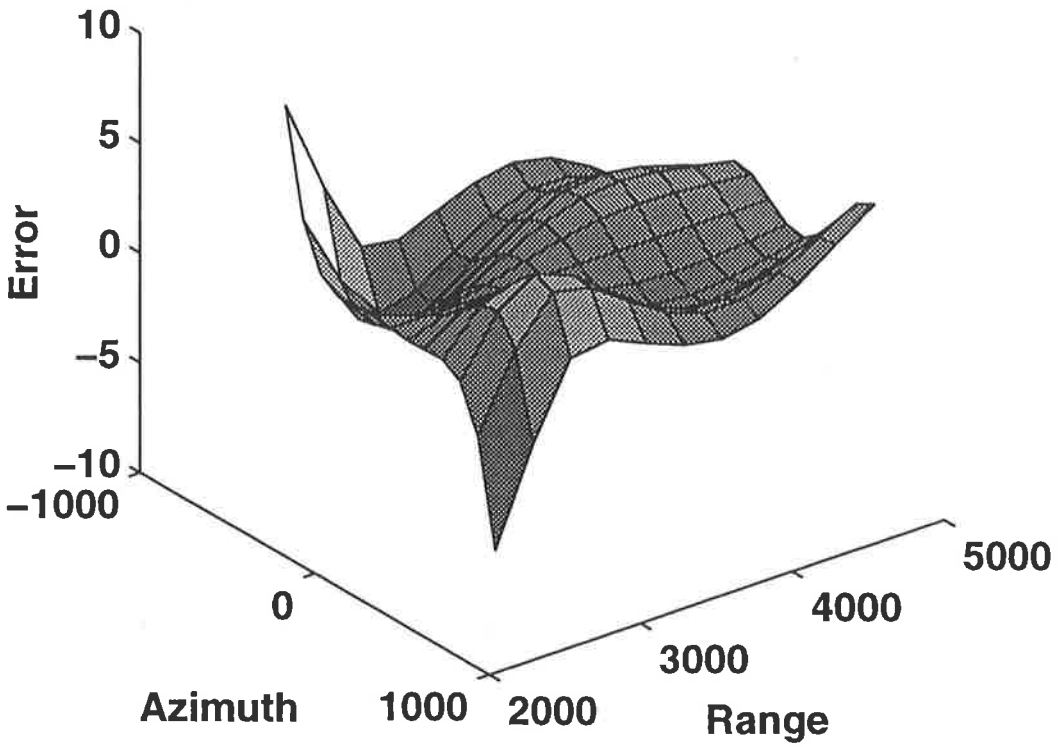

Figure 5.9: Difference between actual field and field modelled by 4 basis functions.

virtual reflecting layers by variables h_E and h_F, respectively. The variables h_E and h_F take on values which represent a wide range of ionospheric conditions; these values lie within the bounds specified by [32]. The values of h_E and h_F are selected from the pair of sets:

$$h_E \in \{90, 94, 98, 102, 106, 110\} \quad \text{(in kilometres) and} \tag{5.14}$$

$$h_F \in \{200, 240, 280, 320, 360, 400\} \quad \text{(in kilometres).} \tag{5.15}$$

Note that we do not impose any interdependence on the variables; we perform the simulation for every combination of the variables h_E and h_F. The total number of such combinations is $C_1^6 \times C_1^6 = 36$. We simulate ten scenarios of each combination of h_E and h_F, making a total of 360 scenarios. Each scenario contains ten targets, and each target has a random range and azimuth, chosen from uniform distributions within the following range of values:

$$\begin{aligned} 800 < \quad R \quad &< 2800 \ \text{(in kilometres) and} \\ -800 < \quad A \quad &< 800 \ \text{(in milliradians),} \end{aligned}$$

where R and A denote the actual range, and actual azimuth of a target, respectively. Thence we calculate some radar measurements for each target: the slant range R_s and the apparent azimuth A_s, and thence the azimuthal disparity ΔA and the range disparity ΔR. We demonstrate the modelling of the disparity field between the pair of modes EE and EF, since the disparity $\mathrm{d}_{EE,FF}$ between modes EE and EF has both an azimuthal component ΔA, and a range component ΔR.

The empirical technique operates on values of the disparity field at fixed locations. Yet the disparity field will rarely, if ever, be available at these locations. Hence we interpolate the components of the disparity vector, ΔA and ΔR to fixed locations, referred to as grid-points, in the radar measurement space. The interpolation scheme is the same as that used in section 5.4.2 (see [42]). The grid-point locations may be arbitrarily chosen, but for the sake of simplicity, we choose the grid-points to be in an evenly spaced, rectangular grid in the radar measurement space. The grid-points take every combination of R_s and A_s from the following sets:

$$R_s \in \{2500, 2750, 3000, \ldots, 5000\} \quad \text{(in kilometres) and} \tag{5.16}$$

$$A_s \in \{-600, -500, -400, \ldots, 600\} \quad \text{(in kilometres).} \tag{5.17}$$

We have 11 values of range, and 13 of azimuth; thus the total number of grid-points is $11 \times 13 = 143$. We estimate the azimuthal disparity at the grid-points, using the azimuthal disparity of every target in the scenario. We use the interpolation function $\mathcal{F}$ (introduced in equation (5.8)) to estimate the azimuthal disparity at grid-point i; thus

$$\Delta A(\mathbf{y}_i) = \mathcal{F}(\mathbf{T}_{\Delta A}, \mathbf{y}_i), \tag{5.18}$$

where $\mathbf{T}_{\Delta A}$ is a 10×3 matrix, containing the pivotal points for the interpolation. Each row of $\mathbf{T}_{\Delta A}$ contains the relevant radar measurements for one target: the delay R_s, the apparent azimuth A_s, and the azimuthal disparity ΔA. Similarly, we estimate the range disparity at grid-point i thus

$$\Delta R(\mathbf{y}_i) = \mathcal{F}(\mathbf{T}_{\Delta R}, \mathbf{y}_i). \tag{5.19}$$

$\mathbf{T}_{\Delta R}$ is a 10×3 matrix of the pivotal points for the interpolation. Each row of $\mathbf{T}_{\Delta R}$ contains the relevant radar measurements for one target: the delay R_s, the apparent azimuth A_s, and the range disparity ΔR.

We form a sample data matrix for the azimuthal disparity, denoted $\mathbf{X}_{\Delta A}$, and another sample data matrix for the range disparity, denoted $\mathbf{X}_{\Delta R}$. Each sample data matrix contains 360 observations of the 143 variables; each observation is a scenario and each variable is the estimated disparity at a grid-point. We perform the PCA on sample data matrices $\mathbf{X}_{\Delta A}$ and $\mathbf{X}_{\Delta R}$, using the SVD. We demonstrate the empirical technique by displaying the eigenvectors; the principal eigenvector of the azimuthal disparity is shown in figure 5.10. Note that the form of this eigenvector closely resembles the actual field of the azimuthal disparity, shown in figure 5.2.

To measure the success of the modelling demonstration, we define ζ_{kq} as the proportion of the total spatial variation accounted for by the first q (of n) eigenvectors, calculated as a percentage of the total variation; thus

$$\zeta_{ki} = \frac{\sum_{i=1}^{q} \lambda_{ki}}{\sum_{j=1}^{n} \lambda_{kj}}, \tag{5.20}$$

where λ_{ky} denotes the j^{th} diagonal element of matrix $\mathbf{L}_k$, which is the square root of the eigenvalue corresponding to eigenvector $\mathbf{v}_{kj}$ of the matrix $\mathbf{X}_k^T\mathbf{X}_k$. Note that the expression in equation (5.20) is a measure of the quality of the error fit at the observation points; it is not intended as an absolute guide to the intrinsic quality of the estimated disparity function. The proportion of the total spatial variation accounted for by the first eigenvector, shown in figure 5.10 is $\zeta_{\Delta A1} = 46.7\%$ (from equation (5.20)). For comparison, we show the 2nd eigenvector of the azimuthal disparity in figure 5.11. The proportion of the total spatial variation accounted for by a linear combination of the first 2 eigenvectors is $\zeta_{\Delta A2} = 58.0\%$. The eigenspectrum of the sample covariance matrix is also of interest. We can inspect the relative 'significance' of the eigenvalues $\lambda_{ki} \forall i$. The eigenspectrum of $\mathbf{X}_k^T\mathbf{X}_k$ for the azimuthal disparity is shown on a logarithmic scale in figure 5.12. The values of $\zeta_{\Delta Ai}$ are computed via equation (5.20), and appear in table 5.1 for several values of i.

We show the first and second eigenvectors of the range disparity in figures 5.13 and 5.14. The eigenspectrum of the corresponding $\mathbf{X}_k^T\mathbf{X}_k$ matrix is shown on a logarithmic scale in figure 5.15. Note that the first eigenvalue is significant, but thereafter the eigenvalues diminish quickly. The first eigenvector accounts for $\zeta_{\Delta R1} = 93.6\%$ of the total spatial

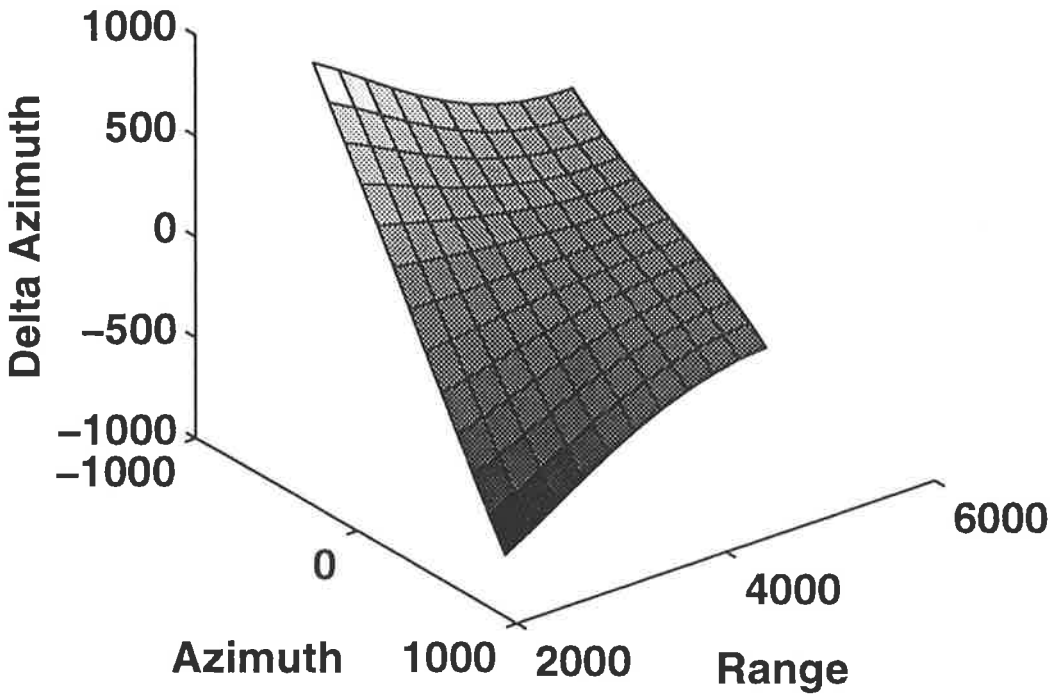

Figure 5.10: First eigenvector at grid-points for azimuthal disparity ΔA.

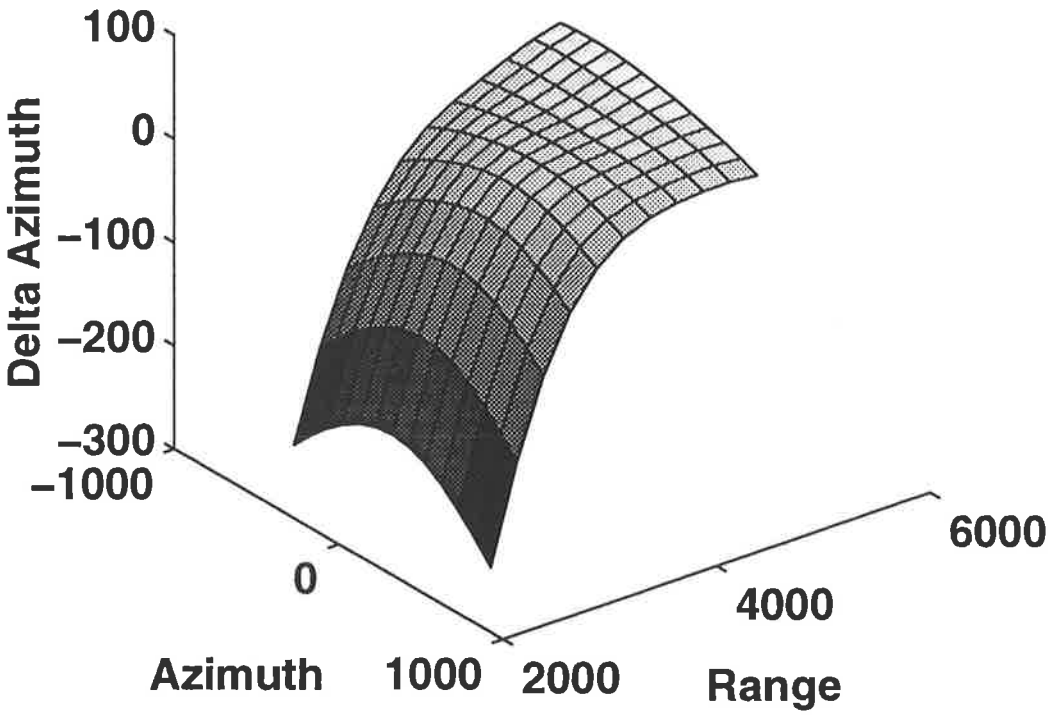

Figure 5.11: Second eigenvector at grid-points for azimuthal disparity ΔA.

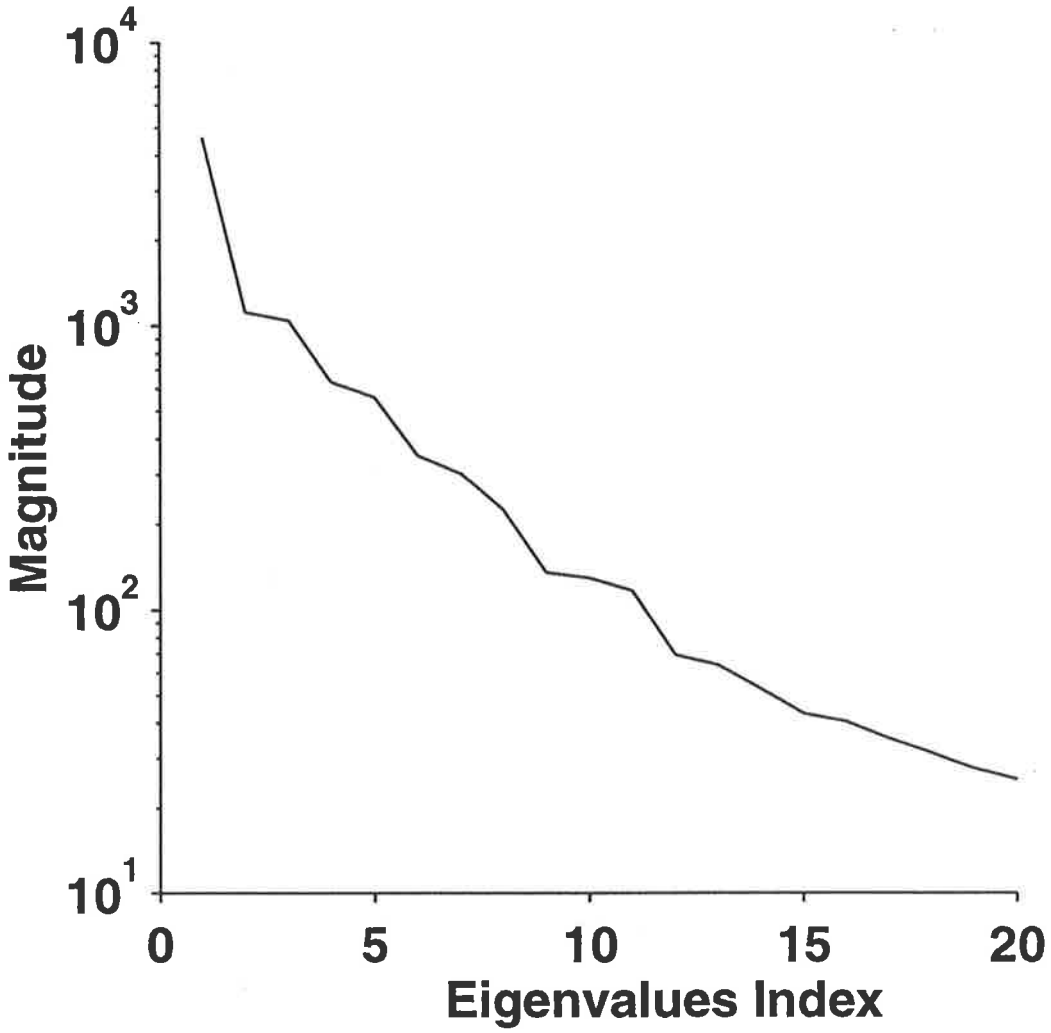

Figure 5.12: Eigenspectrum of $\mathbf{X}_k^T\mathbf{X}_k$ for ΔA.

Components	$i = 1$	$i = 2$	$i = 5$	$i = 10$
$\zeta_{\Delta Ai}$	46.7 %	58.0 %	80.6 %	92.1 %
$\zeta_{\Delta Ri}$	93.6 %	96.2 %	98.3 %	99.3 %

Table 5.1: Proportion of total spatial variation of eigenvectors.

variation, whereas the first two eigenvectors account for $\zeta_{\Delta R2} = 96.2\%$ of this variation. The values of $\zeta_{\Delta Ri}$ are computed via equation (5.20), and appear in table 5.1 for several values of i.

We combine the azimuthal disparity and the range disparity of figures 5.10 and 5.13 to figure 5.16. In this figure, we illustrate the direction and relative magnitude of the disparity throughout the radar coverage. For the sake of clarity, we have only displayed the disparity at half of the grid-points.

5.6.3 *Combined technique*

In section 5.5 we introduced the combined technique, and, in this subsection, we perform a limited demonstration of this technique. The purpose of this demonstration is to measure the error in the estimated disparity function $\hat{\mathrm{d}}_{mn,k}$ when a limited number of basis functions are available. We perform the DCT on grids of simulated data, in a similar way to the technique of section 5.3. The cosine basis function coefficients, the cosine function coefficients, for the grid of data are obtained by the transform. We remind the reader that we refer to these coefficients as variables, and we refer to an instance of these variables as an observation (see section 5.5.3).

Since the purpose of this demonstration is to measure the error in the estimated disparity function with respect to the number of basis functions used, we do not want the basis functions themselves to introduce an error. Therefore we allow the basis functions to be as accurate as possible, by computing them from a dense source of data.

To obtain the cosine coefficients for this demonstration, we require a grid of samples of the disparity field. Since we do not have a way of directly computing the disparity function at the grid-points, we obtain the values of the disparity field via simulation.

We simulate a high density of targets in the target space, and calculate the radar measurements, and thus the disparities, of the corresponding multimode detections. We interpolate the dense field of measurements to obtain the values of the disparity field at the grid-points. Figure 5.2 shows a typical grid of data for the azimuthal component ΔA of the disparity field.

Some aspects of the simulation in this section are the same as the simulation in section 5.6.2. We simulate two ionospheric layers; the E layer and the F layer. We denote the heights of the corresponding virtual reflecting layers by variables h_E and h_F, respectively.

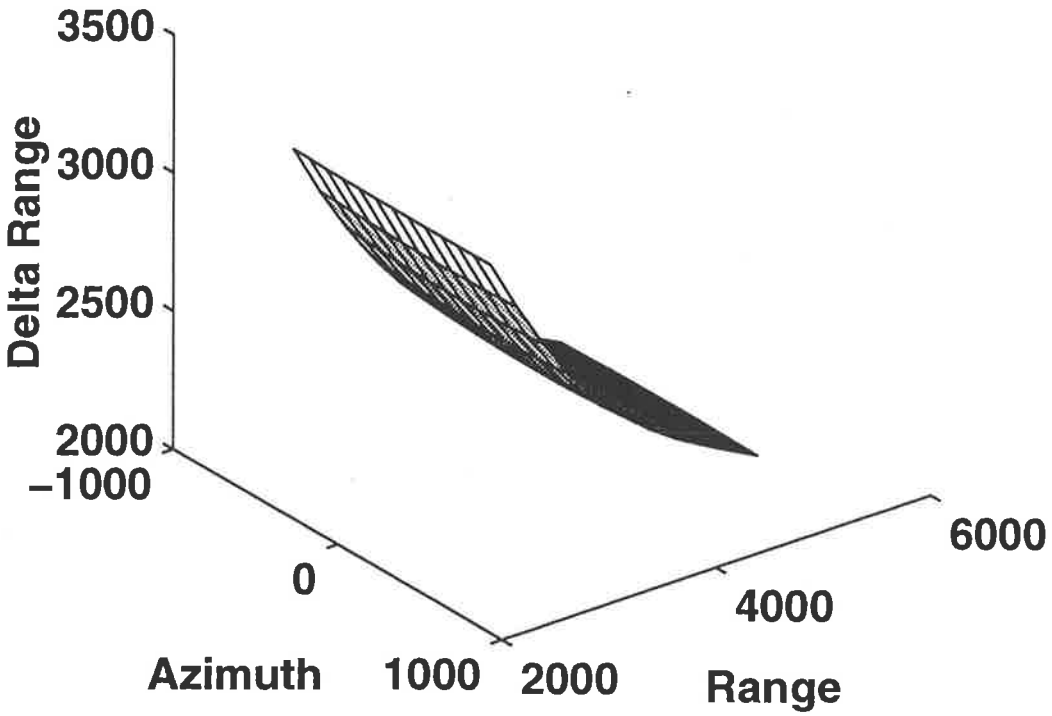

Figure 5.13: First eigenvector at grid-points for range disparity ΔR.

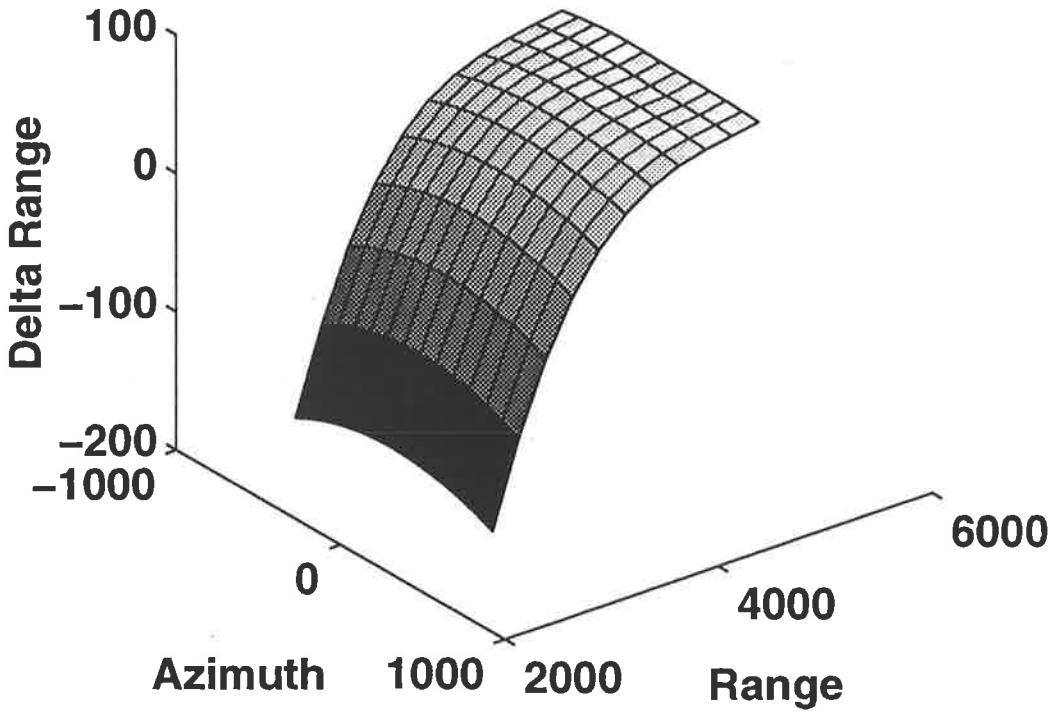

Figure 5.14: Second eigenvector at grid-points for range disparity ΔR.

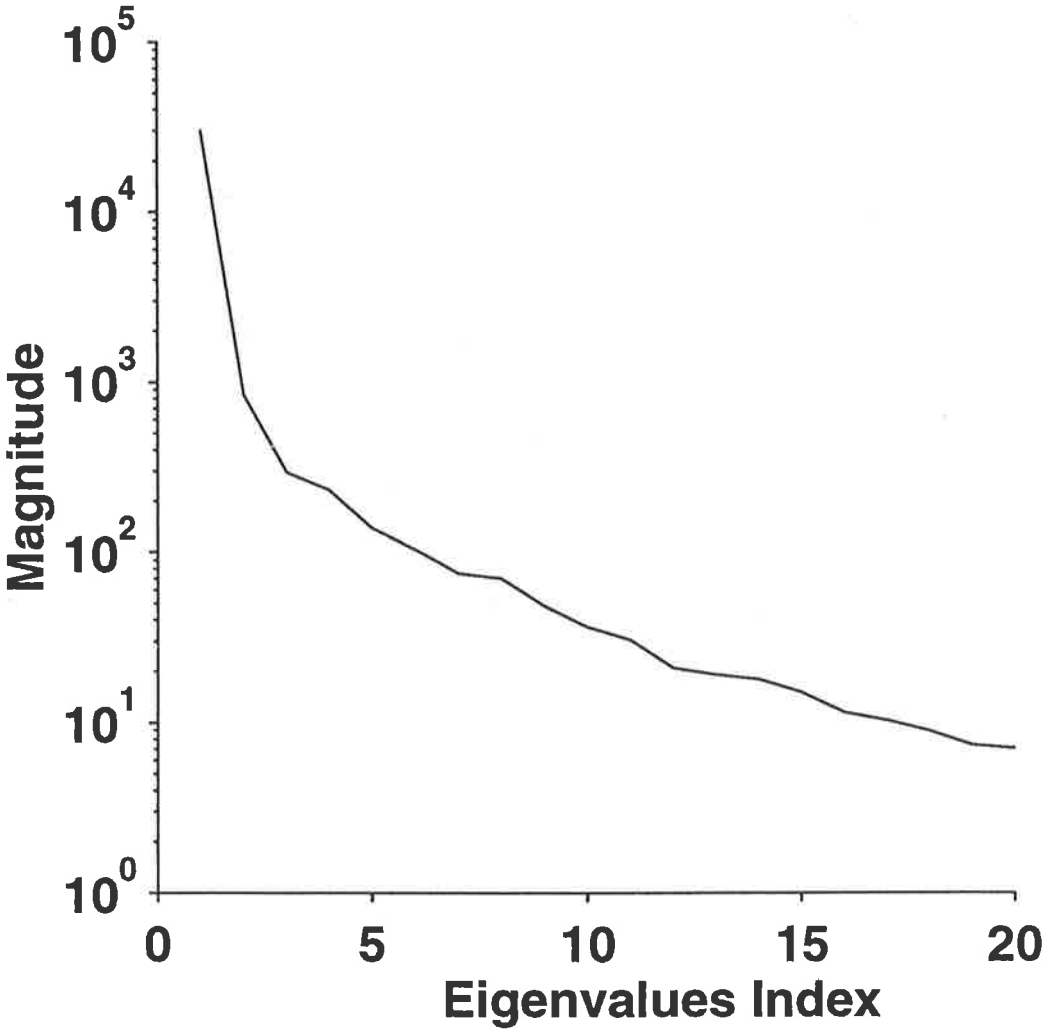

Figure 5.15: Eigenspectrum of $\mathbf{X}_k^T \mathbf{X}_k$ for ΔR.

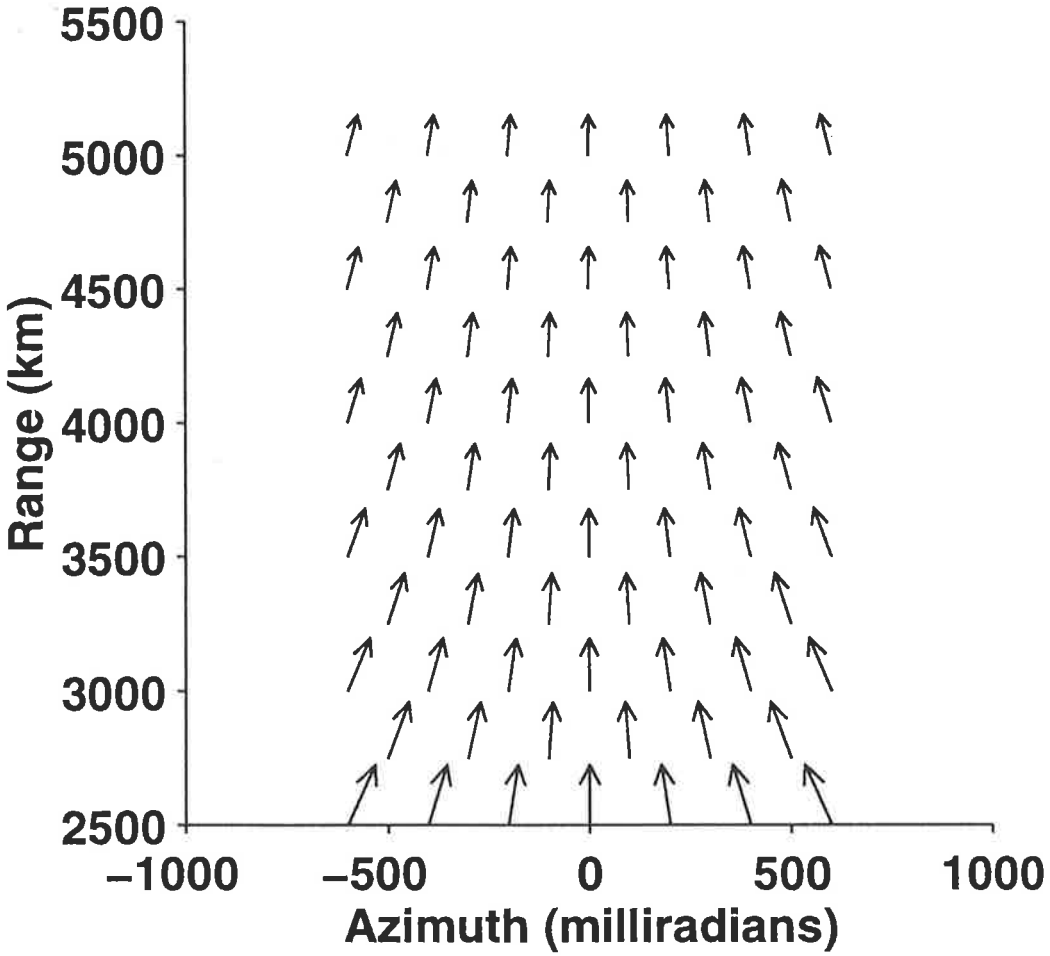

Figure 5.16: Relative magnitude and direction of the disparity between modes EE and EF.

As in section 5.6.2, we select the values of h_E and h_F from the sets in equations 5.14 and 5.15. We simulate every combination of h_E and h_F; 36 combinations in total.

The DCT of the combined technique operates on an evenly spaced grid of disparities in the radar measurement space; either ΔA or ΔR. We generate the evenly spaced grid by interpolating the disparities corresponding to the multimode detections of simulated targets. We first simulate a dense grid of targets in the target space. We choose a dense grid because we want to eliminate, as near as practicable, any bias the interpolation function may introduce to the grid of data. The grid-points take every combination of R and A from the following sets:

$$R \in \quad \{800, 900, 1000, \ldots, 2800\} \quad \text{(in kilometres) and} \tag{5.21}$$

$$A \in \quad \{-800, -700, -600, \ldots, 800\} \quad \text{(in kilometres).} \tag{5.22}$$

The total number of grid-points is $21 \times 17 = 357$. We then calculate the radar measurements of the corresponding multimode detections for each simulated target using the propagation rules in Appendix A. Thence we calculate the corresponding value of the disparity function components for each target: the azimuthal disparity ΔA and the range disparity ΔR. As in section 5.6.2, we demonstrate the modelling of the disparity function between the pair of modes EE and EF.

The DCT of the combined technique, as implemented by the author, operates on an evenly spaced rectangular grid in the radar measurement space. The grid-points take every combination of R_s and A_s from the sets in equations 5.16 and 5.17. To estimate the disparity function component at each grid-point, we use the biharmonic spline interpolation, referred to in section 5.4.2:

$$\Delta A(\mathbf{y}_i) = \mathcal{F}(\mathbf{T}_{\Delta A}, \mathbf{y}_i).$$

$\mathbf{T}_{\Delta A}$ is a (357×3) matrix, containing the pivots of the interpolation. Each row of $\mathbf{T}_{\Delta A}$ contains the relevant radar measurements for one target: the delay R_s, the apparent azimuth A_s, and the azimuthal disparity ΔA. Similarly, we estimate the range disparity by analogy with equation (5.19).

We perform the DCT on each grid of data, and we refer to the resulting set of p coefficients as an observation of the p variables. Each observation is stored in sample matrix $\mathbf{A}_k$, which contains n observations on the p variables. Having obtained a matrix of DCT coefficients, we decompose $\mathbf{A}_k$ using the SVD of equation (5.10). One of the results of the decomposition is the transformation matrix $\mathbf{V}_k$.

We calculate the proportion of the variation in the coefficients accounted for by eigenvectors of the sample covariance matrix, using equation (5.20) to perform this calculation.

In the case of sample matrix $\mathbf{A}_{\Delta A}$, the disparity field resulting from applying the inverse discrete cosine transform (IDCT) [23] to the first PC is shown in figure 5.17. The proportion of the total variation in the coefficients accounted for by this PC is $\zeta_{\Delta A}1 = 97.8\%$; whereas

Components	$i = 1$	$i = 2$	$i = 5$	$i = 10$
$\zeta_{\Delta Ai}$	97.9 %	99.9 %	100.0 %	100.0 %
$\zeta_{\Delta Ri}$	99.3 %	100.0 %	100.0 %	100.0 %

Table 5.2: Proportion of variation of coefficient eigenvectors.

the first two PCs account for a total of $\zeta_{\Delta A}2 = 99.9\%$. The disparity field resulting from the IDCT on the second PC is shown in figure 5.18. table 5.2 contains the proportion of the total variation in coefficients accounted for by a number of principle components, calculated as a percentage of the total variation. The eigenspectrum of the sample covariance matrix is shown in figure 5.19.

In the case of sample matrix $\mathbf{A}_{\Delta R}$, the disparity field resulting from the IDCT of the first PC is shown in figure 5.20; this PC accounts for 99.3 % of the total variation in the cosine basis function coefficients. The disparity field resulting from the IDCT on the second PC is shown in figure 5.21. The eigenspectrum of the sample covariance matrix is shown in figure 5.22

5.6.4 Discussion

The demonstration of section 5.6.1 illustrates that the disparity function can be represented by cosine functions, which is hardly surprising. Moreover, we note that the majority of the spatial variation of the disparity function can be represented by only a few of the low frequency cosine functions. There may, however, be better choices of basis function. A set of basis functions which requires fewer basis functions than another set to adequately represent the same disparity function, is an improved choice; with fewer coefficients to be determined, the set of basis functions can represent the disparity function in situations where there are fewer multimode samples available.

The demonstration of section 5.6.2 contrasts clearly with the demonstration in section 5.6.1. The majority of the spatial variation in the disparity function can be represented by a few functions from a heuristically chosen set of basis functions (the cosine functions). Contrastingly, the dominant basis functions of the empirical technique represent a much larger portion of the spatial variation in disparity function. The advantage of the empirical technique is that it can represent far more of the spatial variation of the disparity field with less functions than the cosine technique. Nonetheless, a disadvantage of the empirical technique is its reliance on the assumption of a maximally smooth field. While a rudimentary simulation of a disparity field may approach maximal smoothness between sampled points, the assumption may not be justified in the case of real OTHR data.

The technique demonstrated in section 5.6.3 is a combination of the cosine technique and

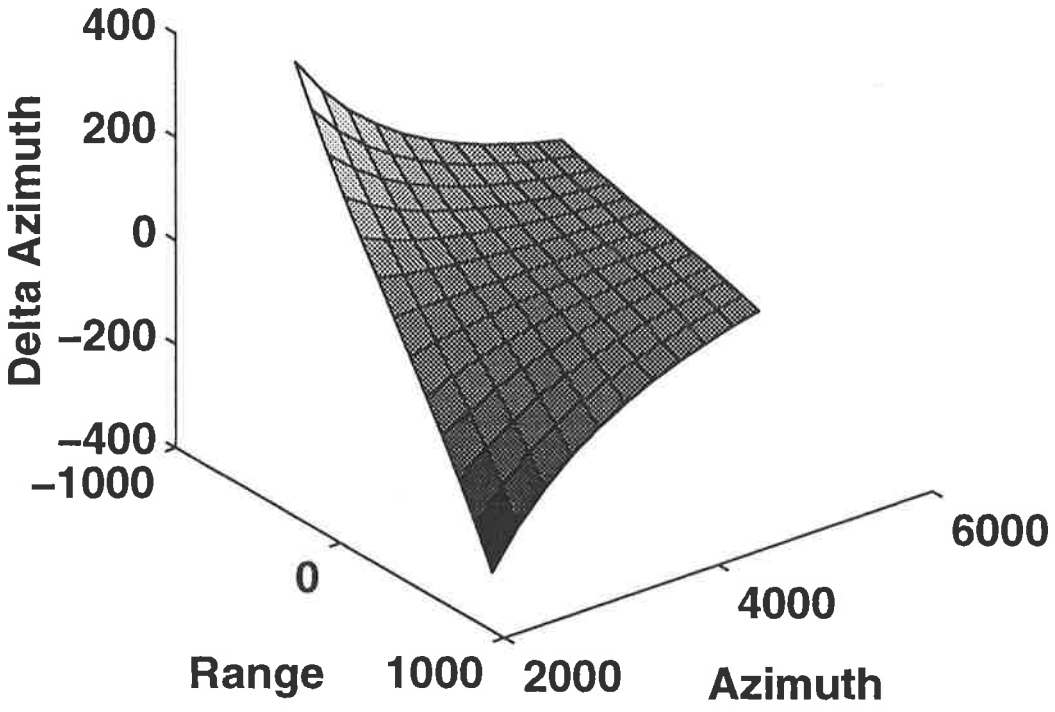

Figure 5.17: IDCT of first PC of ΔA sample cov. matrix.

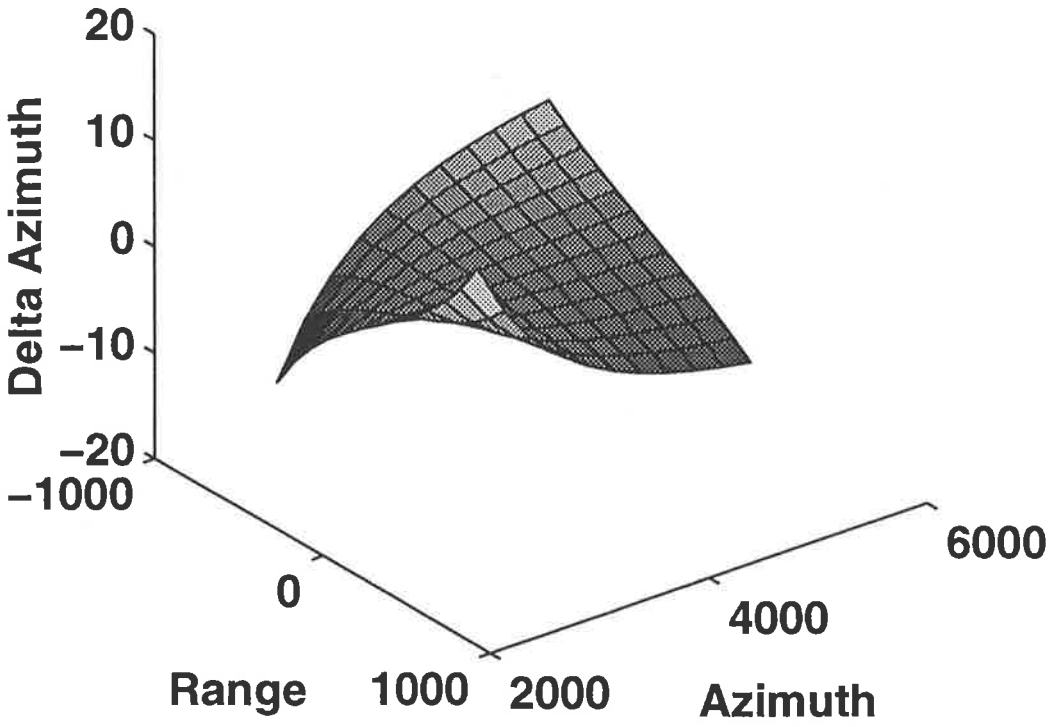

Figure 5.18: IDCT of second PC of ΔA sample cov. matrix.

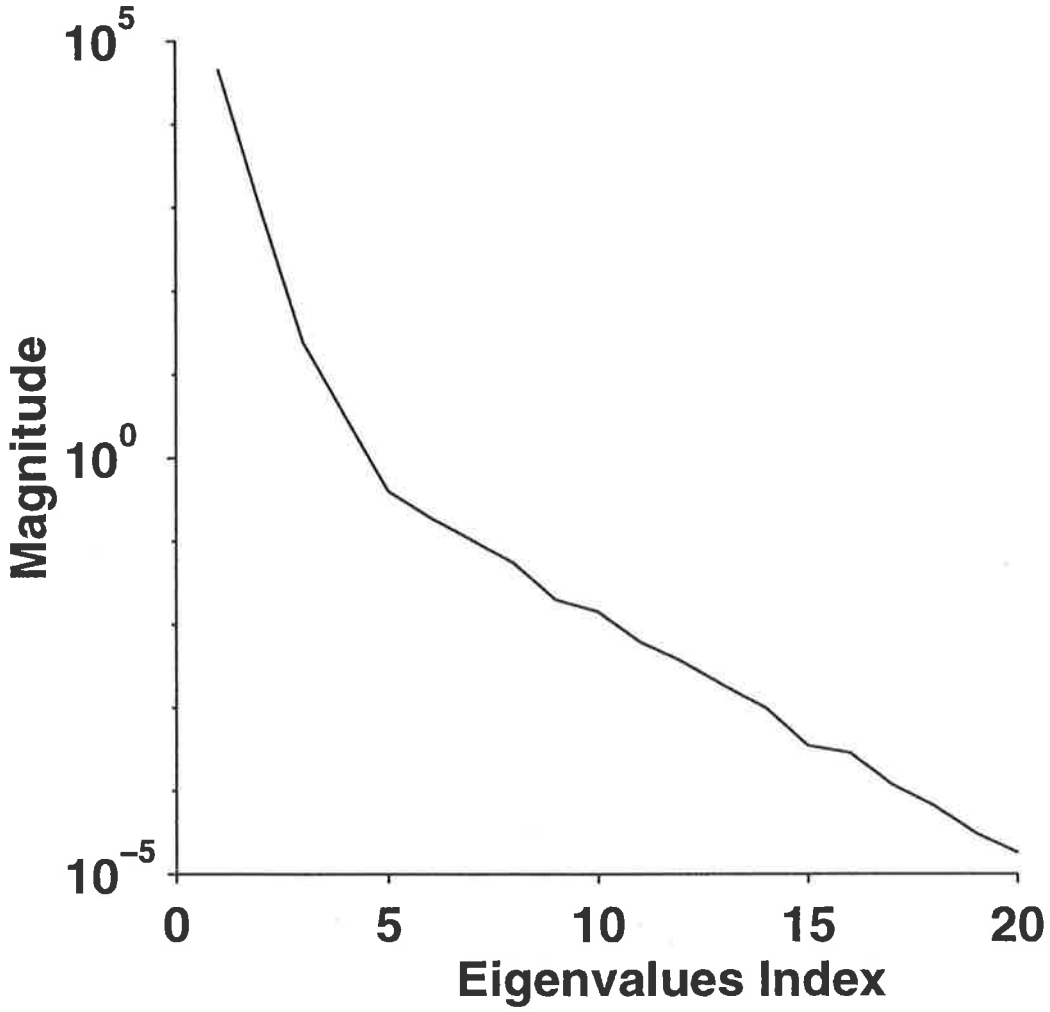

Figure 5.19: Eigenspectrum of ΔA sample cov. matrix.

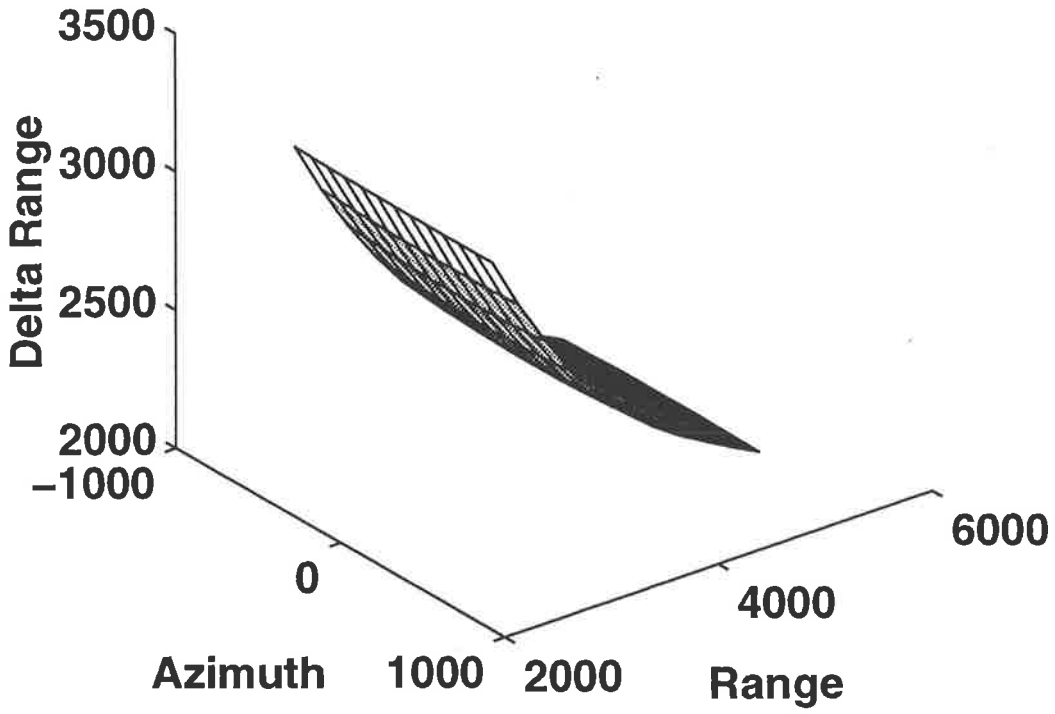

Figure 5.20: IDCT of first PC of ΔR sample cov. matrix.

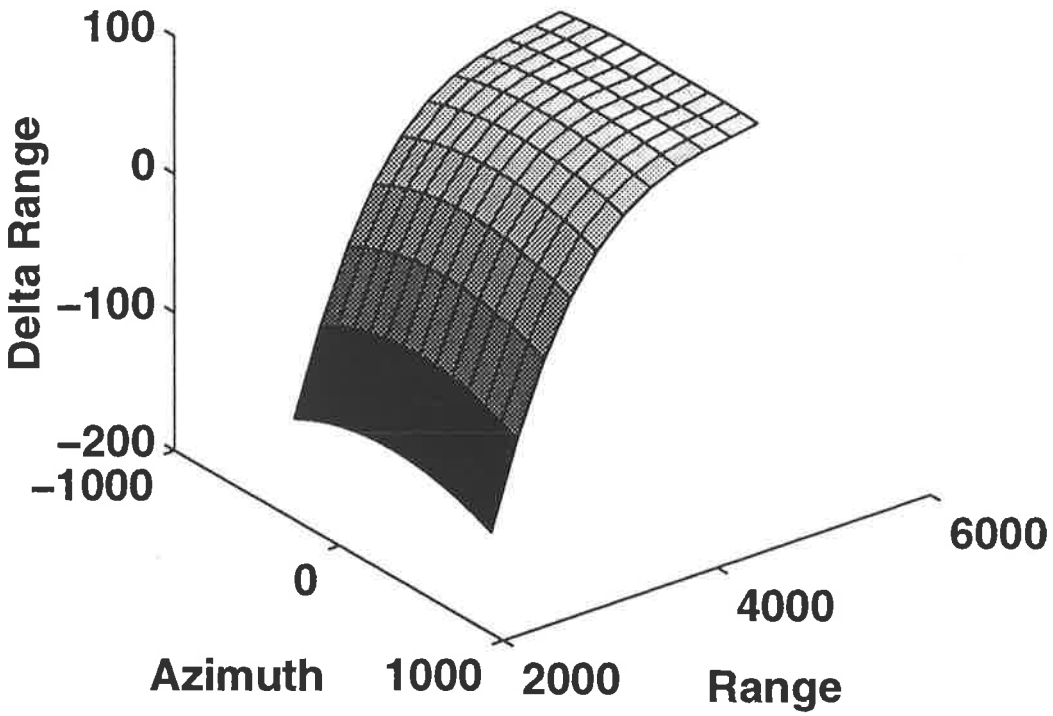

Figure 5.21: IDCT of second PC of ΔR sample cov. matrix.

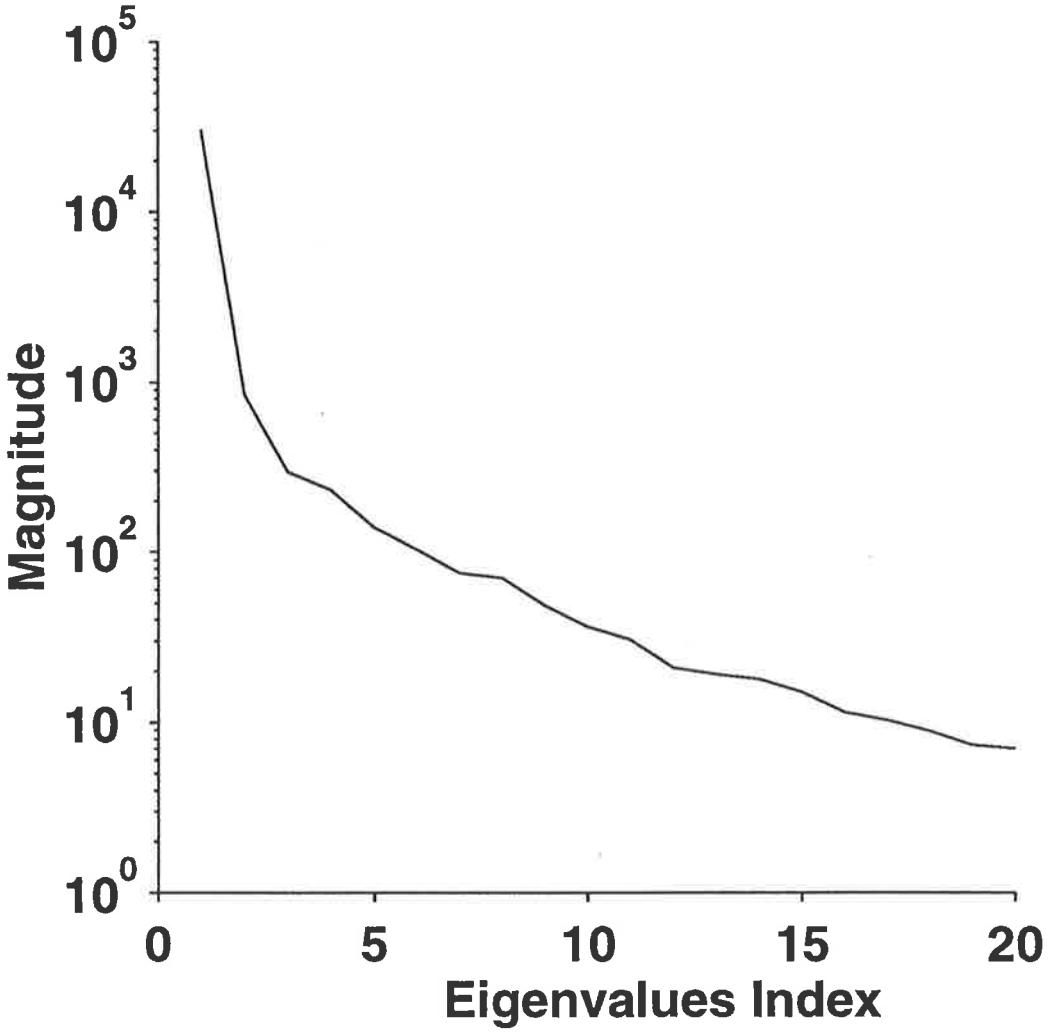

Figure 5.22: Eigenspectrum of ΔR sample cov. matrix.

the empirical technique. Not surprisingly, the first eigenvector represents the majority of the variation in the cosine function coefficients. The IDCT of the principle eigenvectors of the sample covariance matrix are very similar to the corresponding eigenvectors of the empirical technique. This fact is not surprising, since the cosine coefficients are merely a transformation of the data at the grid-points. The major difference between the empirical technique and the combined technique is the function between the grid-points: the empirical technique uses the maximally smooth interpolation function, whereas the combined technique uses a linear combination of cosine functions. The choice of cosine functions over another set of analytical functions is heuristic.

The cosine technique and the combined technique both use cosine functions, one explicitly and one implicitly. The PCA of the combined technique weights the cosine functions. The combined technique produces a better estimate of the disparity function, with respect to the spatial variation criterion in section 5.2, when the number of basis functions available is limited.

In sections 5.6.1, 5.6.2 and 5.6.3, we demonstrated the three modelling techniques proposed in this chapter. Each technique has its strengths and weaknesses, and can be tuned to real data by changing the choice of basis functions, or, in the case of the empirical technique, changing the choice of interpolation function. The OTHR data necessary for choosing the basis functions does not exist publicly; therefore we do not speculate on an appropriate choice of basis functions. However, we do discuss how these basis functions might be chosen: From a choice of suitable candidates, we choose the basis functions which minimise the sum of the squared error of the estimated disparity field at the grid-points.

5.7 Comparative study

In this section, we compare the three techniques proposed in this chapter. The techniques are statistically compared for their ability to model the azimuthal component of a simulated disparity field. Simulated targets provide sampled values of the azimuthal disparity; the sampled values are used for determining the coefficients of each technique's basis functions.

5.7.1 Training

The training data for the statistical comparative study is exactly the same as the data used for demonstrating the combined technique in section 5.6.3. Therefore we do not repeat the details of the simulation here. We simulate one scenario of each combination of the ionospheric heights in equations 5.14 and 5.15; making $n = 36$ scenarios in total. Each scenario provides values of the azimuthal disparity at p evenly spaced grid-points. These values form a $(n \times p)$ sample matrix, labelled $\mathbf{X}_{\Delta A}$, containing n observations of the p grid-points. We obtain a

similarly dimensioned sample matrix of the cosine coefficients via the DCT. This matrix is also $(n \times p)$, containing n observations of the p cosine coefficients. For each of the proposed techniques, we calculate the values of the top five basis functions, by dominance, at the p grid-points. The basis functions for each technique are denoted Υ_j, $j = 1 \ldots 5$ here.

5.7.2 Testing

To generate the set of test data for the comparative study, we choose an arbitrary but plausible combination of the virtual heights of ionospheric layers E and F. The values chosen are $h_E = 100$ and $h_F = 250$. We then compute the value of the estimated disparity function $\hat{\mathrm{d}}_{mn,k}(\mathrm{y}_i)$ at the grid-points in the radar measurement space, whose locations are denoted y_i $i = 1 \ldots p$. The computed disparity function is used for comparison against the modelled disparity functions.

The test data for the statistical comparison contains 1,000 scenarios, with 10 targets in each scenario. The radar measurements of the FE mode of target i^{th} are denoted x_i, and the corresponding azimuthal disparity is denoted ΔA_i. To determine the basis function coefficients, we solve the following linear system of equations in the least squares sense:

$$\begin{array}{ccccccccc} a_1\Upsilon_1(\mathrm{x}_1) & + & a_2\Upsilon_2(\mathrm{x}_1) & + & \ldots & + & a_5\Upsilon_5(\mathrm{x}_1) & = & \Delta A_1 \\ a_1\Upsilon_1(\mathrm{x}_2) & + & a_2\Upsilon_2(\mathrm{x}_2) & + & \ldots & + & a_5\Upsilon_5(\mathrm{x}_2) & = & \Delta A_2 \\ \vdots & & \vdots & & \vdots & & \vdots & = & \vdots \\ a_1\Upsilon_1(\mathrm{x}_{10}) & + & a_2\Upsilon_2(\mathrm{x}_{10}) & + & \ldots & + & a_5\Upsilon_5(\mathrm{x}_{10}) & = & \Delta A_{10} \end{array}, \tag{5.23}$$

where ΔA_i is the azimuthal disparity at x_i in the radar measurement space, and a_j is the coefficient of the j^{th} basis function, Υ_j. We solve such a system of equations for each of the proposed techniques. We use the coefficients to compute the corresponding modelled field at the p radar measurement space grid-points. In the case of the cosine technique,

$$\hat{\mathrm{d}}^{cos}_{mn,k}(\mathrm{y}_i) = \sum_{j=1}^{5} a_j \Upsilon_j(\mathrm{y}_i), \tag{5.24}$$

where y_i is the location of the i^{th} grid-point (in the radar measurement space). We compute the disparity field for the empirical technique and combined techniques via analogous equations to equation (5.24). In the analogous equations, the functions Υ_j, $j = 1 \ldots 5$, denote the basis functions for the technique in question.

Our criterion for comparing the proposed techniques uses the error between the modelled field and the actual field at the p grid-points. The most successful technique has the minimum sum of the squared errors:

$$\sum_{i=1}^{p} (\hat{\mathrm{d}}^{cos}_{mn,k}(\mathrm{y}_i) - \hat{\mathrm{d}}_{mn,k}(\mathrm{y}_i))^2.$$

5.7.3 Results

The results of the comparative study appear in Table 5.3 and 5.4. The first tabulates the errors from fitting only the dominant basis function, whereas the second tabulates the errors from fitting 5 basis functions. The units in each case are milliradians squared.

	Cosine	Empirical	Combined
Mean	6090	80.4	83.8
Std. dev.	677	38.3	42.0

Table 5.3: Error (in mrads^2), using one basis function.

	Cosine	Empirical	Combined
Mean	3070	4.1	10.6
Std. dev.	3510	44.3	36.9

Table 5.4: Error (in milliradians-squared), using five basis functions.

When only the dominant basis function is used, the empirical and combined techniques perform similarly, whereas the cosine technique has far less success. As one would expect, the performance of all three techniques improves when more basis functions are used.

While the empirical technique performs the best, it has the distinct advantage in that maximally smooth assumption used is the same as the maximally smooth interpolation function used in generating the simulated data. The cosine technique performs the worst, which reflects the fact that uses arbitrarily chosen basis functions. In contrast, the combined technique is based on the same arbitrarily chosen basis functions, but it performs similarly with the empirical technique. The combined technique transforms the original basis into a basis in which the bulk of the spatial variation of the disparity field is represented by far fewer basis functions; thus requiring fewer coefficients.

5.8 Summary and Discussion

In this chapter, we introduced three techniques for modelling components of the disparity function. Each technique is essentially a methodology for choosing a set of basis function for representing the disparity. The first technique, in section 5.3, involves choosing the basis functions heuristically. This technique is termed the cosine technique, since the basis functions are chosen to be the cosine functions. The second technique, in section 5.4, employs PCA to determine eigenvectors which represent the disparity at discrete points.

This technique is termed the empirical technique, since its basis functions are determined from empirical data. The third technique, in section 5.5, transforms the heuristically chosen basis of the cosine technique, by performing PCA on the cosine function coefficients. This technique is termed the combined technique, since it combines aspects of the previous two techniques. We demonstrate each of the three proposed techniques in section 5.6.

In section 5.7, we find that the performance of the cosine technique is the worst of the three, which reflects the fact that its basis functions are heuristically chosen. The empirical technique performs the best, which indicates that its assumption of maximal smoothness provides an advantage in modelling the simulated data. This fact is not surprising, since the simulated data is also generated using the same maximally smooth interpolation function. Encouragingly, the performance of the combined technique is not far behind that of the empirical technique. The combined technique does not have the same peculiar advantage on the simulated data as the empirical technique. The basis functions of the combined technique are linear combinations of heuristically chosen basis functions. Essentially, the combined technique provides a mechanism for transforming heuristically chosen basis functions, into basis functions which approaches optimality in the *Karhunen-Loéve* sense. For this reason, we hypothesise that, in the case of real data, the combined technique would be the most successful of the three proposed techniques. Unfortunately, this hypothesis cannot yet be tested on real data, as there are no suitable data publicly available.

CHAPTER VI

Conclusion

We have presented a systematic approach to the challenge of OTHR track association. Our objective was to develop a system which associates multimode tracks from a common target by exploiting the characteristic patterns of multimode propagation. These characteristic patterns have been under utilised in the past.

The ionosphere is the medium by which long range surveillance can be achieved. However, there are many challenges in the interpretation of OTHR returns due to the complex nature of the ionosphere as a medium for propagation. Many of the processing tasks in OTHR are interrelated, and the success of one affects the success of the others. Multimode track association is a key operation, which is related to several OTHR signal processing tasks. Therefore, we anticipate that the proposed system for track association has the potential to contribute to these signal processing tasks.

Multimode track association is a difficult problem; the transformation from radar measurements to ground coordinates can only be roughly estimated. The difference in multimode radar measurements from a common target is one available source of data, which has been under exploited. Multimode data can be used to assist the track association task, and also to assist other related OTHR processing tasks, such as coordinate registration. However, previous methods for multimode track association have significant limitations in that they do not exploit the multimode patterns to their full potential.

The systematic approach was designed to exploit the information contained in the multimode patterns. Fundamental to the proposed track association system is the concept of representing the intermodal coordinate transform by a vector function of both the radar measurements, and the ionospheric propagation conditions. We also proposed several components of the proposed system:

- A decision system was proposed for determining which tracks correspond to common targets. The decision system involves the testing of multiple association hypotheses using an association metric whose parameters are modelled by a partial model of ionospheric propagation. The decision system is designed to avoid conflicting association decisions.

- An association metric was proposed as a tool for estimating the probability that a pair of tracks are due to a common target.

- A model of the disparity vector was proposed, which estimates parameters of the disparity vector function as functions in the radar space.

The proposed association metric is the Mahalanobis distance of the disparity vector function. We demonstrated the success of the proposed association metric over alternative, heuristically chosen methods for both easy association scenarios and difficult association scenarios. The proposed metric provides better discrimination between pairs of associated tracks and pairs of non-associated tracks than the alternative metrics. The success of the proposed metric is due to the incorporation of a model of the multimode propagation. The fundamental difference between the proposed metric and the alternative metrics is the prior knowledge of disparity vectors used for the proposed metric. The alternative association metrics, by comparison, are based on heuristically chosen similarity measures, and they perform significantly worse, since they do not exploit knowledge of the disparity vectors. In short, we have demonstrated that knowledge of the multimode patterns permits great improvement in the association decision.

We proposed three ways of computing a cumulative association metric from the proposed association metric. While the proposed association metric performs well using one dwell, a cumulative association metric, using several dwells, will enhance the discrimination ability of the association metric, and hence the performance of the entire track association system.

We proposed three techniques for modelling components of the disparity field. Each technique is essentially a methodology for choosing a set of basis function to represent the disparity function.

1. The first technique involves choosing the basis functions from a visual inspection of the field to be modelled; the basis functions are chosen to be the cosine functions.

2. The second technique employs principle component analysis (PCA) to empirically determine discrete orthogonal basis vectors which represent the disparity function.

3. The third technique combines advantages of the previous two techniques; it transforms the heuristically chosen basis of the cosine technique to a more suitable basis, by performing PCA on the cosine function coefficients.

We found that the performance of the cosine technique is the worst of the three proposed techniques; this performance is indicative of the fact that its basis functions are heuristically chosen. The empirical technique had the best performance, which could be misleading, since the assumption of a maximally smooth disparity field is peculiar to the simulated data. We demonstrated that the combined technique performs almost as well as the empirical technique,

although not having the same peculiar advantage on the simulated data as the empirical technique. The combined technique provides a mechanism for transforming heuristically chosen basis functions into a more appropriate set of basis functions. For this reason, we hypothesise that, in the case of real data, the combined technique would be the most successful of the three proposed techniques. Unfortunately, this hypothesis cannot yet be tested on real data, as there is no suitable data publicly available.

Summary of Contributions

The major contribution of this thesis is a systematic approach for *associating* OTHR tracks corresponding to the same target. The approach exploits the patterns which are characteristic of multimode propagation. Significant components of the association system are an association metric for track association, and a model of the multimode patterns in the radar measurement space. We summarise specific contributions of the thesis as follows:

- There are two contributions which lie at the heart of the systematic approach for track association:

    1. The formulation of the coordinate transform between propagation modes as a function of the radar measurements and ionospheric propagation conditions (see equation (3.1) on page 30).
    2. The concept of modelling the statistical parameters of the disparity vector as functions of the radar measurements (see equation (3.4) on page 31).

- We modelled the statistical parameters of the disparity function using basis functions (see section 5.2). We compared (see section 5.7) three techniques for finding a suitable set of basis functions:

    1. A technique for modelling the disparity vector as a linear combination of heuristically chosen basis functions: the multidimensional cosine functions (section 5.3).
    2. A technique for modelling the disparity vector as a linear combination of empirically determined, discretely sampled functions using principle component analysis, in section 5.4.
    3. A technique for modelling the disparity vector which combines the advantages of the previous two approaches: modelling the disparity vector via principle component analysis (PCA) on the coefficients of multidimensional cosine functions (see section 5.5).

- We derived and tested an association metric as a tool for determining the probability that a pair of tracks is associated (see chapter 4). The association metric is designed

to discriminate between pairs of associated tracks and pairs of non-associated tracks. The association metric is based on the Mahalanobis distance of the disparity vector function (see equation (4.2) on page 38). The disparity vector function is used so that the warping caused by multimode transmission is accounted for, and thus the metric provides a measure of track similarity with uniform accuracy across the radar coverage. We conducted a comparative study of the proposed metric and alternative metrics (see section 4.3), and demonstrated the advantage of exploiting the patterns characteristic of multimode propagation.

- We described three ways of enhancing the association metric by accumulating sequential association metrics (section 4.4).

APPENDIX A

Simplified Model of Disparity Function

In chapter 4, we require statistical parameters of the disparity function to compute the proposed association metric. To maintain focus on the association metric in the comparative study of section 4.3, we use a simplified model for the computation of the disparity function. This appendix contains details of the simplified model for computing parameters of the disparity vector. These parameters are the estimated disparity vector $\hat{\mathbf{d}}_{mn}$ and its covariance Σ_{mn}. The estimated disparity vector $\hat{\mathbf{d}}_{mn}$ is a vector function over the radar coverage, and the covariance Σ_{mn} is a matrix function.

The parameters for a specific mode pair are a function of location in the radar measurement space, denoted by the vector $\mathbf{y}$. In section A.1 we outline the simplifications which make the model a "simplified" model. Under these simplifications, we state, in section A.2, the geometrical relationship between a target's location and the corresponding radar measurements. In section A.3, we derive analytical expressions for the parameters of the disparity vector.

We outline the numerical evaluation of the disparity vector in section A.4. Finally, in section A.5, we discuss the ionospheric priors used for the simplified model.

A.1 Simplifications to propagation geometry

The model described in this appendix is based on simplified ionospheric propagation geometry. We make these simplifications, so that analytical expressions for the components of the disparity vector between associated tracks can be derived. These components include the difference in slant range and apparent azimuth of tracks from a common target. The simplifications do not detract from the validity of the comparative study in section 4.3. The simplifications to the ionospheric geometry are:

Radar measurement errors are ignored.

Only the ionospheric contribution to intermodal variation is considered. Data dependent quantities such as radar measurement errors are ignored to maintain focus on the comparative study. The inclusion of radar measurement errors is straightforward, but

would extend the study in an unnecessary direction.

Only two ionospheric layers are considered.

We only consider the case of propagation from the E and F layers of the ionosphere. This choice results in four possible modes of propagation. Other scenarios could be considered in the same way.

Spherical ionospheric layers are assumed.

It is assumed that the ionospheric layers are spherical and concentric with the earth. A spherical model was chosen in order to simplify the propagation geometry for the purposes of the demonstration, but such a model is not necessary for the method.

Ionospheric priors are known.

It is assumed that the distributions of the ionospheric heights are known *a priori*. This simplification is made so that the distribution of the disparity vector can be calculated. The heights of the spherical ionospheric layers are represented by the normal random variables $X_E \sim N(\mu_E, \sigma_E)$, for the E layer and $X_F \sim N(\mu_F, \sigma_F)$, for the F layer. We assume that the heights of the ionospheric layers vary independently.

Transmitter and receiver are colocated.

It is assumed that the transmitter and receiver are the same distance from the target for the purposes of the simulation. This assumption is made to avoid data dependent complexities in the geometry of the propagation paths and is not significant for the comparative study of the association metrics. Note that in practice, the transmitter and receiver cannot be within line of sight because the transmitted power causes the receiver to saturate.

Only range and azimuth are considered.

Only the range and azimuth components of the disparity vector are considered. The remaining components of the disparity vector (Doppler shift, signal strength) are ignored to restrict the volume of this paper. The distribution of the remaining components can be calculated in an analogous way.

A.2 Propagation Geometry

Denote by R and A the actual range and azimuth of a target with respect to the radar. The height of the ionospheric layer used for transmission of the radar signal is denoted by h_t, and the layer used for the reception of the radar signal is denoted by h_r. Let R_s denote the slant range between the radar and the target, which is a function of the ground range to the target, R, and the height of the ionospheric layer used for reflection, denoted by h. This function is

derived from the propagation geometry via the cosine rule and is given by

$$R_s(h,R) = 2\sqrt{e^2 + (e+h)^2 - 2e(e+h)cos\left(\frac{R}{2e}\right)}$$

where e is the radius of the earth (taken to be 6380km). Denote by R_t the sum of the slant range from transmitter to target and the slant range from target to receiver. R_t is formulated as

$$R_t(h_t, h_r, R) = R_s(h_t, R) + R_s(h_r, R) \tag{A.1}$$

The apparent azimuthal angle is also derived from the simplified geometry. We denote the apparent azimuthal angle of the target by A_t. A_t is a function of R and A and the height of the layer used for reception of the signal from the target, h_r. From the propagation geometry, the apparent azimuthal angle is

$$A_t(h_r, R, A) = \arcsin\left[\sin(A)\sin\left(\frac{R}{2e}\right)\frac{2}{R_s}(h_r + e)\right] \tag{A.2}$$

A.3 Analytical formulation of disparity vector

Under the simplifications made in appendix A.1, the disparity vector is a function of the target location and the ionospheric conditions, which are known. We derive the parameters of the disparity vector analytically for a specific mode pair at a specific location. As an example, we derive these parameters for the specific mode pair used in the comparative study of section 4.3.

Example Consider that an estimate of the disparity vector between modes EF and EE is required. The difference in total slant range for this example is

$$\begin{aligned} \Delta R(X_F, X_E) &= R_t(X_E, X_F, R) - R_t(X_E, X_E, R) && \text{(A.3)} \\ &= R_s(X_F, R) - R_s(X_E, R) && \text{(A.4)} \end{aligned}$$

The difference between the apparent azimuthal angles of the two modes is

$$\Delta A(X_F, X_E) = A_t(X_F, R, A) - A_t(X_E, R, A) \tag{A.5}$$

By integrating over the known range of possible ionospheric conditions, the estimated value of the disparity vector's range component can be formulated as

$$\begin{aligned} \left[\hat{\mathrm{d}}_{EE,EF}\right]_{\Delta R} &= E\left[\Delta R(X_E, X_F)\right] && \text{(A.6)} \\ &= \int_{-\infty}^{\infty}\int_{-\infty}^{\infty} \Delta R(x_E, x_F) f(x_E, x_F)\, dx_E\, dx_F && \text{(A.7)} \end{aligned}$$

where $f(x_E, x_F)$ is the jointly normal probability density function; thus

$$\begin{aligned} f(x_E, x_F) &= \frac{1}{2\pi\sigma_E\sigma_F} \\ &\exp\left(-\frac{1}{2(1-r^2)}\left[\frac{(x_E-\mu_E)^2}{\sigma_E^2} - \frac{2r(x_E-\mu_E)(x_F-\mu_F)}{\sigma_E\sigma_F} + \frac{(x_F-\mu_F)^2}{\sigma_F^2}\right]\right) \end{aligned}$$

where r is the correlation coefficient between random variables x_E and x_F.

The variance of the range component of the disparity vector can be formulated similarly

$$\sigma^2_{\Delta R} = \int_{-\infty}^{\infty}\int_{-\infty}^{\infty}(\Delta R(x_E, x_F) - \overline{\Delta R(x_E, x_F)}^2) f(x_E, x_F)\, dx_E\, dx_F \tag{A.8}$$

The remaining parameters of the disparity vector are the mean and variance of the azimuthal component, $[\mathrm{d}_{EE,EF}]_{\Delta A}$ and σ_a respectively, and the covariance between the azimuth and the range components, σ_{ra}. Expressions for these parameters are formed by analogy with Equations A.7 and A.8. The estimated value of the azimuthal component of the disparity vector is formulated as

$$\begin{aligned}\left[\hat{\mathrm{d}}_{EE,EF}\right]_{\Delta A} &= E\left[\Delta A(X_E, X_F)\right] &\text{(A.9)}\\ &= \int_{-\infty}^{\infty}\int_{-\infty}^{\infty}\Delta A(x_E, x_F) f(x_E, x_F)\, dx_E\, dx_F. &\text{(A.10)}\end{aligned}$$

The variance of the azimuthal component of the disparity vector is formulated as

$$\sigma^2_{\Delta A} = \int_{-\infty}^{\infty}\int_{-\infty}^{\infty}(\Delta A(x_E, x_F) - \overline{\Delta A(x_E, x_F)}^2) f(x_E, x_F)\, dx_E\, dx_F. \tag{A.11}$$

The covariance between the range and azimuthal components of the disparity vector is formulated as

$$\begin{aligned}\sigma^2_{\Delta R,\Delta A} = \int_{-\infty}^{\infty}\int_{-\infty}^{\infty} &(\Delta R(x_E, x_F) - \overline{\Delta R(x_E, x_F)})\\ &(\Delta A(x_E, x_F) - \overline{\Delta A(x_E, x_F)})\quad f(x_E, x_F)\, dx_E\, dx_F. \quad\text{(A.12)}\end{aligned}$$

A.4 Numerical computation of the disparity vector

The components of the mean of the disparity vector are calculated from equations A.7 and A.10. The components of covariance matrix

$$\Sigma_{mn} = \begin{bmatrix} \sigma^2_{\Delta R} & \sigma^2_{\Delta R,\Delta A} \\ \sigma^2_{\Delta R,\Delta A} & \sigma^2_{\Delta A} \end{bmatrix}$$

of the disparity vector can be calculated from equations A.8, A.11 and A.12.

The model computes the parameters of the disparity function, $\hat{\mathrm{d}}_{mn}$ and Σ_{mn}, from track measurements in the radar space. The integrals in section A.3 are difficult to evaluate analytically, but can be evaluated numerically using the ionospheric priors and the target position in ground coordinates. However, the precise position of an observed target in the target space is not known.

To evaluate the parameters numerically, we must do so at many locations in the radar space. A set of data is computed to form the basis for the model of disparity vectors. This data set is referred to as the *example set*, and it consists of precomputed mean vectors

and covariance matrices, indexed by mode pair and location in radar coordinates. These parameters are precomputed for every combination of mode pairs at many locations across the radar coverage. We model the mean vector functions over the space element-wise. In contrast, we model the eigenvectors, instead of the elements, of the covariance matrix functions. The eigenvectors are modelled similarly to the mean vector functions: as vector functions, element-wise. In making the matrix eigenvectors smooth over the space, instead of the matrix elements, we ensure that the computed covariance matrix has similar characteristic properties to the adjacent precomputed covariance matrices in the example set.

For a specified mode pair at a specified location in radar coordinates, we estimate the parameters of the disparity vector from the nearest (in the radar space) precomputed parameters in the example set. For simplicity, this estimate is made via bilinear interpolation of the nearest precomputed parameters.

A.5 Ionospheric priors

We arbitrarily choose a set of priors to generate the example set for the comparative study. The range of possible heights of the ionospheric layers for all latitudes can be found in [32]. The E layer exists between 90km and 130km, so X_E was chosen to be N(110km,10km). The F layer typically exists between 200km and 400km, so X_F was chosen to be N(300km,50km). The heights of the different ionospheric layers are assumed to be independent.

Bibliography

[1] N. Ahmed and K. R. Rao. *Orthogonal transforms for digital signal processing*. Springer-Verlag, 1975.

[2] Y. Bar-Shalom and T.E. Fortmann. *Tracking and data association*. Academic Press, 1988.

[3] B.M. Bell and T.E. Ewart. Separating multipaths by global optimization of a multidimensional matched filter. *IEEE Transactions on Acoustics, Speech amd Signal Processing*, ASSP-34(5):1029–1037, October 1986.

[4] W.D. Blair, G.W. Groves, Y. Bar-Shalom, and E. Daeipour. Frequency agility and fusion for tracking targets in the presence of multipath propagation. In *Record of the 1994 National Radar Conference*, pages 166–70. IEEE, New York, USA, March 1994.

[5] R.E. Bogner. Signal processing principles for over-the-horizon radar. Technical report, University of Adelaide, 1989. An educational report for DSTO Australia.

[6] R.E. Bogner, A. Bouzerdoum, K. Pope, M.L. Southcott, and J. Zhu. Data association studies for potential othr applications: Design of mlps and statistical decision systems for othr track association. Technical Report Sig-1-1994, Centre for Sensor Signal and Information Processing, Technology Park Adelaide, SA 5095, 1994.

[7] R.E. Bogner, A. Bouzerdoum, K. Pope, M.L. Southcott, and J. Zhu. Data association studies for potential othr applications. Technical Report Sig-2-1995, Centre for Sensor Signal and Information Processing, Technology Park Adelaide, SA 5095, 1995.

[8] R.E. Bogner, A. Bouzerdoum, K. Pope, M.L. Southcott, and J. Zhu. Data association studies for potential othr applications: Affinity selection and performance analysis. Technical Report Sig-1-1995, Centre for Sensor Signal and Information Processing, Technology Park Adelaide, SA 5095, 1995.

[9] R.E. Bogner, A. Bouzerdoum, M.L. Southcott, and J. Zhu. Report to defence science and technology organisation: Investigations into othr track association using neural

networks. Technical Report DFT-2-93, Centre for Sensor Signal and Information Processing, Technology Park Adelaide, SA 5095, 1993.

[10] R.E. Bogner, A. Bouzerdoum, M.L. Southcott, and J. Zhu. Report to defence science and technology organisation: Resolving ambiguities in othr tracks using neural networks. Technical Report DFT-3-93, Centre for Sensor Signal and Information Processing, Technology Park Adelaide, SA 5095, 1993.

[11] P.A. Bradley. Use of ionospheric models in hf radio planning and ohd target location. In *Fifth International Conference on HF Radio Systems and Techniques*, pages 178–82. IEE, London, UK, July 1991.

[12] S.B. Colegrove, A.W. Davis, and J.K. Ayliffe. Track initiation and nearest neighbours incorporated into probabilistic data association. *Journal of Electrical and Electonic Engineers, Australia*, 6(3):191–198, 1986.

[13] S.B. Colegrove and P.J. Edwards. Review of the automatic tracking of targets in clutter. In *Proceedings of the 21st International Electronics Convention and Exhibition*, pages 681–684, Sydney, September 1987. IREE.

[14] I.W. Dall and D.J. Kewley. Track association in the presence of multipath propagation. In *Proceedings of the International conference on Radar 92*, pages 70–73. IEE, October 1992.

[15] I.W. Dall and A.J. Shellshear. Evaluation of a model based data fusion algorithm with multimode othr data. In *Proceedings of the 27th Asilomar conference on signals, systems and computers*, 1993.

[16] I.W. Dall and A.J. Shellshear. Performance of an improved model based data fusion algorithm for othr data. In *Proceedings of the International Conference on Radar 94*, pages 625–9, May 1994.

[17] K. Davies and C.M. Rush. High frequency ray paths in ionospheric layers with horizontal gradients. *Radio Science*, 20(1), 1995.

[18] T.M. Georges and J.A. Harlan. New horizons for over-the-horizon radar? *IEEE Antennas and Propagation Magazine*, 36(4):14–24, 1994.

[19] J.M. Headrick. Looking over the horizon. *IEEE Spectrum*, pages 36–39, 1990.

[20] O. Heaviside. Telegraphy i, theory. *Encyclopaedia Britannica*, 33:215, 1902.

[21] Robert V. Hogg and Elliot A. Tanis. *Probability and Statistical Inference*. Macmillan, 1988.

[22] R. Ignetik and B.J. Jarvis. On the importance of earth geometry for over-the-horizon radar coordinate registration. In *Proceedings of the International Conference on Radar 94*, pages 398–402, May 1994.

[23] Anil K. Jain. *Fundamentals of Digital Image Processing*, chapter 5, pages 150–154. Prentice-Hall, 1989.

[24] R. K. Jarrott. The processing of hf skywave radar signals. In *ICASSP 94, Proceedings of the 1994 International Conference on Acoustics, Speech and Signal Processing*, volume VI, pages 165–168. IEEE, 1994.

[25] I.T. Jolliffe. *Principle Component Analysis*. Springer-Verlag New York Inc., 1986.

[26] Erwin Kreyszig. *Advanced Engineering Mathematics*. John Wiley and Sons, 1983.

[27] T. Kurien, M. Peyman, D. Logan, and W.P.Jr. Berry. Propagation mode estimation: A prerequisite for oth radar fusion. In *Proceedings of the 1994 IEEE International Conference on Multisensor Fusion and Integration for Intelligent Systems (MFI'94)*, pages 543–50. IEEE, New York, 1994.

[28] M. L. Lees. An overview of signal processing for an over-the-horizon radar. In *ISSPA 87, signal processing, theories, Implementations and Applications*, pages 491–495, 1995.

[29] M. Lewis and K. Perry. Over-the-horizon radar. *Miltronics*, 11(1):17–20, 1990.

[30] M. Lockwood. Modelling the high-latitude ionosphere. In *IEE Colloquium on "National Radio Propagation Programme"*, pages 10/1–6. IEE, London, UK, Jan. 1991.

[31] R. H. Maryon. Eigenanalysis of the northern hemispherical 15-day mean surface pressure field and its application to long-range forecasting. Meteorological Observations 13 Branch Memorandum No. 82, UK Meteorological Office, Bracknell, 1979.

[32] L.F. McNamara. *The ionosphere: communications, surveillance, and direction finding*. Krieger Publishing Company, 1991.

[33] L.F. McNamara. *The ionosphere: communications, surveillance, and direction finding*, chapter 4, pages 44–45. Krieger Publishing Company, 1991.

[34] L.F. McNamara. *The ionosphere: communications, surveillance, and direction finding*, chapter 15, page 212. Krieger Publishing Company, 1991.

[35] D.J. Netherway and J.K. Ayliffe. Impulsive noise suppression in hf radar. In *Proceedings of the 21st International Electronics Convention and Exhibition*, pages 673–676, Sydney, September 1987. IREE.

[36] D.J. Netherway, G.E. Ewing, and S.J. Anderson. Reduction of some environmental effects that degrade the performance of hf skywave radars. In *Proceedings of the Australian Symposium on Signal Processing and its Applications*, volume 2, pages 288–292, 1989.

[37] G.W. Pulford and R.J. Evans. State estimation in systems with multiple simultaneous measurements. In *Proceedings of the 33rd Conference on Decision and Control*, Florida, 1994.

[38] G.W. Pulford and R.J. Evans. Probabilistic data association for systems with multiple simultaneous measurements. *Automatica*, April 1995.

[39] J.A. Ratcliffe. *Sun, Earth and Radio: An introduction to the ionosphere and magnetosphere.* World University Library, 1970.

[40] C.M. Rush. Ionospheric radio propagation models and predictions - a mini-review. *IEEE Transactions on Antennas and Propagation*, AP-34(9):1163–1170, September 1986.

[41] John C. Russ. *The Image Processing Handbook.* IEEE Press, 1994.

[42] David T. Sandwell. Biharmonic spline interpolation of geos-3 and seasat altimeter data. *Geophysical Research Letters*, 14(2):139–142, 1987.

[43] D.H. Sinnott. Jindalee - dsto's over-the-horizon radar project. In *Proceedings of the 21st International Electronics Convention and Exhibition*, pages 661–664, Sydney, September 1987. IREE.

[44] D.H. Sinnott. *The Development of Over-the-Horizon Radar in Australia.* Australian Government Publishing Service, Canberra, 1988.

[45] M.L. Southcott and R.E. Bogner. An association metric for track association of multi-mode othr tracks. on offer to IEEE transactions on Aerospace and Electronic Systems, March 1995.

[46] S.S. Swords. *Technical history of the beginnings of RADAR.* Peter Peregrinus Ltd., London, 1986.

[47] A.H. Taylor. An investigation of transmission on the higher radio frequencies. *Proceedings of the Institute of Radio Engineers*, 13:677, 1925.

[48] M. Turley and M.L. Lees. An adaptive impulsove noise suppressor for fmcw radar. In *Proceedings of the 21st International Electronics Convention and Exhibition*, pages 665–668, Sydney, September 1987. IREE.

[49] J.S. Wadsworth. Recent advances in track fusion techniques. In *IEE Colloquium 'Algorithms for Target Tracking'*, pages 8/1–4. IEE, London, May 1995.

[50] K. A. White, I. W. Dall, and A. J. Shellshear. Association of over-the-horizon radar tracks with tracks from microwave radar and other sources. In *Proceedings of SPIE, Signal Processing, Sensor Fusion and Target Recognition V*, volume 2755, pages 335–346. SPIE, June 1996.

[51] J. Zhu, R. Bogner, and A. Bouzerdoum. A comparison of neural networks and statistical methods for track association in over the horizon radar. In *Proceedings of SPIE International Symposium on Optical Engineering in Aerospace Sensing: Sensor Fusion and Aerospace Applications II*, volume 2233, pages 224–235. SPIE, June 1994.

[52] J. Zhu, R. Bogner, A. Bouzerdoum, and M.L. Southcott. Application of neural networks to track association in over the horizon radar. In *Proceedings of SPIE International Symposium on Optical Engineering in Aerospace Sensing: Sensor Fusion and Aerospace Applications II*, volume 2233, pages 224–235. SPIE, June 1994.

[53] B. Zolesi, Lj. R. Cander, and G. de Franceshi. A simple mid-latitude ionospheric model. In *Sixth International Conference on Antennas and Propagation*, volume 2, pages 243–6, 1989.

Addenda

We have added the following text to clarify some questions raised by readers.

- In **Chapter 3, Section 3.3.4.** we add the following two sentences to the end of the second paragraph (at the top of page 32),:

The covariance matrix is decomposed into its eigenvectors, which are modelled in the same way as the disparity vector itself. The interested reader can find details of this modelling in section A.4 of the Appendix.

- In **Chapter 4, Section 4.2** we add three sentences in the middle of the final paragraph (on page 38), which becomes (the existing text is italicised):

The primary benefit of using the M-distance as the association metric is the fact that it accounts for the covariance between radar measurements. We do not ignore the possibility that there may be a choice of association metric which provides better discrimination between associated and non-associated pairs of tracks. Since the distribution of the intermodal disparity vector is unknown, and there is no data available from which the distribution of the intermodal disparity vector might be measured, we do not attempt to assert that this proposed metric might satisfy any optimality criterion. The M-distance would be the optimal metric, in the least squares sense, if the distribution of the intermodal disparity vector were multivariate Gaussian. For now, the criterion which we use to measure the success of a metric is based on its ability to discriminate between tracks from a common target and tracks not from a common target. *We expect an association metric with greater discriminatory performance to improve the performance of the track association system. However, to maintain the focus of this thesis, we omit a rigorous investigation into the merits of different metrics. We perform a limited comparison of the proposed association metric to other association metrics in section 4.3.*

- At the end of the concluding chapter, **Chapter 6** (on page 100), we add the following unnumbered section:

Future work

This thesis would not be complete without a recommendation for the direction of future work to enhance the accuracy and reliability of the techniques introduced in this thesis. Due to the highly sensitive nature of over-the-horizon radar data, it was impossible to apply the ideas introduced in the thesis to real data. In my opinion, the task with the greatest urgency is to establish the reliability of the techniques using real over-the-horizon radar data. Normally distributed disparity vectors were used for illustrating the ideas introduced in this thesis. One might be able to achieve a more accurate model of the disparity vector once a suitable model of the disparity vectors has been obtained using real data.